UNIVERSITY OF CAPE COAST

INVESTIGATIONS OF STAFF DOSES DURING COMPUTED TOMOGRAPHY-FLUOROSCOPY PROCEDURES USING MONTE CARLO SIMULATION

BY

PRINCE KWABENA GYEKYE

Thesis submitted to the Department of Physics of the School of Physical Sciences, College of Agriculture and Natural Sciences, University of Cape Coast, in partial fulfilment of the requirements for the award of Doctor of Philosophy degree in Physics

APRIL 2019

DECLARATION

Candidate's Declaration

I hereby declare that this thesis is the result of my own original research and that no part of it has been presented for another degree in this university or elsewhere.

Candidate's Signature: .... Date: 23-4-19

Name: Prince Kwabena Gyekye

Supervisors' Declaration

We hereby declare that the preparation and presentation of the thesis were supervised in accordance with the guidelines on supervision of thesis laid down by the University of Cape Coast.

Principal Supervisor's Signature: .... Date: 23-4-19

Name: Prof. Samuel Yeboah Mensah

Co-Supervisor's Signature: .... Date: 23/4/19

Name: Dr. Frank Becker

ABSTRACT

Radiation dose to staff during Computed Tomography (CT) fluoroscopy procedures has been investigated using Monte Carlo N-Particle code 6 (MCNP6). Four (4) CT machines located at Korle-bu Teaching Hospital, Sweden Ghana Medical Centre, Karlsruhe Hospital and FOCOS Orthopaedic Hospital respectively were modelled using SimpleGeo software. The patient (supine) and staff (standing) were represented both by Female Adult meSH (FASH) and Male Adult meSH (MASH) computational voxel phantoms. Seven scenarios consisting of staff use of protective equipment, CT gantry and staff positioning in the CT room, CT room size variation, the use of lead drape and patient cover on patient, the use of protective face mask and apron by staff, scatter radiation distribution in the CT room, and the effective estimation of staff effective dose were investigated for occupational staff protection. A systematic approach for validating CT scanners with unknown bowtie-filter was proposed and tested. The use of protective equipment, lead drape and patient cover, protective face mask and apron, diagonal positioning of CT fluoroscopy gantry, and staff standing away from walls of room were observed to reduce effective dose to staff by a factor of 4.5, 4.4, 2.8, 1.1 and 1.2 respectively. Sex based single and double TLD effective dose estimation algorithm was proposed. The staff dose reduction factors observed for applying protection measures for this study varied by a factor of 1.6 – 6.9 compared with other studies. The use of conventional protection equipment at all times is recommended and complemented with alternative one (that is, standing position) to further reduce doses.

KEY WORDS

Computed Tomography

Effective dose

Fluoroscopy

Monte Carlo

Photon

Staff Protection

ACKNOWLEDGEMENTS

I would like to thank the International Atomic Energy Agency (IAEA) for the award of 18 months PhD sandwich research fellowship at Karlsruhe Institute of Technology (KIT), Karlsruhe, Germany. I would like to thank KIT and Karlsruhe Hospital for the experience and knowledge acquired in computational simulations, and making their facilities available for the simulations during my fellowship. My appreciation goes to Korle-Bu Teaching hospital (Accra), Sweden Ghana Medical Centre (Accra) and FOCOS Orthopaedic Hospital (Accra). My sincere thanks also go to the Department of Physics, University of Cape Coast for their guidance, support and the opportunity given to me to undertake my studies. I would like to acknowledge Prof. Geoffrey Emi-Reynolds of the School of Nuclear and Allied Sciences, University of Ghana for his supervisory role throughout the entire duration of my programme. I would also like to thank Dr. Stefan Pölz of KIT for his immense support and guidance throughout this work. Appreciation goes to my two supervisors Prof. Samuel Yeboah Mensah and Dr. Frank Becker for their intellectual support and contribution to a successful completion of this study. Lastly, I would like to thank my wife, children, extended family and friends for their emotional support and encouragement throughout the course of this study.

DEDICATION

In memory of my late grandmother, Ms. Florence Taylor.

TABLE OF CONTENTS

LIST OF TABLES

LIST OF FIGURES

Figure Page

LIST OF ACRONYMS

IAEA	International Atomic Energy Agency
KIT	Karlsruhe Institute of Technology
CT	Computed Tomography
US	Ultrasound
MRI	Magnetic Resonance Imaging
TLD	Thermoluminescence Dosimeter
ICRP	International Commission on Radiological Protection
MCNP6	Monte Carlo N-Particle code 6
3D	Three Dimensional
SPET	Single Photon Emission Tomography
PET	Positron Emission Tomography
2D	Two Dimensional
EBCT	Electron Beam Computed Tomography
WL	Window Level
WW	Window Width
HU	Hounsfield Unit
FOV	Field of View
GE	General Electric
1D	One Dimensional
ALARA	As Low As Reasonable Achievable
ICRU	International Commission on Radiation Units and Measurements
LET	Linear Energy Transfer

CTDI	Computer Tomography Dosimetry Index
MCNP	Monte Carlo N-Particle
CAD	Computer Aided Design
CSG	Hierarchal Constructive Solid Geometry
FASH	Female Adult Mesh Phantom
MASH	Male Adult Mesh Phantom
$CTDI_c$	Computed Tomography Dose Index at centre
$CTDI_w$	Weighted Computed Tomography Dose Index
$CTDI_{vol}$	Volume Computed Tomography Dose Index
$CTDI_{air}$	Computed Tomography Dose Index in Air
LiF	Lithium Fluoride
kVp	Peak Kilo-Voltage
F6:p	Photon Energy Deposition Average over a Cell
PEDEP	Average Energy Deposition per Unit Volume
CF	Calibration Factor

CHAPTER ONE

INTRODUCTION

Radiation diagnostic imaging modalities have improved medical care to people. One of the innovations of radiation diagnostic imaging is Computed Tomography (CT) fluoroscopy. Therefore, this chapter discusses the background of CT's, problems identified to be investigated, main objectives in addressing the problem, the importance of this study, the focus area and organisation of the study.

Background to the Study

The evolution of CT scanner technology in the past 26 years has brought about tremendous discoveries, that is, slip ring scanning, fast (sub-second) rotation times, greater computation power (Keat, 2001) and multiple detector scans. Currently, medical interventional procedures have clinically improved due to the introduction of CT fluoroscopy (Carlson, et al., 2001) and other advance modalities in medical radiology. CT fluoroscopy produces cross sectional images rebuilt at minimum spatial resolution and continuously updated at a rate of several frames per second, permitting real-life time imaging of organs in motion (Carlson, et al., 2001; Irie, et al., 2001).

CT fluoroscopy is a technological innovation resulting from slip-ring technology, X-ray tubes with improved heat capacity, high-speed array processors, and partial reconstruction algorithms (Paulson, Sheafor, Enterline, McAdams, & Yoshizumi, 2001; Katada, et al., 1996). The images from CT can be rebuilt at a rate of approximately six or more frames per second, permitting near real-time imaging similar to that of ultrasonography (US). The advantage of this technology is it combines the localizing strengths of CT with real-time images.

CT fluoroscopy has been used extensively for interventional procedures like tissue biopsy, drainage of fluid-filled lesions (Keat, 2001) and other interventional procedures. This is due to its wide dynamic range to imaging air, soft tissues and bones, and further provisions of acceptable image quality that allows for improved distinction of human anatomical system and minimum influence of patient motion and respiration (Katada, et al., 1996; Froelich, et al., 1998; Buls, Vandenbroucke, & De Mey, 2012).

Clinical studies (Silverman, et al., 1999; Froelich, et al., 1998; Daly, Krebs, Wong-You-Cheong, & Wang, 1999; Meyer, White, Wu, Futterer, & Templeton, 1998) have shown that CT fluoroscopy guide is a safe and effective guidance tool for percutaneous interventional examinations in the pelvis, spine, chest and abdomen. With this technology, procedures are performed more quickly than with traditional CT (Sheafor, Paulson, Kliewer, De-Long, & Nelson, 2000).

Several imaging modalities such as fluoroscopy, US, CT or magnetic resonance imaging (MRI) may be used alone or in combination with the others for guidance in percutaneous interventional examinations. In recent years CT-guided interventions in particular have become essential clinical tool due to associated high spatial resolution, superior reproducibility, wide field of view, and applicability to air-filled, soft tissue and bony structures (Katada, et al., 1996; Froelich, et al., 1998).

Although conventional CT allows assessment of puncture localization, needle direction and evaluation of needle positions within the body, it is time-consuming. Due to the lack of real-time imaging capability of CT-guided interventions compared with sonography and fluoroscopy image guidance, the later were preferable (Sheafor, Paulson, Kliewer, De-Long, & Nelson, 2000). CT guided procedures are cumbersome leading to high radiation doses when lesions are located at respiratory areas. The lesion may shift or disappear in the course of conventional CT-guided procedure due to movement (Froelich, et al., 2002). Therefore, CT fluoroscopy systems were invented to address this problem by providing real-time image reconstruction and display of CT images on a monitor.

Several studies (Katada, Anno, Koga, Ida, & Sata, 1993; Katada, Anno, Ogura, Nonomura, & Kanno, 1995; Katada, et al., 1996) have been conducted to investigate the possibility and applicability of the CT fluoroscopy to nonvascular and vascular interventions, after the introductory report on CT fluoroscopy innovation by Katada *et al*. in 1993 (Katada, Anno, Koga, Ida, & Sata, 1993). Clinical applications of CT fluoroscopy have increased hence there is the concern of radiation exposure to staff and patients. This study investigated radiation dose reduction techniques for the staff involved in CT fluoroscopy guided procedures, that is, drainage, biopsy and other interventional examinations. Monte Carlo simulations approach was employed to investigate all possible scenarios for possible clinical implementation.

Statement of the Problem

The influence of patient breathing and motion on image formation during radiology has reduced due to the intrinsic functionality of the CT fluoroscopy (Buls, Vandenbroucke, & De Mey, 2012). Other significant improvements in images of air-filled, soft tissue and bony structures have led to the increase in the use of CT fluoroscopy as a guide for percutaneous procedures. Due to the increase, significant concern that comes to bare is the radiation doses involved in the applicability of CT fluoroscopy.

Staff exposure to radiation has been detected to be high as observed in other studies (Nawfel, et al., 2000; Silverman, et al., 1999; Stoeckelhuber, et al., 2005; Teles, et al., 2017; Ferrari, et al., 2016). This is because exposure times during CT fluoroscopy guided procedures could be long compared with conventional CT acquisitions. Additionally, the tube voltage and current are relatively high with CT fluoroscopy compared with general fluoroscopy (Buls, Vandenbroucke, & De Mey, 2012; Buls, Pages, de Mey, & Osteaux, 2003; Joemai, Zweers, Obermann, & Geleijns, 2009).

The medical doctor is required in the CT room during percutaneous interventional procedures to manipulate the needle for efficient application of CT fluoroscopy (Kato, et al., 1996). Increased radiation exposure to the hands, body and eye lens of the radiologist is expected due to their proximity to the scan plane on the patient. The scatter radiations to the radiologist are a contribution of scatter radiations from the patient, CT fluoroscopy gantry, patient table (Gyekye, Becker, Mensah, & Emi-Reynolds, 2016; Siebel, Sehnert, & Schmit, 1997; Kato, et al., 1996) and walls of the CT fluoroscopy room (Gyekye, Becker, Mensah, & Emi-Reynolds, 2016; Buls, Vandenbroucke, & De Mey, 2012).

Conventionally, radiologists are expected to protect themselves with lead aprons, goggles, thyroid shield (Pereira, et al., 2011) where applicable and necessary to reduce their exposure to radiation. Alternatively, dose reduction techniques investigated by other authors are the use of protective gloves and needle holder (Yoshimatsu, et al., 2008; Daly, Krebs, Wong-You-Cheong, & Wang, 1999; Silverman, et al., 1999; Kato, et al., 1996), angular beam modulation application (Hohl, et al., 2008), and recommendation of the use of pulse CT fluoroscopy rather than continuous fluoroscopy (Bissoli, Bison, Gioulis, Chisena, & Fabbris, 2003).

With the tremendous increase in the use of CT fluoroscopy for percutaneous procedures and the evident high staff exposures recorded in other studies (Nawfel, et al., 2000; Silverman, et al., 1999; Stoeckelhuber, et al., 2005; Teles, et al., 2017; Ferrari, et al., 2016), the problem at hand is the further reduction of the staff dose apart from the conventional means. The International Commission on Radiological Protection (Stewart, et al., 2012) through its recommendation has suggested equivalent dose limit of 20 mSv per year (averaged over 5 years) for the eye lens in known radiation exposure situations. This is observed as a reduction from the 150 mSv per year reported in earlier publications (ICRP, 1990). The drastic reduction in the dose limit suggests alternative means of dose reduction to the eye lens of staff should be explored as well in CT fluoroscopy guided procedures.

Objective of the Study

The main aim of this research was to effectively contribute to occupational radiation protection during CT fluoroscopy through:

1. proposing a user friendly computational CT modelling protocol for computational radiation protection studies;
2. effective recommendation of appropriate staff dosimetry using thermoluminescence dosimeter (TLD) of occupationally exposed workers/staff;
3. assessment and investigations into the effectiveness of conventional and occupational dose reduction techniques from literature;
4. investigations into alternative occupational dose reduction technique;
5. make suggestions and recommendations on occupational dose reduction for clinical application or manufacturing considerations.

The aims of this study would be achieved through physical radiation output measurements from identified CT machines. The architectural layout of the CT room, position of CT gantry and patient couch in the room, schematic details of CT and computational voxel phantoms would aid in achieving the task through Monte Carlo computational simulation.

Relevance of the Study

Studies in the direction of radiation dose reduction of staff in CT fluoroscopy are important because of reported high doses with the procedure. Fluoroscopy procedures have resulted in majority of radiation doses received by hospital staff using X-rays. This is because the procedure requires direct involvement of medical and clinical staff to guide invasive procedures. Minor repairs of vasculature using instruments through catheters are introduced into the human body (Martin, 2009).

Occupational doses in interventional radiology procedures are generally higher than those received in other radiology practices (Pereira, et al., 2011; ICRP, Avoidance of radiation injuries from medical interventional procedures, 2000). Personal protective devices such as lead aprons, gloves, thyroid shields and goggles are recommended for use by the medical doctor. These protective devices may be complemented depending on the practise with protective screens and table shields. Individual monitoring of staff also raises some questions on the number and correct positioning of whole body and extremity dosimeters (Pereira, et al., 2011). The recommendations from Vano *et al.* (Vano & Faulkner, 2005) suggest the use of a robust and adequate monitoring regime for staff in interventional procedures.

Investigations into staff dosimetry (appropriate dosimetry) and dose reduction methods are of relevance to the staff. This study would inform medical staff on the appropriate measures and techniques to employ to reduce dose to the whole body, hands and eye lens. The reduction of the equivalent dose from 150 mSv to 20 mSv averaged over 5 years as recommended by International Commission on Radiological Protection (ICRP) (ICRP, 2007) also warrants this study to investigate into alternative dose reduction techniques to the eye lens apart from the conventional means, that is, goggles.

The conclusion of this study would also guide future researchers and CT manufacturers on the major areas of concern for further studies. Hence this study is beneficial for the radiation protection community and manufacturers to strengthen the protection of the staff.

Scope of the Study

The research is mainly investigating into dose reduction techniques to medical doctor during CT fluoroscopy interventional procedures. High radiation doses to staff have extensively been reported (Nawfel, et al., 2000; Silverman, et al., 1999; Stoeckelhuber, et al., 2005; Teles, et al., 2017; Ferrari, et al., 2016) and it is of a major concern to the community of medical application of radiation. The focus is on medical staff protection through computational simulation.

CT machine and CT room at Korle-Bu Teaching hospital, Accra (KBTH), Sweden Ghana Medical Centre, Accra (SGMC), Karlsruhe Hospital, Germany (KH) and FOCOS Orthopaedic Hospital, Accra (FOCOS) were considered for the study. Monte Carlo N-Particle 6 (MCNP6) was employed for the computational simulations using a computational male and female mesh phantom in supine and standing positions to mimic the patient and staff respectively. The use of MCNP6 for dosimetry in CT has proved to be effective from comparative studies with realistic computational phantoms (Deak, vanStraten, Shrimpton, Zankl, & Kalender, 2008).

Organisation of the Study

Chapter one discusses background, problem, objective, relevance and scope of the study. Chapter two discusses the literature behind CT fluoroscopy, radiation protection programme, Monte Carlo, SimpleGeo three dimensional modelling tool and computational phantoms. Chapter three identifies all materials required and the approach engaged for the study. Chapter five discusses the outcome of the study and recommendations to target groups.

Chapter Summary

Medical interventional procedures have clinically improved due to the introduction of CT fluoroscopy. But the use of CT fluoroscopy has recorded high doses to staff. Therefore, staff dose reduction techniques are to be investigated and proposed. The outcome of this study is going to be beneficial to the staff, researchers and CT manufacturers. The approach of the staff dose investigation will be through computational Monte Carlo simulation.

CHAPTER TWO

LITERATURE REVIEW

Introduction

This chapter discusses the theory of the study covering all the equipment and other principles utilised in this study.

Evolution of Computed Tomography

CT for clinical usage was introduced in 1971. The technology then was only used for axial scanning of the brain in neuroradiology. With time, it metamorphosed into an all-purpose three-dimensional (3D) full body imaging modality for oncology, vascular radiology, cardiology, traumatology and interventional radiology. Numerous medical procedures are done by employing CT that is diagnosis and follow-up studies of patients, planning of radiotherapy treatment, and screening of healthy subpopulations with specific risk factors (IAEA, 2014a).

Currently, dedicated CT scanners are available for special clinical applications. It is used for applications such as radiotherapy treatment planning. Radiotherapy treatment planning CT's are designed to offer an extra wide bore, allowing the CT scans to be made with a large field of view. Another application is the integration of CT scanners in multi-modality imaging applications, that is single photon and/or positron emission tomography (SPECT/PET) scanner (IAEA, 2014a). Additional innovation of the CT technology is the application of CT for real-time 3D imaging of internal organs and biological process, that is, CT fluoroscopy.

Other current achievements for dedicated diagnostic imaging concerns are the development of a dual source CT scanner, which is a CT scanner that is furnished with two X-ray tubes, and a volumetric CT scanner, that is a 320 detector row CT scanner that enables scanning of the entire organs within one rotation (IAEA, 2014a).

CT imaging procedure is appropriately suited for obtaining 3D images for cardiac, brain, musculoskeletal and whole body. The images can be presented as impressive coloured 3D rendered images, but two dimensional (2D) axial images or reformats in black and white are relied on by radiologists (IAEA, 2014a).

First Generation CT

The patient or object being scanned is axially divided into virtual slices. A single X-ray beam is collimated to obtain a narrow (pencil-width) X-ray beam. A dimension of 3 mm x 13 mm within the plane and perpendicular to the slice respectively defines the single X-ray beam. This dimension is along the axis of the patient. The slice thickness of the image represents the beam width. The X-ray tube is linked to a detector positioned on the other side of the patient. The X-ray tube along with the detector scans axially across the patient using a narrow X-ray beam (Hounsfield, 1973). The detector measurements transmitted X-ray through the patient at several locations during translation motion. The arrangement of X-ray tube, detector and subject is shown in Figure 1 (Goldman, 2007).

The tube–detector assembly is rotated around the subject by 1° after c-

-ompletion of translation. The translation is repeated at a tube-detector assembly angle of 1° to collect a second view. The scanner repeats this process in 1° increments to collect 180 views over 180°. Recent scanners may typically collect 1,000 or more views over 360° (Goldman, 2007).

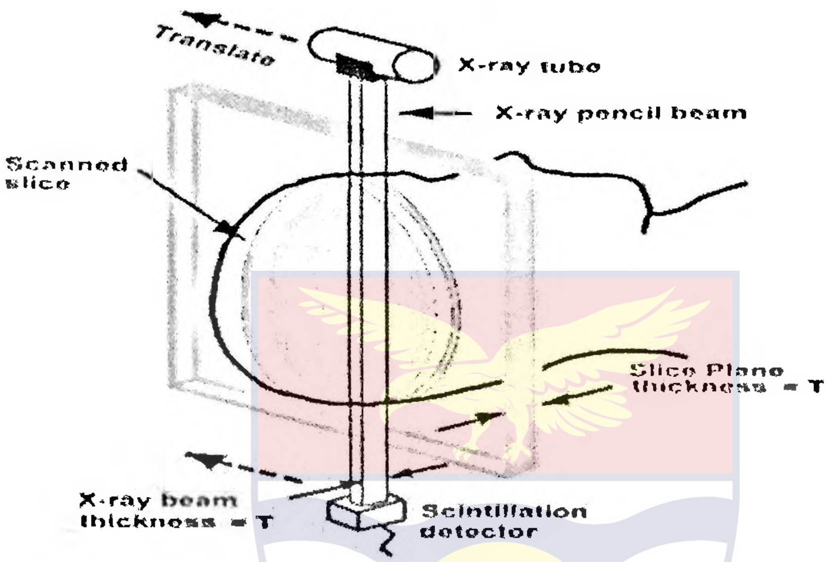

Figure 1: Single beam axial slice Computed Tomography scan

Source: (Goldman, 2007)

Second Generation CT

First generation CT took too long for scans and hence the introduction of second-generation CT geometry in the late 1974 (Ketteringham & Gempel, 1978). Second-generation CT employed multiple detectors and narrow beams engaging rotate–translate motion. A second-generation scanner with three narrow beams and three detectors is shown in Figure 2. Second generation CT can minimise scan time by a factor of 1/(number of detectors) generally. Designs engaging 20 or greater narrow X-ray beams and detectors gathering equivalent numbers of instantaneous views were clinically introduced (Goldman, 2007). This minimised scan times to 20 s or less. There was an improvement in body scan image quality because scans could be completed within a breath hold for most patients. However, the automated rotate-translate geometry complications hindered further speed improvements. The rotate-translate motion arrangement had to be performed swiftly and accurately without causing the gantry (X-ray tube, detectors and associated electronics) to vibrate (Goldman, 2007).

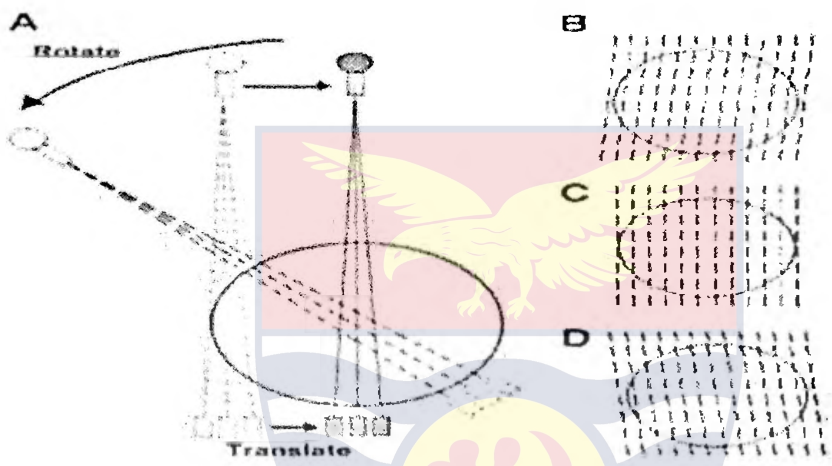

Figure 2: Multiple beam axial slice Computed Tomography scan

Source: (Goldman, 2007)

Third Generation CT

Simpler and smoother rotational motion replaced the translation motion for improvement. This was achieved by opening up the X-ray beam into a fan beam to occupy the entire patient width and with array of detectors to intercept the transmitted beam. Figure 3 details detector and X-ray beam arrangement. The mechanism of the movement of detector array and the X-ray tube is arranged such that both of them rotate together at the same speed around the patient (Seeram, 2010). About 750 or greater detectors fixed enable numerous measurements to be made of the transmitted beam across the scan c-

-ircle path (Goldman, 2007).

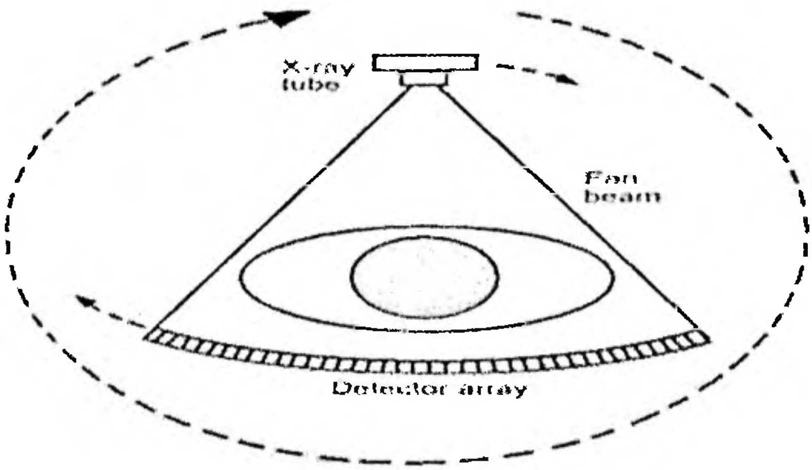

Figure 3: Rotating tube and array of detectors

Source: (Goldman, 2007)

In 1975, third generation CT scanners were introduced. The scanners could achieve a complete scan in less than 5 s. Current designs can achieve a complete scan in one third of a second. Detector stability with matching response is needed in this generation CT. The X-ray tubes and detectors are strictly linked and hence each detector intercepts rays passing only at a particular distance from the centre of rotation. The detector interception is dependent on the position of the detector in the array. Any inaccuracies in the adjustment of a detector relative to the other detectors is back predicted along these ray paths and strengthened along a ring where the rays cross. Dynamic readjustment of the detectors is prohibited because most of the detectors are behind the patient during the entire scan. Therefore, ring artefacts resulting from the detector errors are as small as 0.1% (Goldman, 2007).

Xenon detectors were used to resolve ring artefacts based on the intri-

-nsic properties of the material (Goldman, 2007). Xenon detector arrays were eventually replaced by solid state detectors. Ring artefacts in third-generation CT images were never completely eliminated. The quality of design and calibration of detectors reduced the occurrence of ring artefacts. Residual ring artefacts in images are then removed by image-processing algorithms, without which rings would likely be seen in every CT image. Detector failure or drift may still cause ring artefacts to occasionally appear. The success of third-generation CT has made it the fundamental geometry upon current scanners is based on (Goldman, 2007).

Fourth Generation CT

Under 1s scans were achieved with stationary ring of detectors and X-ray tube alone rotating around the patient by the year 1976 (Goldman, 2007). This approach is illustrated in Figure 4. Fourth generation technology was developed to address the engineering challenges of the third-generation approach. The detector of fourth generation CT gathers a complete fan beam view. Each fourth-generation detector intercepts and gathers transmitted X-ray at any distance from the centre of rotation. Additionally, the detector can dynamically be calibrated before it goes into the patient's shadow such that ring artefacts are not a problem (Goldman, 2007).

Setbacks such as size and geometric dose efficiency of fourth generation CT were observed (Goldman, 2007). The X-ray tube was designed to rotate inside the detector ring and hence a large ring diameter (170–180 cm) was required. In addition, for a good spatial resolution for generating acceptable images, the detector aperture was limited to approximately 4 mm. The cost consideration of the detectors limited the number to 600 instead of proposed 1,200. This resulted in gaps between detectors thereby generating low geometric efficiency. The design was improved by arranging the detectors close to the patient (to reduce the size of gantry) whilst the X-ray tube rotated outside the ring of detectors. Increased scatter radiation was another issue observed with fourth-generation CT designs. This is because scatter-absorbing septa could not be used due to the design of fourth generation CTs. In all, fourth-generation CT was not an advanced model of third-generation CT (Goldman, 2007) but rather different way of detector arrangements.

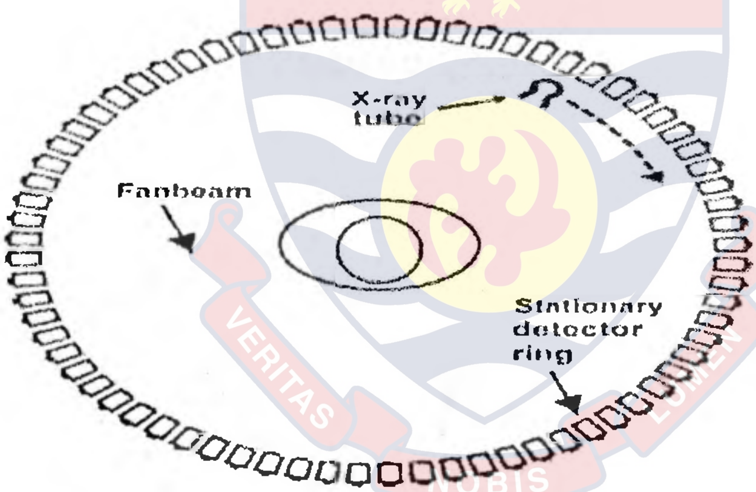

Figure 4: Fixed detector ring and rotating X-ray tube

Source: (Goldman, 2007)

Other Developments of CT

CT scanners have undergone other developments to improve upon its diagnostic capabilities. Slip ring scanners, helical scans, electron beam scanners and the ability to couple fluoroscopy during scans are the developments.

Slip Ring Scanners and Helical CT

Beyond the fourth generation CT technology, not much was innovated (other than incremental improvements) until 1987 (Goldman, 2007). Inter-scan delays contributed much to the total time spent for CT examination. This was because the cables connecting to the rotating parts of the gantry after a complete rotation (360 degrees) have to be reversed. Reeled cables were released during rotation, and then re-wound during reversal. Scanning, braking, and reversal delayed the scan for at least 8–10 s, of which only 1–2 were spent acquiring image. This resulted in poor resolution (temporal for contrast enhanced motion studies) and long examination times (Goldman, 2007).

Low-voltage slip technology was introduced to eliminate inter-scan delays by employing continuous (non-stop) rotation. The technology enabled electrical power to be connected to the rotating components (e.g., X-ray tube and detectors) without connecting cables. Slip ring technology consisted of a drum with channels along which electrical conducting brushes slide. The wireless innovation passed data from detectors enabling non-reversible rotations to exist. Slip ring has allowed the complete elimination of inter-scan delays although the time required moving the table to the next slice position remains. The solution to resolve the delay in time for table movement was to continuously rotate and continuously acquire data as the table (patient) is smoothly moved though the gantry. The ensuing path of the tube and detectors relative to the patient creates a spiral or helical pathway as shown in Figure 5 (Kalender, Seissler, Klotz, & Vock, 1990; Toki, 1993). This enabled fast scans to be performed in a required region of the patient in the direction of the table movement (z-axis) in sometimes within a single respiratory hold (Goldman, 2007).

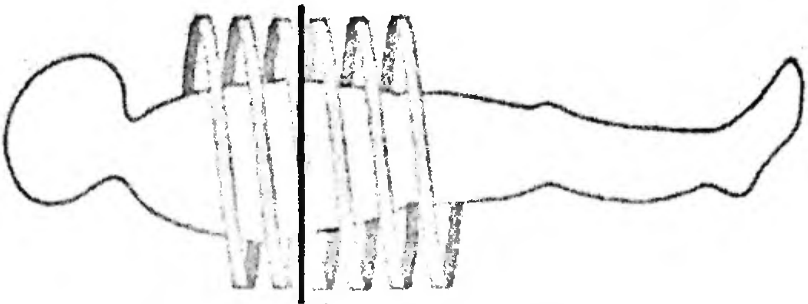

Figure 5: Helical Computed Tomography

Source: **(Goldman, 2007)**

Electron Beam-CT (EBCT)

The mechanical problem encountered with fast scans under a second drained the X-ray tubes. This is because about 250 mAs per slice is needed to generate an appropriate body CT scan (that is 0.25 s scan would require 1,000 mA). However, cardiac CT scans need superfast scans (about 50 ms) to stop cardiac motion from interfering with the image. A novel electron beam-CT with the capability of performing scans between 10 - 20 ms was designed to address the issue of cardiac CT. The ultrafast CT utilised a large, bell-shaped X-ray tube (Iinuma, Tateno, Umegaki, & Wantanbe, 1977). A narrow beam of electrons is generated from a collection of electrons released from a cathode. This narrow beam is then deflected to a small focal spot located on tungsten target anode (angulated) electronically to eventually produce X-rays. The electron beam (and consequently the focal spot) is then electronically directed along the entire 360 circumference of the target. X-rays are generated along and shaped into a fan beam whenever the electron impinges on the angular tungsten target (Goldman, 2007).

Swift scans of the heart without table (patient) movement needed four anodes and two detector banks to be used along the z-axis to obtain eight interleaved slices occupying 8 cm of the cardiac space (heart). The electron beam – CT (EBCT) achieved faster scans through the innovation but slower (50 – 100 ms) due to limited tube current (650 mA) needed to obtain appropriate mAs value for an image of good quality (McCollough, 1995). EBCT is mainly used for cardiac screening because the produced diagnostic image quality was lower than that of conventional CT (this was due to low mAs values) and also the equipment is expensive. However, the introduction of multi-slice CT's has made cardiac screening cheap and easily accessible (Goldman, 2007).

CT Fluoroscopy

Real-time CT fluoroscopy is feasible due to the dynamic, continuous scanning made possible by the innovation of slip ring technology. A slip ring scanner is modified to allow real-time tableside image viewing and table positioning via foot pedal–controlled acquisitions and joy stick–controlled table positioning. This innovation has enabled percutaneous aspirations and biopsies to be performed using the innovation as a guiding tool. Since a slip ring scanner can continuously acquire views at a fixed z-axis, temporal resolution can be considerably better than expected on the basis of rotation speed; acquired images are updated many times per second by consistent addition of new data generated to replace old ones (Goldman, 2007; Cho, 2014).

CT fluoroscopy has proved to be of relevance for interventional procedures but creates the potential for significant radiation doses if too many images are acquired at a given position (Silverman, et al., 1999). Considering minimizing radiation exposure, a recent trend has been to replace continuous acquisition with a series of discrete, rapidly acquired images to guide biopsies (Goldman, 2007).

Principles of Computed Tomography Technology

Computed tomography image acquisition is achieved by measuring X-ray transmitted through an object (patient) for a large number of views. Different views are obtained in computed tomography primarily by using detectors with hundreds of detector elements along the detector arc (generally 800 - 900 detector elements). The rotation of the X-ray tube around the patient takes about 1000 angular measurements and hence generating more views. Additionally, there are tens or even hundreds of detector rows aligned next to each other along the axis of rotation (IAEA, 2014a) by so doing enhancing the view.

Values representing pixels in CT images are linked with the average linear attenuation coefficient μ (m^{-1}) of tissues. The linear attenuation coefficient (μ) relies on the composition and density of the material, and the energy of the photon as illustrated by Beer-Lambert law:

$$I\,(x) = I_o e^{-\mu x} \qquad (1)$$

where I(x) - intensity of transmitted X-ray; I_o - intensity of the incident X-ray; x - material thickness. Beer's law describes the attenuation of the primary beam and does not consider the intensity of scattered radiation that is generated. For poly-energetic X-ray beams, Beer's law should be applied by integrating all photon energies in the required X-ray spectrum. The back projection procedures developed for CT reconstruction algorithms is generally not used but rather a pragmatic solution is to assume one value representing the average photon energy of the X-ray spectrum. This assumption results in errors in the reconstruction leading to beam hardening artefact (IAEA, 2014a).

When an X-ray beam passes through a patient, different body tissues exhibit different linear attenuation coefficients. The intensity of the transmitted X-ray through a distance (d), can be expressed as:

$$I(d) = I_o e^{-\int_0^d \mu(x)dx} \qquad (2)$$

where: I(d) - intensity of transmitted X-ray beam at *d*; I_o - intensity of the incident X-ray beam; μ(x) - the linear coefficient; x - material thickness (IAEA, 2014a).

CT images are obtained through a matrix of pixels correlating to the average linear attenuation coefficient in an accompanying volume element (voxels). A simplified 4 x 4 matrix representing the measurement of transmission along one line is shown in Figure 6. In theory, each element in the matrix can have a different value of the accompanying linear attenuation coefficient. Therefore, equation (2) is modified to express as:

$$I(d) = I_o e^{-\sum_{i=1}^{i=4} \mu_i \Delta x} \qquad (3)$$

where: I(d) - intensity of transmitted X-ray beam at *d*; I_o - intensity of incident X-ray beam; μ_i - linear attenuation coefficient at *i*. Δx - the material thickness (IAEA, 2014a).

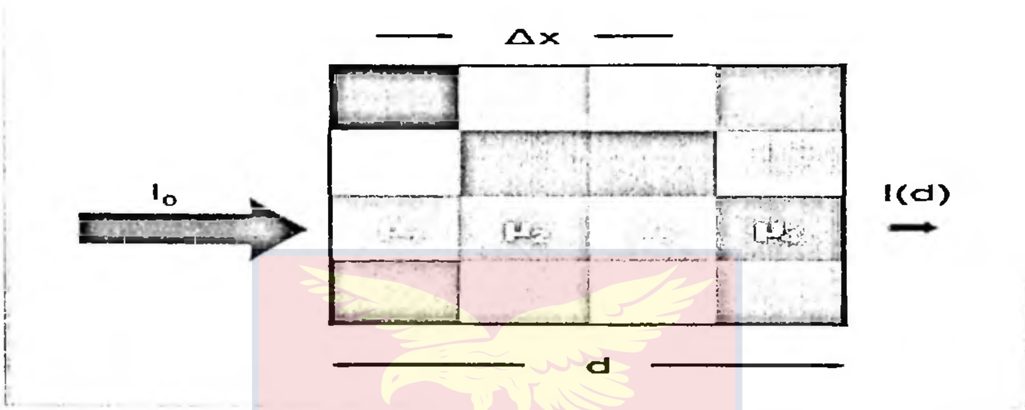

Figure 6: Radiation transmission measurement along one line in a 4 x 4 matrix

Source: (IAEA, 2014a)

Equation (3) shows that to estimate linear attenuation coefficient, the intensity of the attenuated I(d) and un-attenuated (I_o) X-ray beam should be measured. The basis of CT image formation is dependent on the image reconstruction procedures employed to obtain a matrix of linear attenuation coefficient. The matrix of reconstructed linear attenuation coefficients ($\mu_{material}$) is converted into a corresponding matrix of Hounsfield units ($HU_{material}$), where the HU scale is expressed relative to the linear attenuation coefficient of water at room temperature (μ_{water}):

$$HU_{material} = \frac{\mu_{material} - \mu_{water}}{\mu_{water}} x\ 1000 \qquad (4)$$

therefore, $HU_{water} = 0$, when ($\mu_{material} = \mu_{water}$; $HU_{air} = -1000$ when ($\mu_{material} = 0$; $HU = 1$ is associated with 0.1% of the linear attenuati-

-on coefficient of water. The value of Hounsfield unit depends on the composition of a body tissue or material, the X-ray tube voltage, and the existing temperature. Body tissue or substance Hounsfield units are shown in Table 1 (IAEA, 2014a).

Table 1: Table of Materials and Hounsfield Units

Substance	Hounsfield Unit
Compact Bone	+1000 (+300 to +2500)
Liver	+ 60 (+50 to +70)
Blood	+ 55 (+50 to +60)
Kidneys	+ 30 (+20 to +40)
Muscle	+ 25 (+10 to +40)
Brain, Grey Matter	+ 35 (+30 to +40)
Brain, White Matter	+ 25 (+20 to +30)
Water	0
Fat	- 90 (-100 to -80)
Lung	- 750 (-950 to -600)
Air	-1000

Source: (IAEA, 2014a)

Hounsfield units are visualized in eight (8) bit grey scale offering 128 grey values. Window Level (WL) as CT number of mid-grey and window width (WW) as the number of HU from black (> white) are used to define the CT display. The clinical need for WW and WL necessitated for its use because optimal visualization of the body tissues of interest in the CT image relies on the appropriate selection of window width and window level. Different settings of the WW and WL are required to visualize soft tissue, lung tissue, bone etc. The effect of WL and WW is shown in Figure 7 with different settings (IAEA, 2014a).

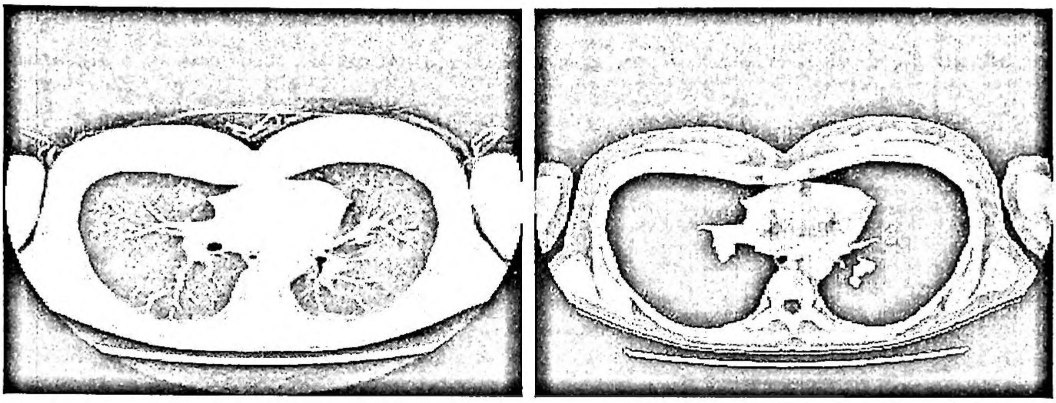

WL -593, WW 529 WL -12, WW 400

Figure 7: Comparison of the effect of window length (WL) and width (WW)

Source: (IAEA, 2014a)

A minimum bit depth of 12 Hounsfield units enables creating a Hounsfield scale that runs from –1024 HU to +3071 HU, hence taking into consideration relevant clinical body tissues. A wider Hounsfield scale is useful with a bit depth of 14 creating a scale up to +15359 HU thus making applicable to high density and high linear attenuation coefficient materials. Generally, an extended Hounsfield scale will allow for better visualisation of body parts with implanted metal objects such as stents, orthopaedic prosthesis's, dental- or cochlear implants. Hounsfield unit for substances and tissues, except for water and air, varies at different tube voltages. This is because substances and tissues exhibit a non-linear relationship of their linear attenuation coefficient relative to water at different photon energies. This effect is dominant in substances and tissues with relatively high (effective) atom number such as contrast bone (calcium) and enhanced blood. In clinical procedures, a deviation between the actual and expected Hounsfield unit is possible. This is due to the dependence of the Hounsfield unit: on the reconstruction filter; on the size and position within the scanned field of view; and on the formation of artefacts in images (IAEA, 2014a).

Computed Tomography Imaging Components

Currently the CT scanners available on the market are mostly helical, multi detector row, dual source and volumetric. These features were developed at the end of the year 1983. Multi detector row and multisource row was explained by a United States patent (#4196352, W.H. Berninger, R.W. Redington, GE company) shown in Figure 8a. Additionally the unique helical scan was also explained in the patent (#4630202, Issei Mori, Tochigi, Japan.) as shown in Figure 8b (IAEA, 2014a).

Gantry and Table

The gantry of a CT scanner houses all the components that are needed to acquire the transmission profiles of a patient. The transmission profiles of a patient are acquired at different angles and hence the components are mounted on a support for the rotation. The components mounted on the gantry for rotation are the beam collimators and shaping filters, X-ray tube with its cooling content (water or air), the arc of detectors, data processing equipment and generator for high voltage. Figure 9 shows the image of an opened gantry with the X-ray tube (T), the X-ray beam (X), the detectors (D), and the rotation direction (R) (IAEA, 2014a).

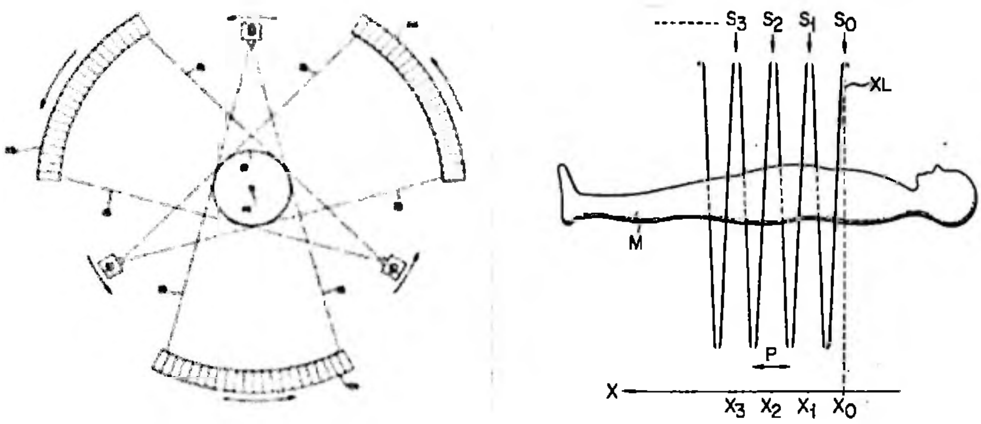

(a) (b)

Figure 8: (a) Patent multi detector row and multi-source arrangement and (b) helical scan illustration of Computed Tomography scanners

Source: (IAEA, 2014a).

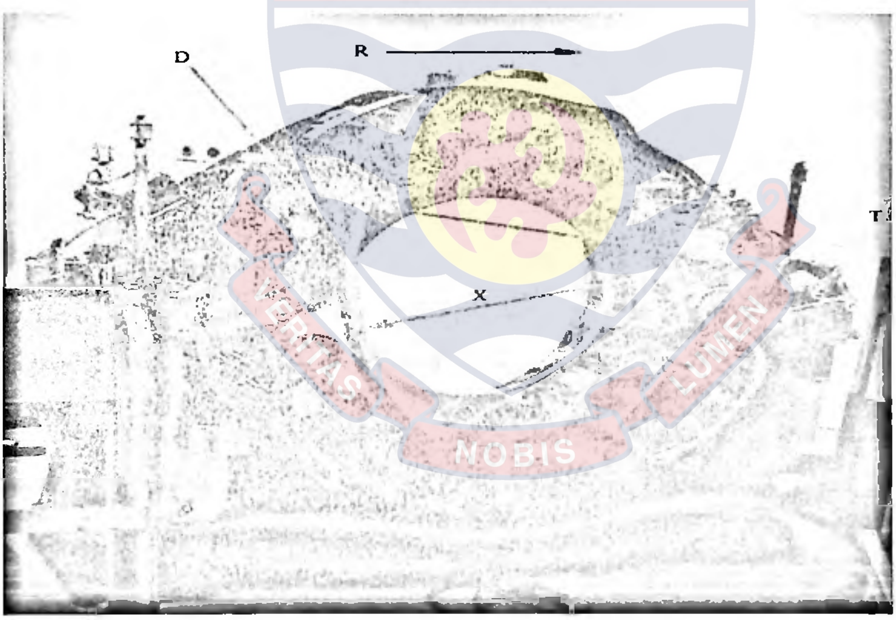

Figure 9: Opened Computed Tomography gantry

Source: (IAEA, 2014a)

The rotating gantry requires electrical power, hence brushes from stationary slip ring technology enables this to be successful. Additionally, projection profiles from the gantry to a computer are transmitted through wireless communication. The patient is positioned on the table of the examination either by head first, feet first, supine or prone. The positioning is entirely based on the type of examination (IAEA, 2014a).

X-ray tube and Generator

A rotating anode type X-ray tube with high voltage generator is used for producing bremsstrahlung X-ray beam for diagnosis. The X-ray beam produced is shaped to form slice or cone. There is a limitation on the tube rotation time, and the related resolution of CT scan due to intense centrifugal (g) force observed at short rotations times. Several tenths of gravitational forces are observed at rotation times in magnitude of 0.35 seconds (IAEA, 2014a).

Collimation and Filtration

The X-ray beam from a CT scanner is either a fan beam or cone beam shaped when the width along the y –axis (longitudinal) is small or big (multi-slice scanners) respectively. Flat and beam shaping ("Bow-tie") filters are mounted close to the entrance of the X-ray tube to fully intercept the whole beam. Radiation intensity gradient is created by the beam-shaping filter. The reason for the beam shaping filter is: to compensate (reduce) the active range of the information recorded by the CT detector; to reduce radiation dose to the edge (thinner than inner region) of the patient; to try normalising the hardening of the beam in aid of detector calibration. The beam-shaping filter material and shape is proprietary and unique (IAEA, 2014a) for different CT machines.

Detectors

About approximately 800-1000 detector elements are along the detector arc and about 1-320 detectors along the z-axis of the Cartesian plane. In the axial plane (x-y plane), the detectors are curved but rectangular along the z-axis (longitudinal). Ionisation chambers filled with Xenon were used as detectors till the year 2000. This was effective in achieving fewer ring artefacts but showed a deficiency of lower radiation measuring efficiency. At the moment, solid-state detectors are used improving upon the radiation measuring efficiency. These solid-state detectors function through scintillation by the photons interacting with the detector to produce light. The light is then changed to electrical signal using photodiodes. An anti-scatter grid may be employed to improve image quality and reduce patient dose (IAEA, 2014a). A typical detector module in a complete CT arc is shown in Figure 10.

Physical attributes for a good CT detector is: it should exhibit good detection efficiency; it must have fast response (and little afterglow) to radiation; it must have good accounting for the generated light (to ensure effective conversion of the produced light using the photodiodes). Additionally, small strips and septa of the anti-scatter grid are needed to increase the effective area of the detector and hence increase the detection of X-rays (IAEA, 2014a).

Resolution of reconstructed image relies on: the detector element size along the x-y plane (detector arc) and the z-axis and the separation of the proj-

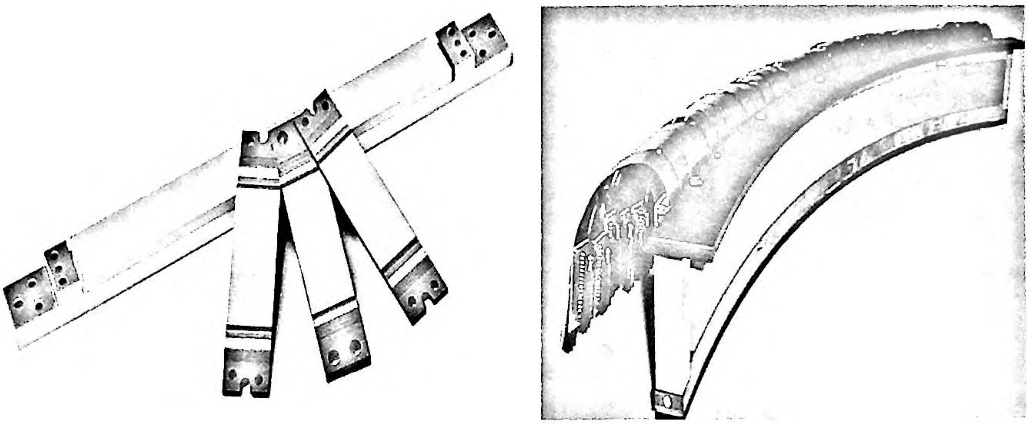

(a) (b)

Figure 10: (a) Detector modules for 4, 16, 64 and 320 slice and (b) the complete detector composed of many detector modules

Source: (IAEA, 2014a)

-ection at every angle. The beam size at the iso-center is the effective size of the detectors. Approximately, two times field of view (2*FOV) divided by spatial resolution (*d*) determines the minimum number of detector elements required to reconstruct image in a CT, that is (2*FOV)/d. Example, for spatial resolution of 1 mm within FOV of 400 mm of reconstructed image, about 800 detector elements are required. Quarter shift of CT detector and focal spot oscillating during gantry rotation resulting in quarter detector shift have improved spatial resolution in CT. The spatial resolution becomes twice as good when detector element is shifted by a distance that is a quarter of the size of the elements (IAEA, 2014a).

The coverage of multi-detector row scanners increased with advancing technology of increasing detector rows. This is illustrated in Figure 11. Multi-slice or multi-row scanners are identified by the maximum number of detector row (data channels) it acquires. However, not all the detector rows or data cha-

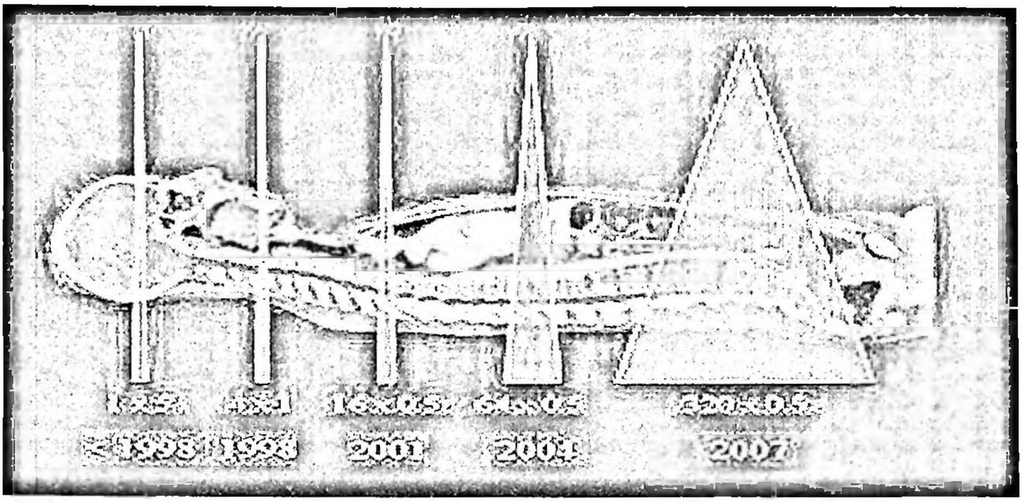

Figure 11: Detector row increase with technology advance

Source: (IAEA, 2014a)

-nnels are often used to acquire a tomographic section or slice. Example is a General Electric (GE) LightSpeed CT scanner with 16 x 1.25 mm detectors (four-slice scanner). This CT scanner can acquire 4 x 1.25 mm, 4 x 2.5 mm, 4 x 3.75 mm, or 4 x 5 mm slices. A multi-slice or multi-row scanner has enhanced thinner tomographic sections (slices), wide (long) scan volumes and fast acquisition (IAEA, 2014a).

Image Reconstruction

Reconstruction of CT images hinges on the techniques of simple and filtered back projection, iterative reconstruction and algebraic expressions. The measurements of transmitted X-ray through the patient at different angles by the detectors during CT scan form the bases for image reconstruction. A linear relationship is observed between the logarithm of normalised X-ray transmission ($\ln(I_o/I(d))$) and, the product of linear coefficient (μ_i) and change in distance (Δx) (IAEA, 2014a).

Figure 12 details the image formation procedures employed by CT scanners. (a) X-ray is transmitted through a patient from an angle. (b) One transmission profile is formed by back projection evenly distribution of measured signal over the area of scan. (c) From the same angle of the projection, transmitted X-ray profiles are measured from several numbers of angles and back projected. (d) The eventual interpretation of the measured X-ray profiles is blurred image. Studies have shown that simple back projection

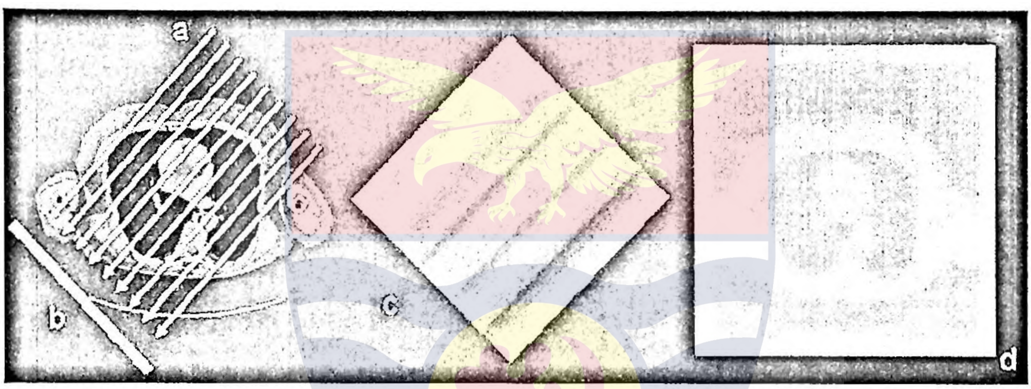

Figure 12: Image formation procedure

Source: (IAEA, 2014a)

of transmitted X-ray profiles is not enough to generate precise image reconstruction in CT. Therefore, the use of filtered back projection is suggested as the standard for CT image reconstruction. Alternative reconstruction techniques identified are algebraic or iterative reconstructions. However algebraic reconstruction is clinically not practical due to large matrices required in medical imaging, and inconsistencies observed in equations (caused by errors in noise and measurement) (IAEA, 2014a).

However, iterative (statistical) reconstructions are recently being used in commercial CT scanners although it has regularly been used in nuclear medicine. Iterative reconstruction is effective on removing streak artefacts; and uses minimal dose in image acquisition. The deficiencies of this technique are the presence of other artefacts, and misidentification of patterns (IAEA, 2014a).

Filtered back projection is currently the most used CT reconstruction technique. This technique functions using three interrelated domains, that is, object space (linear attenuation values), random space (projection values obtained at different angles) and Fourier space (derived from object space by engaging a 2D Fourier transformation) mathematically. The Fourier slice theorem states that the one dimensional (1D) Fourier transform of the projection profile yields an angulated line in (Cartesian) Fourier space at the angle of the projection. A 2D Radon transform translates the object space into radon space. The 2D Radon space is measured raw data of projections during a CT scan. Central slice theorem suggests that many 1D Fourier transforms of transmitted projections under many angles allow for the development of Fourier space of the object space (IAEA, 2014a).

There are four steps mathematically required for a successful filtered back projection. These are as follows: 1. Performance of Fourier transform on Radon space (many 1D Fourier transforms are required). 2. Application of a high-pass filter to each of the 1D Fourier transforms (this can be substituted with convolution of projection kernels in the random domain). 3. Then the application of an inverse Fourier transform to the high pass filtered Fourier transforms to achieve a Radon space with improved transmission profiles. 4.

Finally, the image of the object is achieved by back projection of the filtered transmission profiles (IAEA, 2014a).

The space available for images is usually shown on a regular grid. The definition for a 2D image space is f(x,y), where (x,y) are Cartesian coordinates in the space. Therefore, one 1D projection of the 2D image space with equal distance and along the X-rays direction produces one line in Radon space. The 1D projection is expressed as p(t,θ), where t is the distance of the transmitted X-ray from the iso-center and θ is the transmission angle as illustrated in Figure 13 (IAEA, 2014a).

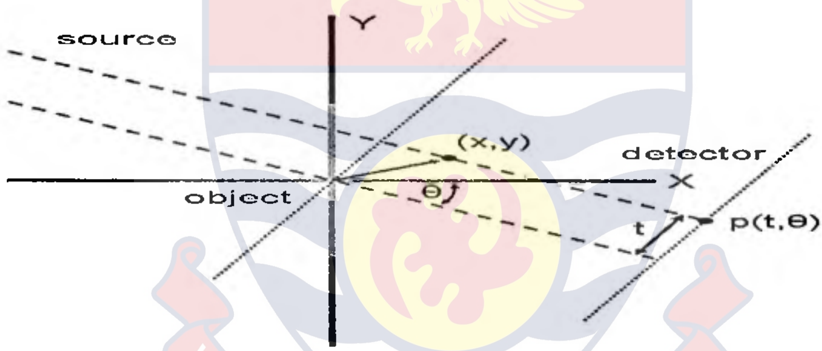

Figure 13: Cartesian coordinate for a 1Dimensional projection

Source: (IAEA, 2014a)

Fourier transform of parallel projection of image space with projection angle θ produces one (1) line in 2D Fourier space F(u,v) at the same angle, where u and v are spatial frequencies in x and y direction. For a projection angle θ = 0, the equivalent line in random space and the projection p(x,0) is explained as in Equation 5 where α is infinity.

$$p(x,0) = \int_{-\alpha}^{+\alpha} f(x,y)dy \qquad (5)$$

The 1D Fourier transform with respect to the x-ray plane of the projection p(x,0) at the projection angle θ = 0 is explained by Equation 6:

$$p(u) = \int_{-\alpha}^{+\alpha} p(x,0)e^{-i2\pi 2\pi}dx = \int_{-\alpha}^{+\alpha}\int_{-\alpha}^{+\alpha} f(x,y)e^{-i2\pi 2\pi}dxdy \qquad (6)$$

The 2D Fourier transform F(u,v) of the 2D image space f(x,y) at v = 0 is explained by Equation 7.

$$F(u,v)\big|_{v=0} = \int_{-\alpha}^{+\alpha}\int_{-\alpha}^{+\alpha} f(x,y)e^{-i2\pi 2\pi}dxdy\big|_{v-0} = \int_{-\alpha}^{+\alpha}\int_{-\alpha}^{+\alpha} f(x,y)e^{-i2\pi 2\pi}dxdy$$

(7)

Hence, it is obvious that the 1D Fourier transform with respect to the x-ray plane for the projection angle θ = 0 equals the 2D. Therefore, Fourier transform F(u,v) of the 2D image space f(x,y) at v = 0 is explained by Equation 8.

$$p(u) = F(u,v)\big|_{v=0} \qquad (8)$$

The conclusion can be applied for any projection angle θ. Theoretically, a reconstruction can be obtained by a generation of the 2D Fourier space F(u,v) by a lot of 1D Fourier transforms of the transmission profiles obtained at different transmission angles and then finally apply a 2D inverse Fourier transform of the 2D (IAEA, 2014a).

Filtered back projection also begins with 1D Fourier transforms of image space, thus generating the matching 2D Fourier space. Selection of the 2D Fourier space F(u,v) is conveniently in a polar grid, hence resulting in the transformation of the coordinates, that is $u = w\cos\theta, v = w\sin\theta$. Where 1D projection angle is θ, |ω| represents the ramp filter in the frequency domain, and α is infinity. Filtered back projection is explained by Equation 9.

$$f(x,y) = \int_0^{\pi} d\Theta \int_{-\alpha}^{+\alpha} P(\omega(\Theta)) \left| \omega \right| e^{i2\pi 2\pi} d\omega \qquad (9)$$

Ramachandran-Lakshminarayanan (Ram-Lak) filter or ramp filter in the filtered back projection, theoretically results in good reconstruction. The filter gives good spatial resolutions in the reconstructed images, and comparatively high image noise levels. Other filters are often used to reduce the noise level in the images reconstructed. Currently, CT scanners offer specific clinical improved purposed reconstruction filters (IAEA, 2014a).

Radiation Protection

Radiation protection involves the protection of people and the environment from the detrimental effects of ionizing radiation (IAEA, 2014b). People are exposed to ionising radiation from natural (existing radiation) and man-made sources (ICRP, 2007). The health effects associated with radiation exposure are deterministic (e.g. cataract, hair loss etc.) and stochastic effects (e.g. cancer and hereditary effect). Due to health effects associated with radiation exposure, it is necessary to provide acceptable level of protection for humans without unnecessarily limiting the benefits of radiation. Basically, the aim of radiation protection is to prevent the incidence of harmful deterministic effects and to reduce the probability of incidence of stochastic effects (ILO, 2018).

The level of radiation protection is grouped into occupational radiation protection, which is the protection of persons who are exposed to radiation by virtue of their work; medical (patient) radiation protection, which is the protection of patients being exposed to radiation for diagnosis or treatment purposes; and public radiation protection, which is the protection of persons who are members of the public and of the entire population (IAEA, 2014b).

Radiation exposure situations need a suitable level of radiation protection to be implemented on a graded approach. That means the level of radiation control implemented must be proportionate with the related risk or risks. Exposure to radiation is classified in terms of planned, emergency and existing exposure situation (IAEA, 2014b).

Planned radiation exposure situations occur during planned radiological activities. The ultimate goal during such situations is to have a good shielding design of the installation, equipment and procedures for operation. Persons likely to be exposed include these categories, that is, workers, patients and the public. Dose limits are used as a means of control for workers and the public. The same does not apply to patients since the ultimate consideration for doses is to ensure effective diagnosis and treatment (IAEA, 2014b).

Accidents, malicious act, or other unexpected events that require a response to minimise its repercussions give rise to emergency exposure situations. Radiation doses may be to the public and/or to workers, who may be relied on in responding to the emergency (IAEA, 2014b).

Existing radiation exposure situations are situations that were in existence before the introduction of man-made radiation or the need for radiation control. Exposure of individuals/population to natural background radiation and radioactive residual from a nuclear or radiological emergency (after elimination of emergency exposure situation) is a perfect example. The magnitude of doses and population are considered in controlling existing exposure situations. In all instances, social and economic factors have to be taken into consideration, in some instances, the existing exposure may not be opened to control (IAEA, 2014b).

Principles of Radiation Protection

A set of identified principles for radiation protection apply to known, emergency, and prevailing exposure situations. The principles are structured to consider radiation sources, individuals, as well as the application of the source related sources to control situations. The radiation source related principles are justification and optimisation of activity and would be applicable to all the exposure situations, which is planned, emergency and existing. The principle of dose limitation is person dependent and is applicable to only planned exposure situations (IAEA, 2014b).

The principle of justification: Any practice or activity changing the prevailing radiation exposure should present more benefit than harm. Thus the introduction of a new radiation source, the reduction of existing radiation exposure, or the reduction of the potential radiation risk should present benefits to persons or population to overweigh the detriments associated (IAEA, 2014b).

The principle of optimisation: this principle considers three areas of interest, which is the possibility of persons being exposed to radiation, the number of persons involved in an exposure, and the magnitude of the persons' doses. Financial and societal reasons should be well-thought-out in keeping the identified three areas as low as reasonably achievable (ALARA). Therefore, the level of radiation protection from all exposure situations should be the best considering the presenting situation, increasing the margin of benefit over harm. In order to control the unfair outcome of the application optimisation principle, there should be dose constraints and reference levels (IAEA, 2014b).

The principle of dose limitation: The overall radiation dose to any person from a controlled source in planned exposure situations should not surpass the applicable dose limits recommended by the ICRP. In applying dose limits, it will not be used for medical exposure of patients. The regulatory authority may determine the dose limits for occupational exposed workers and members of the public taking into consideration the international suggestions for known radiation exposure situations (IAEA, 2014b).

Occupational Radiation Protection

The regulatory body is responsible for providing the duties of employers regarding occupational exposure in known exposure situations. The established requirements for the protection of staff would be enforced by the regulatory body. The staff radiation exposure limits shown in Table 2 would be forced for compliance. Before the use of any new or modified practice, employers would provide evidence in areas of: Equipment design standards and structures regarding radiation and possible radiation exposure of staff in operational or emergency situations; Equipment design standards and structure of systems and monitoring programmes for staff in operational or accidental s-

-ituations (IAEA, 2014b).

Table 2: Radiation Dose Limits for Staff

Dose	Adults	Apprentice 16 to 18 Years Old
Effective Dose	20 mSv per Year (Averaged over five consecutive years)	6 mSv in a Year
Equivalent Dose to Lens of Eye	20 mSv per Year (Averaged over five consecutive years)	20 mSv in a Year
Equivalent Dose to Extremities (hands & feet) or Skin	500 mSv in a Year	150 mSv in a Year

Source: (IAEA, 2014b)

There would be regulatory controls, as appropriate, for: the staff radiation exposure monitoring, recording and control in known exposure situations; staff radiation monitoring programmes of registrants and licensees; service provision of personnel monitoring and equipment calibration services; the reviewing of periodic reports on staff exposures; the maintenance of staff exposure records and results of assessed doses; the confirmation of compliance with occupational exposure of authorized practices through inspection (IAEA, 2014b).

Workers engaged in activities that would expose them to planned radiation exposure situation, employer would ensure that: they are protected against work related radiation exposures; worker doses do not exceed the recommended radiation dose limits; optimisation is applied in the protection and safety of workers; decisions on protection and safety measures are documented and made available at all times; policies, procedures and organizational provisions for protection and safety includes controlling staff exposures; facilities, equipment and services would be provided to staff and will be commensurate with the associated risk; health surveillance programme for staff would be provided; monitoring and personal protective equipment would be provided considering its appropriate use, calibration, testing and maintenance; qualified persons are engaged, and training and retraining in protection and safety would be provided; conditions to promote safety culture are provided to staff (IAEA, 2014b).

Workers at all times should be involved in the optimisation processes for staff protection and safety. The optimisation process should consider dose constraints as well. Workers exposed to radiation but not work related would be classified under members of the public and would have the same level of protection. Administrative measures should be employed to inform workers of their responsibility to ensure protection of themselves and others against radiation exposure. Actions would be taken by the employer upon report of any non-safe practice from a worker (IAEA, 2014b).

Controlled area should be designated for: controlling exposures in a confined region; avoiding or controlling the probability and extent of exposures in known and emergency conditions. The controlled area should be delineated by physical or any appropriate means. A radiation warning symbol and instructions at access points shall be displayed in the controlled area.

Administrative controls, that is, physical barriers should be used to restrict access to controlled areas and these controls should be commensurate with the risk of the radioactive source. Personnel protective equipment, personnel and workplace monitoring should be provided. The boundaries of the controlled area should be reviewed based on monitoring. Persons in the controlled area, which is, occupationally exposed should be given enough information, instruction and training (IAEA, 2014b).

Supervised area is any area not already labelled as a controlled area. The area should be designated but specific protection measures are not necessary although staff exposures review is required. The radiation exposure at the supervised area will consider the nature, probability and extent of exposures. Appropriate means would be considered in the delineation of the area. After the delineation, approved signs at access points to the supervised area will be posted. Periodically, appraisal would be performed at the supervised area to ascertain protection and safety levels (IAEA, 2014b).

Engineering, administrative and personal protective equipment controls would be deployed in the above hierarchy for the protection of staff. Local rules and procedures with investigation levels would be written and made know to all staff or persons concerned. There would be proper supervision during work to ensure local rules are observed at all times. Such supervision should be done by an appointed radiation protection officer. Suitable and acceptable personal protective equipment (that is, protective clothing, respiratory mask, aprons, etc.) would be provided and used by staff during work. The workers would be trained on the appropriate use of the protective equipment and tasked to specific staff during work. This equipment will be stored, maintained and tested at appropriate time intervals. In using the protective equipment for specific tasks, other non-radiological risk and optimisation principles should be considered as well (IAEA, 2014b).

A work place monitoring programme shall be initiated, continued and kept under appraisal by a qualified expert or radiation protection officer. The workplace monitoring programme would be fashioned to account for assessment of radiological conditions in all areas including controlled and supervised areas, and advice revision of the areas if the need be. The workplace monitoring should be based on the type of practise, activity, the probability and extent of exposures in known and accidental situations. The findings of the workplace monitoring programme should be maintained and made available to staff (IAEA, 2014b).

Worker exposed to radiation would be monitored through individual monitoring by a recognised dosimetry service provider. Persons in the controlled area receiving significant amount of radiation would be individually monitored and if not possible, workplace monitoring would be used to assess the doses. All workers in the supervised area would have their doses assessed based on workplace monitoring (IAEA, 2014b).

Dose assessment records of staff would be maintained throughout and after the worker's working life. The dose records would be stored not less than 30 years after retirement of the worker. Dose records of workers would include: the type of work done by the staff; dose assessments and others requiring investigations; dose records at various places of employment; dose records during emergency interventions. Access to the dose records by the staff, regulatory body and the radiation protection officer will be granted. The dose records of staff would be made available to new employers when the staff moves to another radiation related job. Retention of staff records would be made appropriately by maintaining the confidentiality of records (IAEA, 2014b).

Health surveillance programme to assess the initial and continuing fitness of the worker to enable their intended task would be designed and initiated. If worker's task would expose them to uncontrolled radiation source, special health surveillance will be done. Enough information would be provided to staff on occupational health risk related to all the exposure situations , which is, planned, emergency and existing. Workers condition of service will be independent of their exposure to radiation. Special arrangements for benefits (e.g. salary, insurance, vacation, retirement benefits etc.) should not be used as a substitute for protection or safety measures. Alternate employment opportunities are made available to workers if for health surveillance or radiation over exposure reasons, the staff is unable to carry out their duties. Information on radiation risk to foetus and infants would be provided to female staff in the controlled, supervised or under taking and intervention. Persons below the age of 16 years would not be subject to radiation due to work. Persons below the age of 18 years would be allowed to enter a controlled area under supervision and only for the purposes of training or studies (IAEA, 2014b).

Radiation Dosimetry

Effective dose and equivalent dose in a tissue/organ are radiation dose quantities that have been suggested for use in radiation protection situations. It is also clear that the radiation exposure dose limits for staff are expressed in these quantities (that is, effective and equivalent dose). The effective and equivalent dose cannot be measured directly and hence the physical quantities that can be measured with a device are particle fluence (ψ), kerma (K) and the absorbed dose. Operational quantities were proposed by International Commission on Radiation Units and Measurement (ICRU) to practically relate measured (physical) and protection quantity for external radiation exposures (ICRU, 1985; ICRU, 1993). Directional H' (d,Ω) and ambient H^*(d), and personal Hp(d) dose equivalent are perfect examples of operational quantities applicable to area and personnel monitoring respectively (IAEA, 1999a). The three (3) quantities (that is, physical, operational and protection) are interrelated. In order to derive equivalent dose or effective dose, radiation-weighting factors are used as multipliers of absorbed dose. This is done to exhibit the harm of the absorbed dose delivered due to high linear energy transfer (LET) and not low LET. The weighting factors suggested for use are shown in Table 3. Personal, ambient and directional dose equivalent are derived by using radiation quality factors. The quality factors are dependent on a Q–LET relationship (IAEA, 1999b).

The mathematical definition for physical quantities, fluence (ψ), kerma (K) and absorbed dose (D) are given in Equations 10, 11 and 12 respectively.

$$fluence\ (\psi) = dR/da \qquad (10)$$

where dR is the energy of the radiation incident on a sphere of cross-sectional area da.

Table 3: Radiation Weighting Factors for Particles

Type and Energy Range	Radiation Weighting Factor (W_R)
Photon, all Energy	1
Electrons and Muons, all Energy	1
Neutrons, Energy:	
< 10 keV	5
10 keV to 100 keV	10
> 100 keV to 2 MeV	20
> 2 MeV to 20 MeV	10
> 20 MeV	5
Photons other than Recoil Protons, Energy > 2 MeV	5
Alpha Particles, Fission Fragments, Heavy Nuclei	20

Source: (IAEA, 1999a)

$$Kerma\ (K) = \frac{dE_{tr}}{dm} \qquad (11)$$

where dE_{tr} is the total of the initial kinetic energies of all charged ionizing particles liberated by uncharged ionizing particles in a material of mass dm.

$$absorbed\ dose, D = \frac{d\varepsilon}{dm} \qquad (12)$$

where $d\varepsilon$ is the mean energy imparted by ionizing radiation to matter in a volume element and dm is the mass of matter in the volume element (IAEA, 2014b).

The mathematical definition for protection quantities, equivalent (H_T)

and effective (E) dose are given in Equations 13 and 14 respectively.

$$equivalent\ dose, H_T = W_R . D_{T,R} \qquad (13)$$

where $D_{T,R}$ is the absorbed dose delivered by radiation type R averaged over a tissue or organ T and W_R is the radiation weighting factor for radiation type R.

$$effective\ dose, E = \sum_T W_T . H_T \qquad (14)$$

where H_T is the equivalent dose in tissue or organ T and W_T is the tissue weighting factor for tissue or organ T (IAEA, 2014b).

Operational quantities considered in CT dosimetry are computed tomography dose index (CTDI), weighted CTDI ($CTDI_w$), volume CTDI ($CTDI_{vol}$) and dose length product (DLP). The CTDI, $CTDI_w$, $CTDI_{vol}$ and DLP have been defined in Equations 15, 16, 17 and 18 respectively.

$$CTDI = \frac{1}{NT}\int_{-\alpha}^{+\alpha} D(z)dz \qquad (15)$$

where CTDI represents the mean absorbed radiation dose along the z-axis; D(z) is the dose outline along the z-axis; N is the number of tomographic sections acquired in a single axial scan; T is the width of the tomographic section along the z-axis acquired by data channel (s).

$$CTDI_w = \frac{1}{3}CTDI_{100,centre} + \frac{2}{3}CTDI_{100,edge} \qquad (16)$$

where $CTDI_w$ represents the average absorbed radiation dose over x and y directions; $CTDI_{100,centre}$ is the average dose at the centre measured by a 100 mm ionisation chamber; $CTDI_{100,edge}$ is the average dose at the peripherals (0, 90, 180 and 270 degrees) measured by a 100 mm ionisation chamber.

$$CTDI_{vol} = \frac{1}{pitch} x\ CTDI_w \qquad (17)$$

where $CTDI_{vol}$ represents the average absorbed radiation dose over x, y and z directions; pitch is the ratio of the table movement per rotation (I) to the nominal beam width (N, number of slices x T, slice thickness).

$$DLP\ (mGy - cm) = CTDI_{vol}(mGy)\ x\ scan\ lenght\ (cm) \qquad (18)$$

where DLP represents the total energy absorbed by a given scan protocol (AAPM, 2008).

Monte Carlo

Monte Carlo is used to emulate theoretically statistical process (such as the interaction of radiation particles with matter) and is mostly helpful for complicated problems out of the range of computational deterministic methods. The individual probabilistic events that comprise a process are simulated sequentially. The probability distributions governing these events are statistically sampled to describe the total phenomenon. Generally due to the large number of trials required to describe the process, simulations are done on a digital computer. Random selection of numbers is employed and this is similar to dice throwing in a gambling casino, hence the use of the name “Monte Carlo”. Radiation particle transport by Monte Carlo technique is predominantly accurate. It involves following every particle from the source of generation till it’s termination through absorption, escape, etc. Probability distributions are unsystematically sampled using transport information to predict the result at each step of its life (X-5MonteCarloTeam, 2008).

Monte Carlo Method and Deterministic Method

Monte Carlo and deterministic methods are particle transport methods that are not the same in their problem solving and outcome. Discrete ordinates method, a popular deterministic method evaluates particle transport equation for an average behaviour of the particle. On the contrary, Monte Carlo generates solutions by tracking individual particles and saving some (tallies) of their average performance. The average performance of particles of a physical system is then concluded (using the central limit theorem) from the behaviour of the simulated average particles. Apart from the significant different approaches used by Monte Carlo and deterministic methods in solving problems, the constituents of solutions are different. The outcome of Monte Carlo simulations are user defined (that is, specific tally requested) whilst deterministic methods usually give fairly complete outcome (e.g. flux) (X-5MonteCarloTeam, 2008).

A transport equation need not be written to solve a problem by Monte Carlo. Nonetheless, one can derive an equation that describes the probability density of particles in phase space; this equation turns out to be the same as the integral transport equation. Without developing the integral transport equation, it is useful to enquire why the discrete ordinates method is connected with the integral-differential equation and Monte Carlo with the integral equation. The discrete ordinates method envisages the phase space to be divided into a lot of small boxes for particle movement. In the limit when the boxes get increasingly smaller, differential amount of time is required for differential distance in space with particles moving from box to box. In further limit, integral-differential transport equation is approached with derivatives in time and space. Contrary, collision of particles in Monte Carlo transports separated in space and time do not inherit these parameters (that is, space and time). The integral equation for Monte Carlo transport does not have time or space derivatives (X-5MonteCarloTeam, 2008).

Monte Carlo is an appropriate tool for solving complex three-dimensional, time-dependent problems. This is because phase space boxes and averaging calculations in space, time and energy are not required in Monte Carlo methods. This is especially important in allowing detailed representation of all aspects of physical data (X-5MonteCarloTeam, 2008).

Monte Carlo N-Particle Code

Monte Carlo N-Particle (MCNP) is generalised purposed, geometry, time and energy Monte Carlo transport code for neutron, photon, electrons and ions. MCNP can be applied as neutron, photon or electron only, or as combined modes. The neutron, photon, electron, light and heavy ions energy regimes of 10 - 11 MeV to 20 MeV for all isotopes and up to 150 MeV for some isotopes; 1 keV - 100 GeV; 1 KeV - 1 GeV; from 1 MeV/nucleon; from 3 MeV/nucleon respectively are used in MCNP. Light ions from MCNP require an input file to be created by the user for simulation by the code. This input file contains information to specifically solve the problem. Information such as: geometry definition of the problem; explanation of materials used in the geometry and appropriate cross-section assessments; location and the type of source; definitions of desired outcome or tallies; and application of variance reduction technique to increase efficiency (X-5MonteCarloTeam, 2008).

Features of MCNP

MCNP has specific features that enable it to effectively track particles.

These features are nuclear data, tallies of simulation output, error estimation, and variance reduction.

Nuclear Data and Reactions

Nuclear and atomic information libraries with continuous energy are used by MCNP. A system for evaluated nuclear information, initiatives for innovative computational technology, library for evaluated nuclear and photon information, Livermore's initiation library compilations, nuclear physics team 16 group at Los Alamos evaluations are the primary nuclear data. Evaluated information is processed into an appropriate format by codes such as NJOY. Nuclear data libraries processed, retain data from the initial evaluation as possible to generate the evaluators idea (X-5MonteCarloTeam, 2008).

Source Specification

The generalised user input by MCNP allows the user to define any source scenario without having to modify the source code. Source variables (that is, source cells or surface, energy, time, position and direction of propagation) have self-reliable probability distributions. The geometry of the source may be defined to address a specific task. There is also the option to modify the source code to define a source variable being dependent on other source variables. The user can also alter all input functions or distributions (X-5MonteCarloTeam, 2008).

Tallies and Output

Tallies of current, energy deposition and particle flux can be requested by the user. The tallies are standardised to per emitted source particle excluding some situations with criticality sources. Surfaces (that is, segments and total) are the available modes in which current can be tallied to solve a problem. Electrons and positrons are the tallied modes for charges. Fluxes across any set of surfaces (that is, segments and total) and in cells (that is, segment and total) are also available. Similarly, the fluxes at selected detectors (that is, point or ring) are standardised tallies, so is also radiography detector tallies. The fluxes of mesh superimposed over geometry of a problem can also be tallied. Energy deposition in a user defined cell can also be tallied. A pulse height tally defines the energy dissemination of pulses created in a detector by radiation. Particles may also be specifically defined to be tallied separately when they interact with specified surfaces or enter an identified cell. All tally results, except for mesh tallies, can be displayed graphically, either while the code is running or in a separate post processing mode (X-5MonteCarloTeam, 2008).

Estimation of Monte Carlo Errors

MCNP tallies are standardised to per beginning particle and are outputted with a second number R, which represents the estimated relative error. The relative error is one projected standard deviation of the mean S_x divided by the projected mean x. For an accurate tally, R is equivalent to $1/\sqrt{N}$ where N is the number of histories. The projected relative error gives indication of how accurate an outcome is, and hence is a confidence level indicator. The Central Limit Theorem suggests that as N approaches infinity there is a 68 % probability that the expected result will be in the range of x(1 ± R) and a 95 % probability in the range of x (1 ± 2R). These confidence statements are a reflection of how accurate the Monte Carlo simulation is but not the true physical value (X-5MonteCarloTeam, 2008).

Variance Reduction

For an MCNP input file run, the computer time (T) used is comparative to N. Therefore $R = C/\sqrt{T}$, where C is a positive constant value. When T is increased and/or C is decreased, the relative error can be reduced. The reduction of T is highly dependent on the specifications of the computer used for the simulation. For example, if it has taken 1 hour to obtain R = 0.20, then 100 hours will be required to obtain R = 0.02. MCNP has been engineered to variance reduction methods to reduce C. Variance is the square of the standard deviation. The constant C depends on the tally choice and/or the sampling choices (X-5MonteCarloTeam, 2008).

Photon Interaction Process

When photon interacts with matter, pair production, Compton scattering or Raleigh interaction and photo electric effect may occur depending on the energy of the photon.

Pair Production in the Nuclei Field

Pair productions occur only when a 1.022 MeV photon or in excess interacts with matter. Because of the high energy of photons required, this type of process does not occur in diagnostic radiology. Photon interacts with the nucleus such that the photon energy is converted to matter. The matter generated is electron and position pair particles. The mass of the pair particles is the same and equivalent to rest mass energy of 0.511 MeV. The bremsstrahlung interaction of the pair particles in the nucleus also results in more photons being generated. This process is more likely to occur in matter with high atomic number than a low one, that is, pair production is equivalent to atomic number square (Z^2) (Sprawls, 2018).

Compton Interaction (Incoherent Scattering)

In Compton interaction, the photon interacts with electrons in the shell of an atom and loses part of its energy and produces a scatter photon with reduced energy. The recoil photon leaves the interaction site in a different direction. Due to the change in direction of the recoil photon to that of the incident photon, the process is called scattering. The patient's examination part is the main source of scatter radiation in X-ray diagnosis. The scattered radiation may continue to reach the image receptor to reduce the image quality or may be the main source of radiation exposure to personnel (Sprawls, 2018).

Photon Electric Interaction

In this process of interaction, the travelling photon transfers all of its energy to an electron in the interacting matter. The electron is excited and ejected from its positon due to the energy absorbed, and travels a distance in the interacting matter depositing the gained excess energy. The photon is eventually deposited in the matter not too far from the interacting site. This type of interaction is very common for low energy photon interactions. The transfer of energy has been observed to be a two-step process, that is, photon to electron and electron to matter. This interaction occurs with electrons firmly bounded to an atom, that is electron with relatively high binding energy (Sprawls, 2018).

Photoelectric process is premised on the situation that the binding energy of an electron is less than the incident photon energy. This is because high photon energy is required to overcome the binding energy of the electron and the remainder is passed on to the electron as kinetic energy that is eventually deposited in matter. The interaction is typical with an electron in the K or L shell creating a vacancy. Therefore, characteristic X-ray is produced when an electron losses energy to fill the vacancy (Sprawls, 2018).

Rayleigh Interaction (Coherent Scattering)

This type of radiation interaction is sometimes called coherent, Thompson, classical, and elastic. It generally involves scattering (deflection of the photon) without any energy loss to the interacting matter. This type of radiation interaction is not important in medical diagnostic procedures but very common at low photon energies. When a low energy photon interacts with matter (optically thick shield), both Compton and Rayleigh scattering will occur but the proportions of each will be a function of the incident photon energy (Sprawls, 2018).

Tracking Photons using Monte Carlo Simulation

The initial photon parameters are put on STACK and photon transport cut-off has been identified. STACK is an arrangement that contains particle existing characteristics for transport and absorption. It can be ignored since it does not contribute to tally accumulation. The first characteristic used is the transport cut-off to determine if the energy of the particle is sufficient to be transported or terminated. Termination occurs when the energy of the particle is below the transport cut-off and hence ceasing particle history. When the STACK is empty, another particle history is commenced. When the energy of the particle is above the transport cut-off, the distance to the next impact is estimated. The photon then moves to the next point of interaction. If the photon leaves the volume by virtue of its travel, then it is discarded. If it is in the same volume, then branching distribution is used to estimate the next interaction. The existing particles are given their energies, direction and other characteristics required from the necessary distribution. The existing particles are put on STACK with the low energy particle on top. This process is repeated again until all the particles are cut-off or SATCK emptied (Bielajew, 2018).

SpekCalc Software

SpekCalc (Poludniowski, Landry, DeBlois, Evans, & Verhaegen, 2009) is an executable programme for estimating X-ray emission spectra of diagnostic and high voltage radiotherapy X-ray tubes. An X-ray is produced when an electron is accelerated onto a focal spot on an anode (metal). The electrons penetrate the metal and interact with nuclei of the metal generating bremsstrahlung or characteristic X-ray emissions. X-ray spectrum is formed highly based on the X-ray energy emissions from a target anode. The theory behind SpekCalc combines the ideas of semi-empirical models and Monte Carlo simulation approaches. The likelihood of an electron interacting deeply in a target and its energy at that depth has been pre-estimated using BEAMnrc Monte Carlo tool (Poludniowski & Evan, 2007a). The bremsstrahlung cross-section and self-filtration has also been pre-analysed using semi-empirical approaches. Predictions from SpekCalc model have exhibited strong agreement with measured data (Poludniowski, 2007b). This model is applicable to tungsten and tungsten-rhenium alloys but there are discrepancies in the spectrum as the rhenium portion increases. SpekCalc computationally spends less time in its predictions (each calculation spends some seconds). The size of the program and data is small, that is, six megabytes. The user can easily and quickly obtain useful information as half value layers (HVLs) (Poludniowski, Landry, DeBlois, Evans, & Verhaegen, 2009).

There are other computer programmes generating diagnostic spectrums but they are empirical or semi-empirical based , that is, spectrum processor by Institute of Physics and Engineering in Medicine's Report 78 (IPEM78) (Cranley, Gilmore, Fogarty, & Deponds, 1997). The unique nature of SpekCalc is its ability to predict spectrums for orthovoltage X-ray beams (Poludniowski, Landry, DeBlois, Evans, & Verhaegen, 2009).

SimpleGeo Modelling Tool

The SimpleGeo 3D modelling tool for solid objects uses hierarchical constructive solid geometry (CSG). CSG model has proven to be very effective over computer aided design (CAD) model for a good computational run time during radiation transport calculation.

Computer aided design

CAD programmes are used heavily across the scientific, engineering and other research communities. Boundary faces and patches of planer faces are used to represent solid and curved surfaces respectively if the later does not exist in CAD. Eventually, an object would be visualized but losing its original identity. An example is the use of boundary surfaces of polygons for a sphere. The loss of identity of the object is negligible depending upon the applications. Arbitrary face patches is more flexible in the construction process rather than solid face patches (Theis, Buchegger, Forkel-Wirth, Roesler, & Vincke, 2006).

The use of arbitrary or solid face patches to represent objects is very complicated when geometries of the object are to be applied in radiation transport situations. Particle tracking through geometries of objects is done by all Monte Carlo transport packages, therefore appropriate tracking algorithm is important. A test of a point source in sphere would result in one in a polyhedron and this is the deficiency of CAD systems. Computations for such a test would be complicated and trivial since the analytical formula may be readily available. This indicates that using CAD models for radiation transport calculations will have problems due to the computational run time (Theis, Buchegger, Forkel-Wirth, Roesler, & Vincke, 2006).

Hierarchical constructive solid geometry

Hierarchical CSG is a computational modeling structure used to generate 3D solid objects through a tree-graph. The tree-graph has tentacles that are formed of geometric primitives with Boolean and affine operation nodes. CSG uses analytic models and hence makes it more suitable for developing geometries for radiation particle transport. The problems of radiation transport identified in CAD models are not present in CSG. Typical operation of CSG includes: instantiation of basic primitives; development of complex models from primitives in a graded approach; Boolean operations application (union, difference, intersection); employment of affine operations (translation, rotation, scaling) (Theis, Buchegger, Forkel-Wirth, Roesler, & Vincke, 2006).

Method employed by CSG model is premised on image and object space approaches. Image space solutions include scanline, ray tracing, and various z-buffer algorithms. Object space method is preferred for complex geometries. Boundary representations are used to represent analytic models using object space approach. Discrete set of points defined on a surface is used to represent the boundary representation concept. Therefore, connecting the vertices generates a mesh of polygons to represent the solid or object (Theis, Buchegger, Forkel-Wirth, Roesler, & Vincke, 2006).

Computational Phantoms

Radiation dosimetry to human is assessed by detectors on the body surface of the exposed individual. This dosimetry gives an indication of the effective dose to the person but does not show individual organ doses in the human body. To be able to appropriately estimate the tissue/organs doses (appropriate for organ cancer risk estimation), computational or physical human phantoms have been developed. The development started with a simple homogenous water phantom and now anthropomorphic human phantoms about 60 years ago.

The edge to improve on the modelling of human anatomy has had a significant impact on computational phantoms development. The chronology of the development of phantoms for radiation transport studies started with 30 cm slap phantom, then homogeneous elliptical cylinders and with inhomogeneous parts embedded to emulate lungs, then a homogenous and then lastly heterogeneous human phantoms (MIRD5) (Cassola, de Melo Lima, Kramer, & Khoury, 2010).

The organs in the heterogeneous phantoms were modelled using mathematical equations of representative body geometries that is, ellipsoids, truncated cones etc. Therefore, complicated body organs e.g. gastro-intestinal tract could not be modelled but human body size could easily be changed if required. This resulted in the human anatomy phantoms not being accurate but useful for indicative absorbed or equivalent dose estimation for both internal and external radiation exposures (Cassola, de Melo Lima, Kramer, & Khoury, 2010).

Technology advance in computer and image processing aided the will to develop human look-alike phantoms for dosimetry. Voxel phantoms gave the actualisation of the idea of developing an accurate human phantom. The voxel phantoms were developed from images of human body parts obtained from CT, nuclear magnetic response and colour photos. Voxel phantoms gave good representation of humans than mathematical phantoms (Cassola, de Melo Lima, Kramer, & Khoury, 2010).

A lot of voxel phantoms of representative male, female and children have been developed e.g. BABY and CHILD phantoms, VIP-Man phantom, NORMAN and NAOMI phantoms, MAX, FAX, MAX06 and FAX06 phantoms etc. (Cassola, de Melo Lima, Kramer, & Khoury, 2010). Although voxel phantoms are accurate compared with mathematical ones, there are still limitations like: difficulty in organ segmenting due to poor resolution e.g. walls/twists of colon and small intestine; difficulty in segmenting boundaries of organs/tissues due to poor image contrast; difficulty in voxelising changing organ volumes. Applications of non-uniform rational B-spline (NUBS) and polygon mesh addressed the limitations of voxel. Major contribution to the development of computational human phantom was the use of mesh-based concept by G Xu at Rensselaer Polytechnic Institute (RPI) in Troy, USA (Cassola, de Melo Lima, Kramer, & Khoury, 2010).

Male and Female Mesh Computational Phantom

Female Adult meSH (FASH) and Male Adult meSH (MASH) phantoms using polygon mesh concept have been developed with the guidance of ICRP publication 89 (ICRP, 2002). Digital images of human body parts were acquired to be used in the development of the phantoms. The phantoms were developed to address observed limitations in existing current computational phantom (that is, FAX06 and MAX06) to improve radiation transport dosimetry. The use of polygon mesh surfaces makes it easy to model fat distribution and hence the ability to change weight of phantoms. Due to the supine positions of images (during scanning) used in computational phantoms, the positions of liver, lungs, small intestine, stomach, uterus, colon, urinary bladder, ovaries, prostate, abdominal adipose tissue and muscle volume overlying internal organs were abnormal for standing individuals. The channel from the colon showed discontinuity, and the linkage of the stomach and small intestine was left undefined. The skeleton, that is, the cervical vertebra did not reflect the reality. Then eventually, the body shapes of the existing phantoms were bigger than usual and the face, ears, eyes, nose and lips were not present. The observed limitations were all addressed for standing posture phantoms to reflect the reality in terms of organs and tissue positions for male and female as shown in figure 14 (Cassola, de Melo Lima, Kramer, & Khoury, 2010).

FASH and MASH phantoms are the reference models for further improvement in the already existing computational phantoms by other authors (Zankl, Eckerman, & Bolch, 2007; Zankl & Wittmann, 2001; Zhang J. , Na, Caracappa, & Xu, 2009; Zhang, Na, & Xu, 2008a; Zhang, Na, & Xu, 2008b; Kramer, Khoury, Vieira, & Lima, 2006; Sato, et al., 2007). The two modelled phantoms will be additionally improved to alternate weight and height in order to aid patient specific dosimetry (Cassola, de Melo Lima, Kramer, & Khoury, 2010).

Chapter Summary

CT for clinical usage was introduced in 1971 and the technology has transformed from axial scanning to currently all-purpose 3D imaging modality. The arrangement of the detectors and x-ray source has informed the different generations of CT's from first, second, third and currently fourth generation. The CT machine requires gantry, table, X-ray tube, generator, collimator, filtration and detectors to function. In the use of the CT, a set of id-

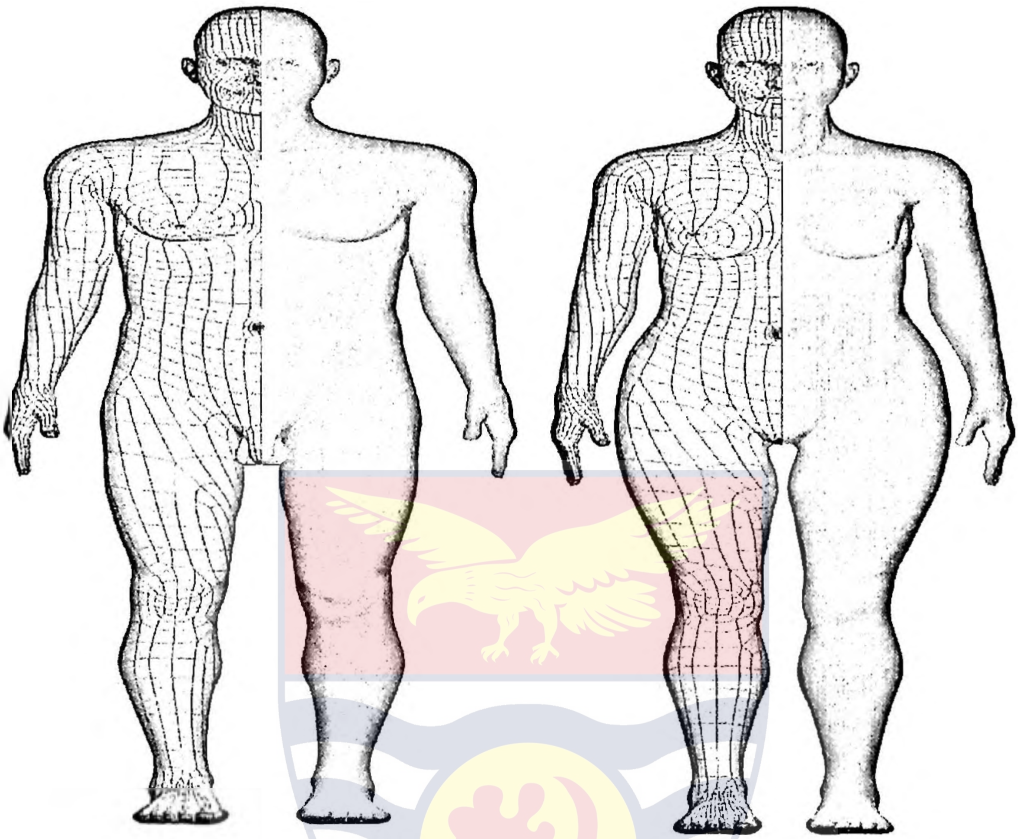

(a) MASH (b) FASH

Figure 14: (a) Male adult mesh and (b) female adult mesh phantoms

Source: (Cassola, de Melo Lima, Kramer, & Khoury, 2010)

-entified principles for radiation protection apply to known, emergency, and prevailing exposure situations. In staff protection through dosimetry, effective dose and equivalent dose in a tissue/organ are the radiation dose quantities.

Monte Carlo is used to predict theoretically statistical process for complicated problems out of the range of computational deterministic methods. SimpleGeo a computational 3D modelling tool uses hierarchical CSG to generate 3D solid objects through a tree-graph. Voxel phantoms developed from actual images of human body parts give the actualisation of the idea of developing an accurate human phantom. Voxel phantoms give good representation of humans than mathematical phantoms.

CHAPTER THREE

METHODOLOGY

Introduction

This chapter discusses the materials, equipment and tools that were utilised in the study. The approach or methods used in achieving the study objectives have been discussed as well.

Materials

A tape measure was used to measure the dimension of the CT rooms, viewing window, entrance doors and CT gantry position in the room. The schematic drawing of the CT machines were downloaded from the internet to aid with the modelling of the CT machines in terms of gantry dimensions, aperture (the opening in gantry) diameter, fan beam angle, focus-isocenter distance, focus-detector distance, movable table dimensions etc. (ITN, 2012). Details of CT machines used for the study are given in Table 4.

A Barracuda quality control kit (Serial Number: BC1-13050013) consisting of a CT dose profiler (Serial Number: DP2-13040061) connected to an Ocean Software (RTIElectronic, 2018) installed on a laptop was used for CTDI measurements on all the identified CT scanners. Schematic diagram with accurate dimensions of a TLD was used for the modelling of personnel monitoring dosimeters.

A 3D solid object modelling tool SimpleGeo developed by Theis *et al.* (Theis, Buchegger, Forkel-Wirth, Roesler, & Vincke, 2006) was used to model the geometry of all the objects of interest for the studies, that is the CT

Table 4: Details of Computed Tomography Machines used for the Study

Facility	Korle-bu Teaching Hospital (Accra)	Sweden Ghana Medical Centre (Accra)	Karlsruhe Hospital (Germany)	FOCOS Orthopaedic Hospital (Accra)
Manufacturer	Toshiba Acquilion One	Siemens Somaton Emotion	GE Discovery PET-CT 710	Philip Brilliance
Slices	640	16	128	16
Model	TSX-301A	10165880	Performix 2	1731
Serial No.	4CA1292037	40310	164630GI6	6821

room, CT gantry and table, lead apron, thyroid shield, protective goggles etc. Voxel2MCNP, a framework for modelling, simulation and evaluation of radiation transport scenarios for Monte Carlo codes developed by Karlsruhe Institute of Technology, Germany (Poelz, et al., 2013) was used to spatially put together all the different models required in a scenario on one platform.

Standing and supine female and male computational mesh phantoms MASH and FASH developed by Federal University of Pernambuco, Brazil were (Cassola, de Melo Lima, Kramer, & Khoury, 2010) used to represent patient and staff for the investigative studies. The two phantoms have body heights, body weights, as well as organ and tissue masses in agreement with data recommended by the ICRP 89 (ICRP, 2002). FASH and MASH have a total mass (60097 g and 72783.4 g respectively) and height (162.5 cm and 175.6 cm respectively). SpekCalc, a radiation spectrum generator developed by Poludniowski et al. (Poludniowski, Landry, DeBlois, Evans, & Verhaegen, 2009) was used to generate X-ray spectra of required filtration and energy. MCNP6, a Monte Carlo radiation transport code developed by Los Alamos National Laboratory (LANL, 2014) was used to track photons emitted from the CT fluoroscopy scanner. The overall results were tabulated for comparison using Microsoft Excel 2010 spread sheet.

GNUPlot is a command-line controlled graphing programme. It can be used to draw 2D or 3D graphs or plots of lines, points, boxes, contours, vector fields etc. (Williams & Kelley, 2014). This programme was used to draw radiation dose contours in a CT fluoroscopy room for dose distribution studies.

Method

The method used to achieve the objective of this study is discussed below.

CTDI Measurement

A cylindrical CT body phantom with dimensions of 15 and 32 cm for height and diameter respectively was used to represent the human body. The CT body phantom has five (5) holes of diameter 1.38 cm each that is 0.7 cm from the surface positioned at 0, 90, 180, 270 degrees and centre of the phantom. The phantom was put on the CT couch and positioned with its centre at the iso-centre of the CT scanner. The CT Dose profiler with sensitive measuring length of 100 mm was then inserted at the centre hole of the using a tape measure. Details of dimensions of operator viewing window, CT room door, CT gantry position in the room were collected as well. This procedure was repeated for all the identified rooms of the CT scanner at the different facilities. The CT scanner specifications collected physically and also from schematic diagrams downloaded from the internet (ITN, 2012) is detailed in Table 5.

Table 5: Specifications of Computed Tomography Scanners considered for the Study

Specification	Toshiba Aquilion One	Siemens Somaton Emotion	GE Discovery PET/CT 710	Philip Brilliance
Aperture (cm)	72	70	70	70
Focus-Isocentre Distance (mm)	600	535	541	570
Focus- Detector Distance (mm)	1072	940	949	1040
X-ray Fan Beam Angle (degree)	49.2	55.8	56	57
Bowtie-filter Thickness (mm)	Unknown	Unknown	Unknown	Unknown
Collimation (mm)	40	10	20	24

phantom with all the remaining four holes blocked as shown in Figure 15. CT

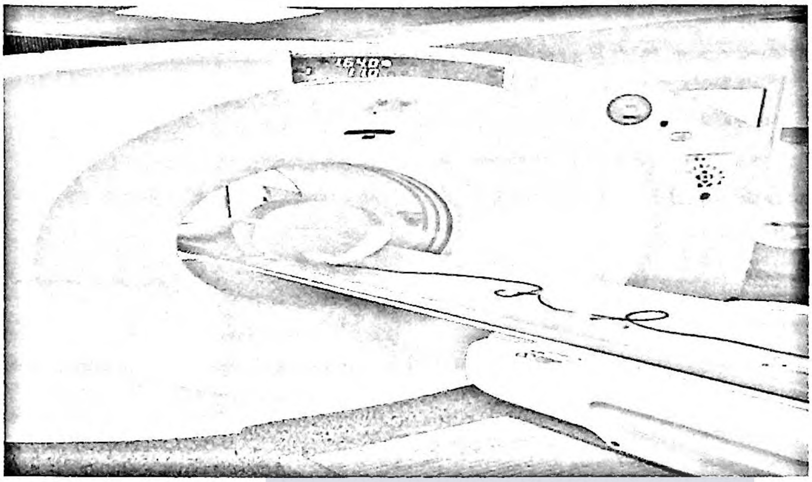

Figure 15: Computed Tomography Dose Iindex measurement setup

parameters of tube voltage 120 and 130 (Siemens Somaton Emotions only) kVp; current of 100 mA; collimation of 40 mm (Toshiba Aquilion 640), 10 mm (Siemens Somaton Emotion), 20 mm (GE Discovery PET/CT 710), 24 mm (Philip Brilliance); and tube rotation time of 1 s (full 360 degree tube voltage rotation) was used to scan the setup helically or spirally to estimate CTDI at the $CTDI_c$. The measured $CTDI_c$ was multiplied by K-factor (chosen based on tube voltage, phantom type and CT scanner name) (RTIElectronics, 2012) to estimate $CTDI_w$ as given in equation 19.

$$CTDI_w = CTDI_c \, x \, k - factor \qquad (19)$$

The same CT scanner parameters and setup but with ionisation chamber in air with the perspex body phantom as holder were also used to estimate CTDI in air ($CTDI_{100,\, air}$) for all the four identified CT scanners (RTIElectronics, 2012).

CT Room and Gantry Data Collection

The CT room length, breath, height and wall thickness were measured

Table 5 Continued				
Gantry Dimension (H x W x L), cm	203 x 243 x 107	178 x 79 x 232	194 x 205 x 104	203 x 239 x 94
Couch Top Length and Width (cm)	219 x 47	218 x 43	239 x 42	243 x 41

H: height; W: width; L: length

Modelling

The collected information on the CT room dimensions (that is, room length, breath and height) and details of doors, operator viewing window positions shown in Table 6 were modelled using 3D solid modelling software SimpleGeo.

Table 6: Computed Tomography Room Structural Information

Specification	Toshiba Aquilion One	Siemens Somaton Emotion	GE Discovery PET/CT 710	Philip Brilliance
Room Size (Length x Breath)- m	5.06 x 6.67	6.20 x 5.92	5.25 x 16.28	5.48 x 5.13
Wall Thickness (cm)	30	35	45	35
Lead Equivalent in Door (mm Pb)	3.0	3.0	3.0	3.0
Viewing Window Lead Equivalence (mm Pb)	2.5	2.0	2.5	2.5

The details of the CT specifications already outlined in Table 5 were followed to model all the four CT scanners using SimpleGeo as illustrated in Figure 16.

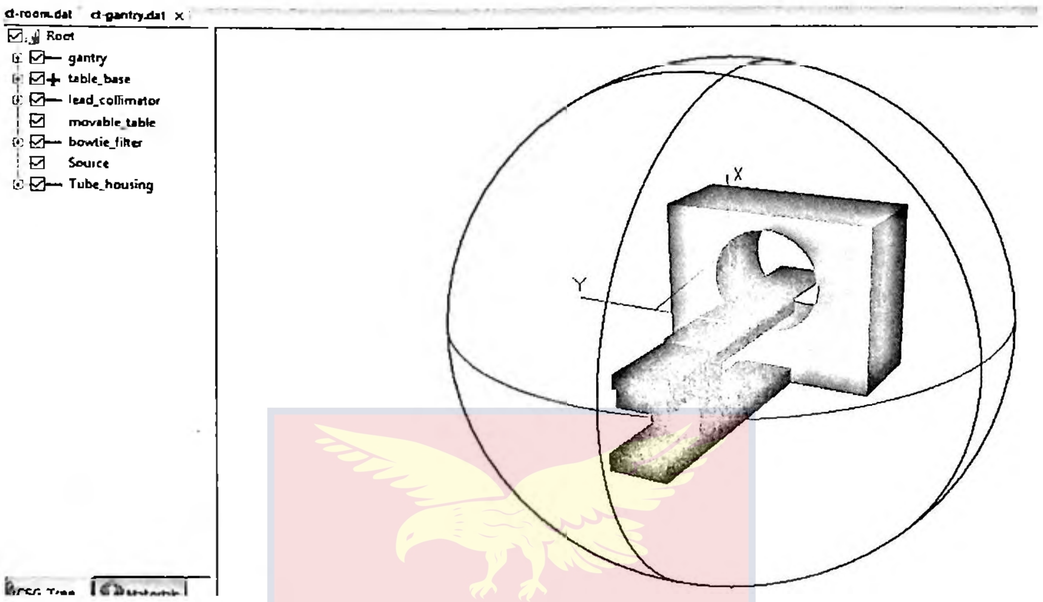

Figure 16: SimpleGeo being used to model Computed Tomography scanner

A bowtie filter was used to compensate for varying body thickness across a tomographic section for improved image and patient dose optimisation. The shape of bowtie filter is complicated (Toth, Cesmeli, Ikhlef, & Horiuchi, 2005) and the thickness was not provided by manufactures due to proprietary rights. Therefore, the shape was assumed to be a parallelepiped shape with an elliptical cut off and made of aluminium (Gu, Bednarz, Caracappa, & Xu, 2009; Figueira, et al., 2013). The elliptical shape was varied (trial-and-error) to change the filter thickness during the CT verification stage.

Protective equipment like goggles (0.75 mm lead equivalence), thyroid shield (0.35 mm lead equivalence) and wrap around lead apron (front: 0.35 mm lead equivalence and back: 0.25 mm lead equivalence) were modelled using SimpleGeo as illustrated in Figure 17.

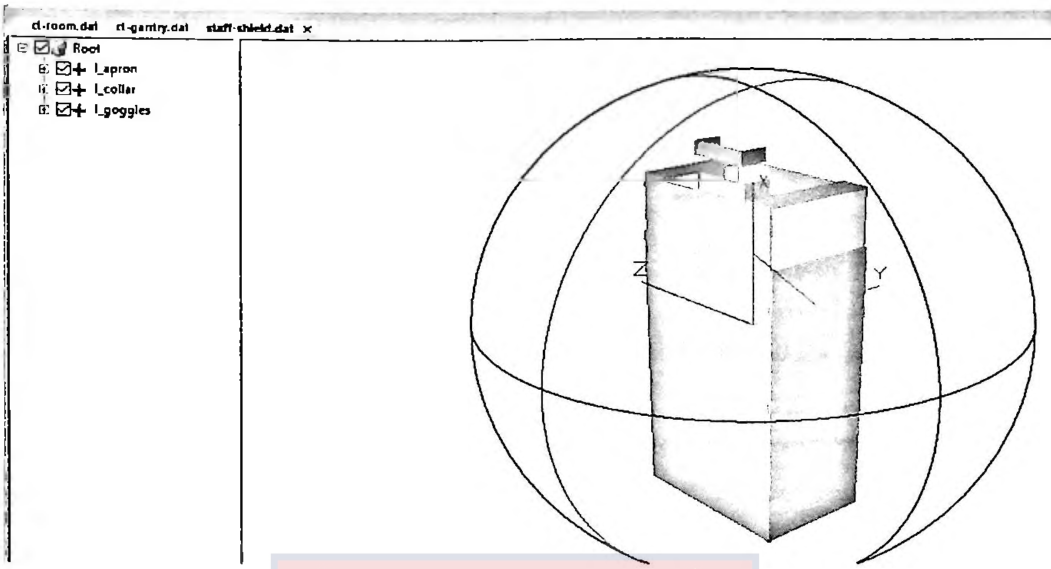

Figure 17: SimpleGeo being used to model staff protective equipment

Lithium Fluoride (LiF) thermoluminescence dosimeter with shape of right circular cone and dimension (height- 0.03 cm, radius – 0.225 cm) in a thin film of the same shape and dimension (height - 0.089 cm, radius – 0.225 cm) were modelled for staff effective dose estimation. A lead drape, lead patient cover and protective face mask (visor) were also modelled with dimension of 0.5 mm lead equivalence each for investigative studies. Perspex body phantom of a cylindrical shape with dimensions of 32 cm diameter, 15 cm height and 1.38 cm diameter of hole in the centre was modelled for the CT verification studies. Three concentric cylinders of radius 0.335, 0.51 and 0.681 cm representing first, second and third cylinders respectively were modelled. The inner part of first cylinder was air-filled (active volume), the wall of the chamber (section between first and second cylinder) was modelled as air equivalent plastic (C-552), and the build-up cup (section between second and third cylinder) was modelled as polyacetal plastic. The chamber had an active length of 10 cm (Gu, Bednarz, Caracappa, & Xu, 2009).

The fan shape of the beam was modelled using lead collimators (Gu, Bednarz, Xu, & Jiang, 2008) opened (along z-axis) positioned (along x-axis) at distance estimated from the CT's collimation and fan angle respectively , that is, the focus to iso-centre distances, the fan angle and the collimation at the iso-centre of each CT scanner is required. Point sources modelled at 36 positions (10 degrees apart from each other) in the gantry were used to track the axial or helical rotational movement of the X-ray tube for one complete rotation (360 degrees). At each position (angle), the source was defined by the point source, collimators and bowtie-filter coordinates. Schematic representation is shown in Figure 18.

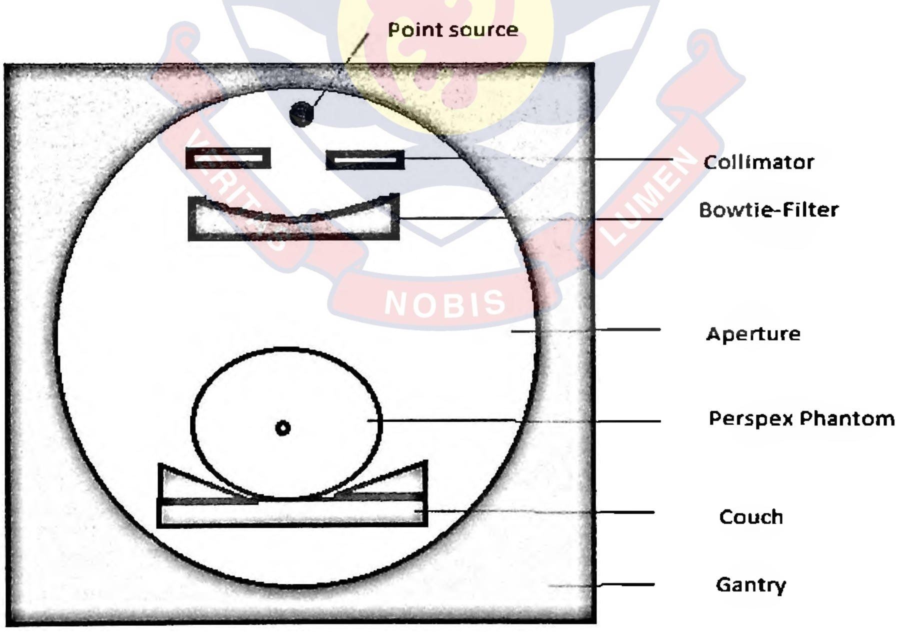

Figure 18: Cross-sectional representation of source, collimator and bowtie-filter arrangement

Energy Spectrum Generation

The photon energy spectrum for 120 and 130 peak kilo-voltages (kVp) were generated using spectrum generation software SpekCalc (Poludniowski, Landry, DeBlois, Evans, & Verhaegen, 2009). The spectrums were generated using a tungsten anode angle of 12 degrees, 2.5 mm thick aluminium filter and the required tube voltage was inputted for SpekCalc to generate the necessary spectrum for diagnosis. Mean energy of 54.4 and 56.8 keV were generated for 120 and 130 kVp respectively. The spectrum generation process is illustrated in Figure 19.

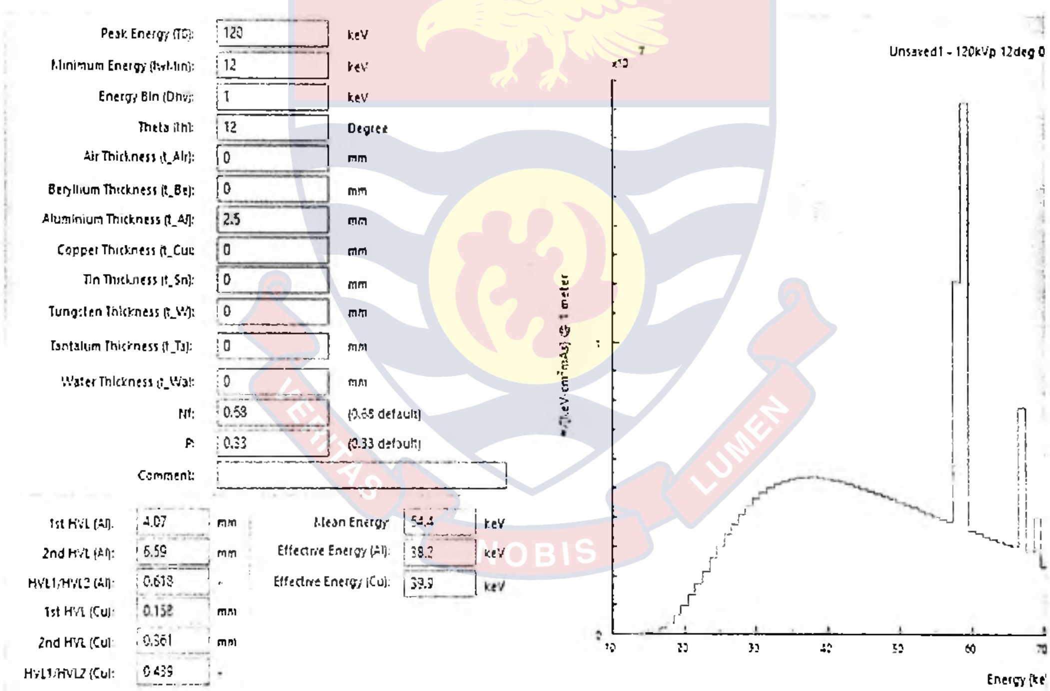

Figure 19: Photon energy spectrum generation using SpekCalc

CT Verification Process

The modelled CT scanner was verified for its true likeness to the real CT scanner by comparing their radiation output in terms of CTDI. MCNP6 simulation input file was created for the CT scanner (that is, point source, collimator, bowtie-filter, gantry and couch), perspex body phantom with ionisation chamber at the centre and in air. MCNP6 was used to track the photon transport for a simulation cut-off at photon energy deposition average over a cell (F6: p) accuracy of 5 % in the air-filled ionisation chamber. A typical CT validation simulation input file is detailed in Appendix A. Conditions of charge particle equilibrium permits the collision kerma to be equated to absorbed dose (that is, energy deposition per mass per particle) accounted for by using F6:p tally of the MCNP6. A conversion factor (CF) is generated per CT scanner to convert MeV/g/particle to mGy/100 mA by simulating $CTDI_{100,air}$ and using equation 20.

$$CF = \frac{CTDI_{100,air,measured\ per\ 100mAs}}{CTDI_{100,air,simulated\ per\ particle}} \tag{20}$$

where $CTDI_{100,air,\ measured\ per\ 100mAs}$ is the measured CTDI in air at the iso-centre using the ionisation chamber (mGy/100mAs) and $CTDI_{100,air,\ simulated\ per\ particle}$ is the simulated CTDI in air of the modelled ionisation chamber (MeV/g/particle) under the same scan protocol (Gu, Bednarz, Caracappa, & Xu, 2009).

The CF was used to convert simulated $CTDI_c$ and $CTDI_w$ from MeV/g/particle to mGy/100mAs for comparison with the measured values. The bowtie-filter thickness was varied to obtain corresponding CTDI percentage deviations. An exponential curve was fit to a scatter graph of filter thickness against percentage deviation as shown in Figure 20. From the curve, an appropriate bowtie-thickness and percentage deviation can be estimated for accurate CT scanner model verification. This procedure was repeated for all the identified CT scanners at their respective operating voltages of 120 and 130 kVp.

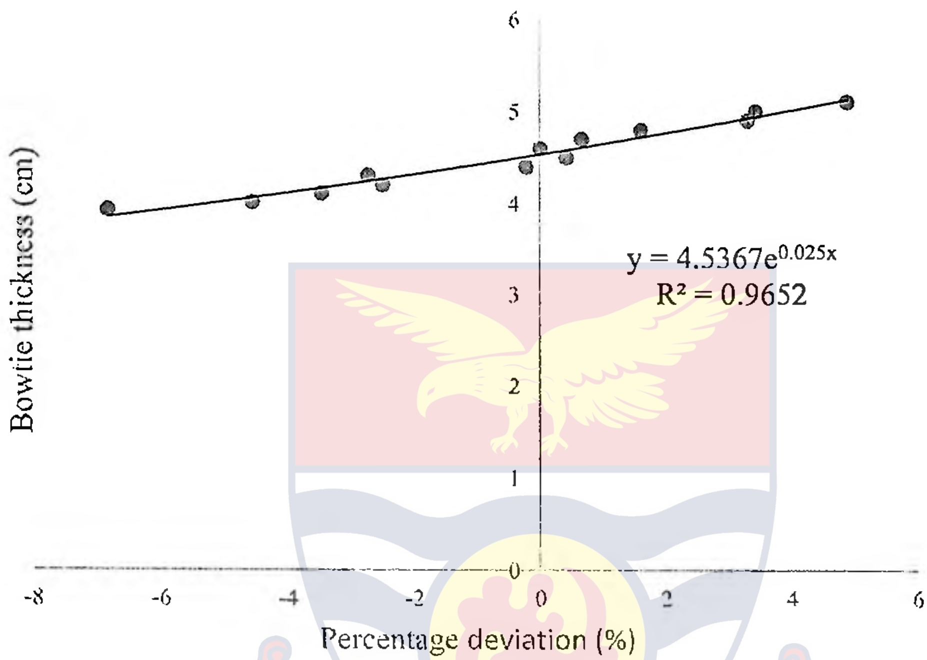

Figure 20: Fitted exponential curve to varying percentage deviation and bowtie filter thickness

Simulation Scenarios using Voxel2MCNP

Voxel2MCNP software developed by Karlsruhe Institute of Technology (Poelz, et al., 2013) enables the different created models to be spatially put together on one platform to create a scenario for simulation studies. It also has the capacity to generate MCNP simulation input file for the created scenario. Illustration of the use of Voxel2MCNP is shown in Figure 21.

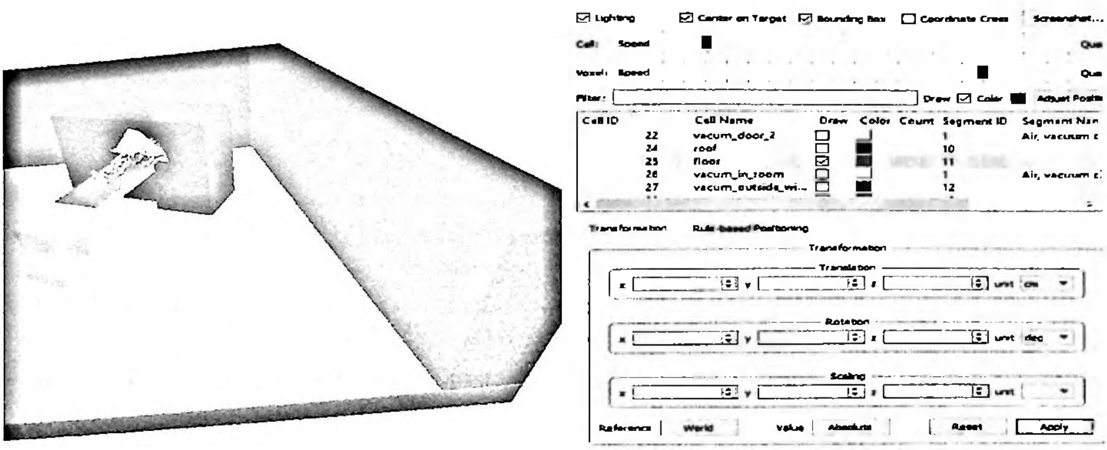

Figure 21: Voxel2MCNP being used to merge the different models

Scenario 1: Investigation into conventional use of protective equipment

Conventional protective equipment, that is, lead apron, thyroid shield and protective goggles used by the staff were investigated to assess their quantum of dose reduction to staff during CT fluoroscopy procedures. Voxel2MCNP was used to simulate the scenario with the computational supine MASH phantom as patient and standing MASH phantom as staff wearing all the protective equipment. A control scenario of staff without protective equipment was simulated as well. Illustrations of the scenarios are shown in Figure 22.

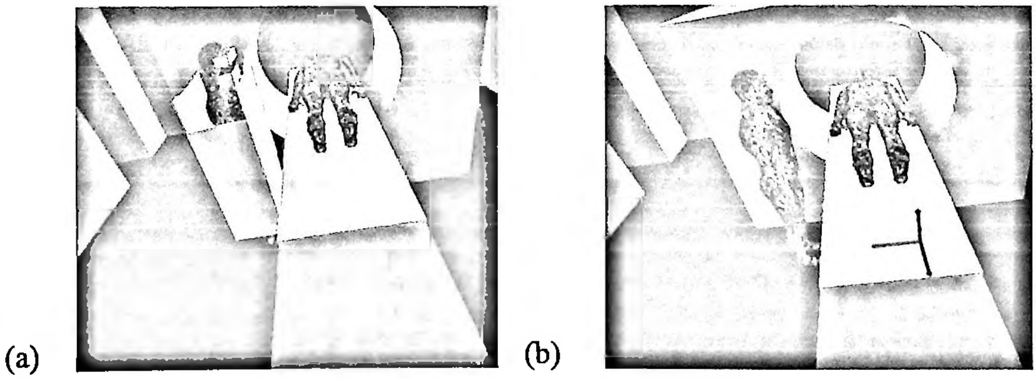

Figure 22: (a) Staff wearing protective equipment and (b) without protective equipment

Scenario 2: Investigations in CT gantry and staff positioning

Gantry positioning in terms of its angulation in the room as seen in most other facilities were investigated to assess their effect on staff dose. The gantry was positioned aligned with the walls of the room (90 degrees) and diagonal in the room (30 degrees clockwise). The staff position at a distance of 5 cm from patient and 10 cm from the gantry was also investigated for their influence on staff doses when staff was standing on the right or left in both CT gantry orientation , that is, 90 and 30 degrees. Figure 23 illustrates the scenario of gantry orientation by using Voxel2MCNP.

(a) 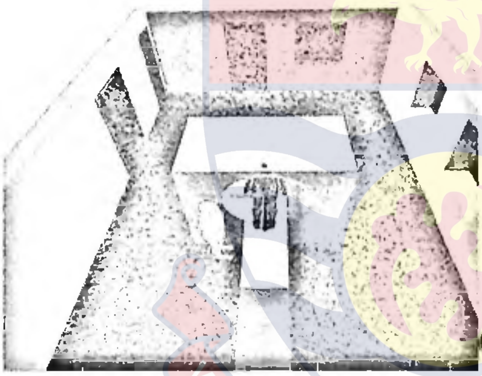 (b) 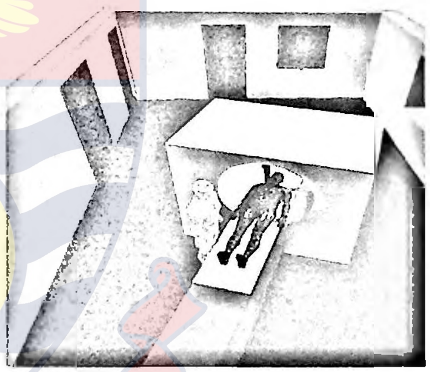

Figure 23: (a) Perpendicular positioning and (b) diagonal positioning of Computed Tomography fluoroscopy gantry in the room

Scenario 3: Investigations in room size variation

The influence of the CT room size on the radiation doses to the staff was investigated by varying the CT room floor area. The minimum room area required by the Nuclear Regulatory Authority, Ghana for X-ray diagnostic facilities is 25 m^2 (NRA, 2018). Therefore, scenarios with room dimension of 25.01 m^2 and 33.75 m^2 were simulated while maintaining all other models constant.

Scenario 4: Investigations into the use of lead drape and patient cover

The use of lead drape on the CT gantry and lead patient cover were investigated to identify their significance on the radiation dose to staff during CT fluoroscopy procedures. Scenarios with the use of both lead drape and patient cover wrapped 180° around the patient was simulated and a control, that is, without them was simulated as well. The alternate use of the drape and patient cover was also investigated to study their influence on staff doses. Figure 24 illustrates the scenario of lead drape and patient cover use, and control scenario using Voxel2MCNP.

(a) (b)

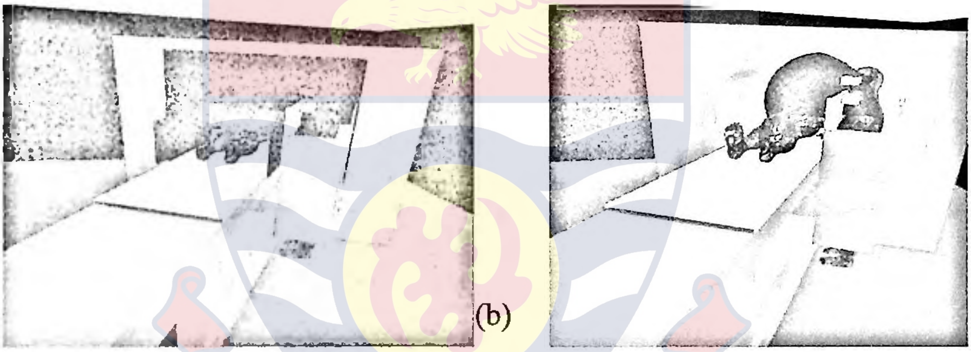

Figure 24: (a) Lead drape use and patient cover and (b) without lead drape and patient cover use

Scenario 5: Investigations into the protective face mask (visor) and apron

The protective face mask (visor) was alternatively used by staff in replacement of thyroid shield and protective goggles. The face mask is used due to its comfortability for long duration CT fluoroscopy procedures and also its capacity to accommodate reading glasses of staff requiring it for vision. The face mask is used in combination with lead aprons in the CT room by the staff. The use of the face mask together with lead apron was investigated to identify its magnitude of influence on FASH staff doses. The scenario considered the FASH phantom standing close to the supine patient phantom. A scenario with the use of face mask and lead apron, and a control without them were simulated. Figure 25 shows the scenarios of a FASH staff with and without face mask using Voxel2MCNP.

(a) (b)

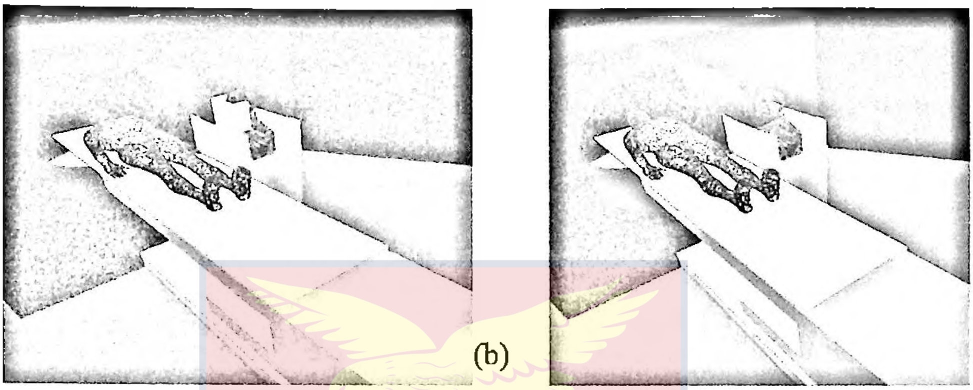

Figure 25: (a) Face mask used and (b) without face mask scenarios

Scenario 6: Investigation into scatter radiation distribution in the CT fluoroscopy room

In order to have a better understanding of the radiation dose distribution in the CT room, the dose distribution at a height of 138.2 cm from the floor of the room was simulated. The scenario with no object on couch, perspex or voxel phantom on couch and boundless room were simulated. Figure 26 illustrates the simulation with voxel phantom and perspex phantom on the couch.

GNUPlot programme was used to draw dose distribution contours in the CT room from the simulation results for all the scenarios considered.

Scenario 7: Investigation into effective dose estimation of staff during CT fluoroscopy procedures

MASH and FASH staff effective dose estimation using TLD badges d-

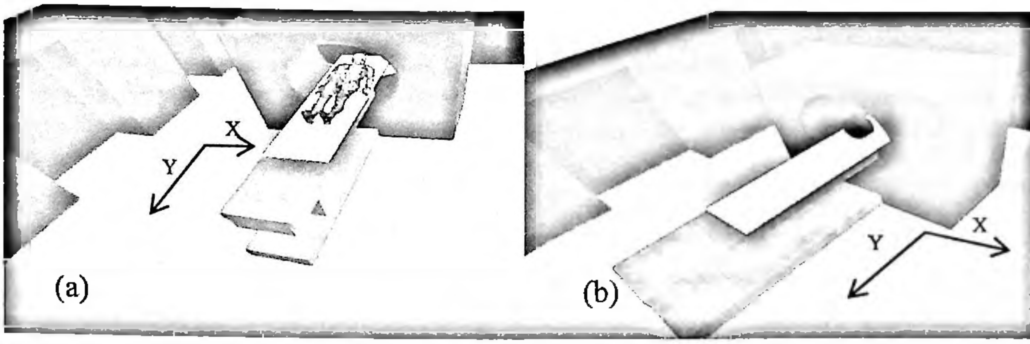

Figure 26: (a) Voxel phantom and (b) perspex phantom on couch scenarios

-uring CT fluoroscopy procedures were investigated at scan voltage of 120 kVp. TLD badges were simulated to be at thorax/neck over collar, thorax under apron and waist under apron. The simulated TLD readings at the various positions were used to estimate effective dose by using published formulas given in Table 7. Additionally, the effective dose was estimated from organ doses of the staff voxel phantom using equation 14 (IAEA, 2014b) as given by IAEA.

Table 7: Effective Dose Estimation Formulae for Dosimeter Readings

Source	Dosimetry Type	Formula
NCRP Report 122 (NCRP, 1995)	Single	$H_p(0.07)_{Neck,Over} \times \frac{1}{21}$
Huyskens et al. (Huyskens, Franken, & Hummel, 1994)	Single	$H_p(0.07)_{Neck,Over} \times \frac{1}{5}$
Padovani et al. (Padovani, Foti, & Malisan, 2001)	Single	$H_p(0.07)_{Neck,Over} \times \frac{1}{33}$

Table 7 Continued		
NCRP Report 122 (NCRP, 1995)	Double	$0.5H_p(10)_{\text{Thorax,Under}} + 0.025H_p(0.07)_{\text{Neck,Over}}$
Niklason et al. (Niklason, Marx, & Chan, 1994)	Double	$0.98H_p(10)_{\text{Thorax,Under}} + 0.02H_p(0.07)_{\text{Neck,Over}}$
Von Boetticher et al. (vonBoetticher, Lachmund, Hoffman, & Luska, 2003)	Double	$0.65H_p(10)_{\text{Thorax,Under}} + 0.017H_p(0.07)_{\text{Neck,Over}}$
Clerinx et al. (Clerinx, Buls, Bosmans, & deMey, 2008)	Double	$1.64H_p(10)_{\text{Thorax,Under}} + 0.075H_p(0.07)_{\text{Neck,Over}}$

$H_p(10)$ is dose equivalent at 10 mm depth in tissue; H_p (0.07) is the skin dose at 0.07 mm depth in tissue.

Monte Carlo Simulation of Scenarios

MCNP6 Monte Carlo code was used to track the photon energies necessary for all the scenario simulations. MCNP6 employs photon cut-off energy of 1 keV. The code assumes that there is generation of secondary electrons during photon transport but the electron energies are deposited at photon interaction sites, generating charge particle equilibrium. This assumption is valid considering the diagnostic X-ray energy and hence collision kerma is equivalent to absorbed dose (Gu, Bednarz, Caracappa, & Xu, 2009; DeMarco, et al., 2005).

MCNP6 simulation input files were generated for all the scenarios considered and the CT verification. An input file has cell, surface and data cards. A detailed scenario based simulation input file is shown in Appendix B.

Two billion (2.0 x 10^9) number of photon were tracked to achieve a good compromise between computational time and relative error. The simulations were performed on an Apple Mac computer (processing speed of more than 30 GHz) installed at Karlsruhe Institute of Technology, Germany.

An output of energy deposition in a unit mass of cell per particle represented by photon mode tally type 6 (F6:p) tally on MCNP6 were tallied for eye lens, thyroid and other organs of the staff required for estimating effective dose for simulation scenario 1 to 5. The photon average energy deposition per unit volume (PEDEP) in air mesh tally on MCNP6 was tallied for the scatter radiation in the room for simulation scenario 6. F6: p tally was used to tally absorbed dose in TLD and organs required for effective dose estimation for simulation scenario 7.

In all the scenarios, the already determined CF per scanner per voltage was used to convert MeV/g/particle or MeV/cm3/particle to mGy/100mAs.

Chapter Summary

A Barracuda quality control kit (Serial Number: BC1-13050013) with a CT dose profiler (Serial Number: DP2-13040061) connected to an Ocean Software installed on a laptop was used for CTDI measurements on all the identified CT scanners. A tape measure was used to collect the CT room dimensions and technical data on CT gantry were obtained. Four CT machines and rooms at different locations, protective equipment (apron, thyroid shield and goggles) were modelled suing SimpleGeo. The x-ray spectrum to be used for the simulation was generated using SpekCalc software. The modelled CTs were verified using the measured CTDI values.

Voxel2MCNP software was used to spatially put all the modelled items and the voxel phantoms on one plate form for scenario generation. The following seven scenarios were generated for the study: investigation into conventional use of protective equipment; investigations in CT gantry and staff positioning; investigations in room size variation; investigations into the use of lead drape and patient cover; investigations into the protective face mask (visor) and apron; investigation into scatter radiation distribution in the CT fluoroscopy room; and investigation into effective dose estimation of staff during CT fluoroscopy procedures.

MCNP6 Monte Carlo code was used to track the energy deposition in a unit mass of cell per particle and photon average energy deposition per unit volume (PEDEP) in air mesh tally for two billion (2.0 x 109) number of photons to achieve a good compromise between computational time and relative error.

CHAPTER FOUR

RESULTS AND DISCUSSIONS

Introduction

This chapter discusses the findings of this study. Detailed, logical, scientific interpretation of the results and comparison with other studies has been discussed.

Measured Computed Tomography Dose Index

Measured $CTDI_c$, air CTDI ($CTDI_{air}$) and estimated $CTDI_w$ for the four different CT scanners are shown in Table 8. The measured CTDI in air, centre

Table 8: Measured Computed Tomography Dose Index for the different Computed Tomography Scanners

CT Scanner	Peak Voltage (kVp)	$CTDI_{air}$ (mGy)	$CTDI_c$ (mGy)	$CTDI_w$ (mGy)
Toshiba Aquilion One	120	44.75	3.34	5.94
Siemens Somaton Emotion	130	69.96	16.27	26.13
GE Discovery PET/CT 710	120	89.73	13.27	21.98
Philip Brilliance	120	57.7	5.75	9.33

and weighted varied among the brand of CT scanners. It was clear that CTDI (centre and weighted) increased with increase in tube voltage. $CTDI_w$ was ob-

-served to be more than $CTDI_c$ by approximately by a factor of 1.7.

Scenario Setup

The model of a staff performing a CT fluoroscopy procedure standing beside the patient in a room is shown in Figure 27. This model formed the basis for all the investigative studies by the generation of scenarios as illustrated in the Method section (scenario 1 to 7). It must be mentioned that the staff is always required to be in the room for effective examination (Kato, et al., 1996; Siebel, et al., 1997). The individual models of the CT room and gantry for all the facilities are shown in Appendices C – F.

(a) (b)

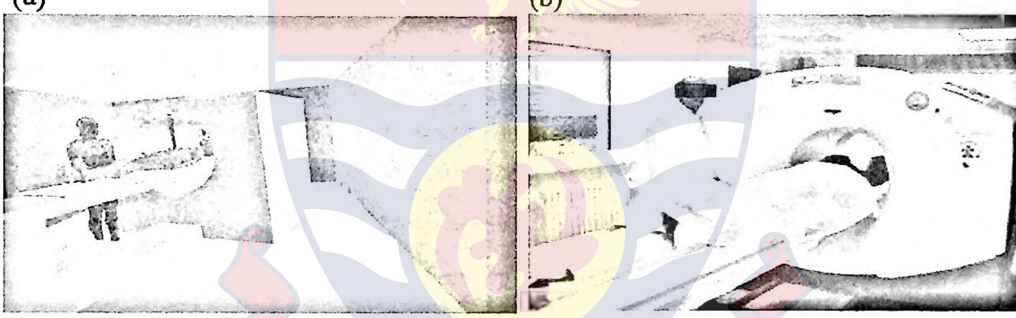

Figure 27: (a) 3D model and (b) picture of a staff performing Computed Tomography fluoroscopy procedure

Generated Photon Energy Spectrum

The radiation energy spectrum of 120 kVp was chosen for all the investigative studies because it is the most used voltage for diagnosis and additionally, it gives a mean representation of the available voltages of CT scanners. The energy spectrum for 120 kVp is shown in Figure 28. The radiation energy spectrum generated by 130 kVp for the CT verification studies has been shown in appendix G.

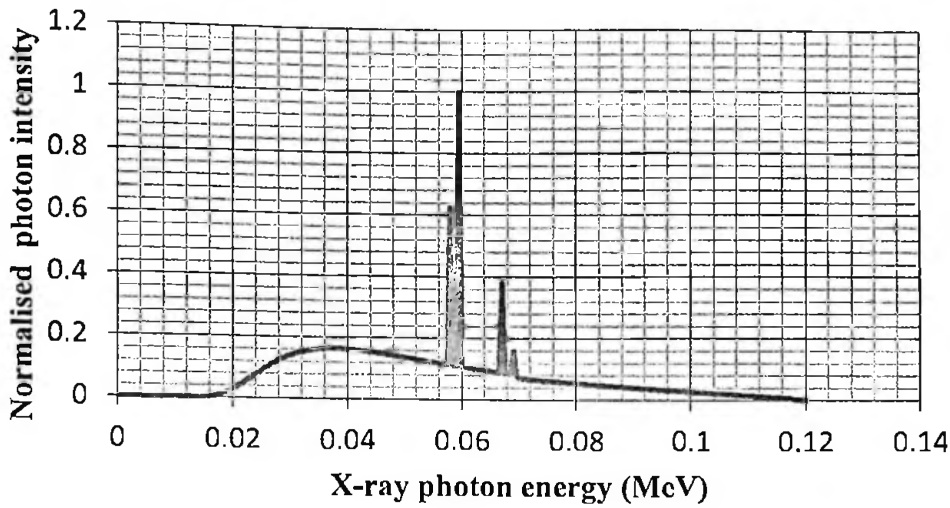

Figure 28: Normalized photon energy spectrum for 120 kVp @ 2.5 mm Al filter and 12 degrees tungsten anode angle

Computed Tomography Fluoroscopy Validation

The MCNP6 tallies (results) are normalized to be per starting particle history. The statistical precision of the fractional results with respect to the estimated mean is given as relative error. MCNP6 performs normality test of the results with a confidence level of 95 %.

Trial-and-error variation of the bowtie-filter (since not known or given in documents) during validation of the CT scanners resulted in an array of bowtie-filter thickness against percentage deviation (deviation of measured $CTDI_c$ from simulated $CTDI_c$). These values were plotted and an exponential curve fitted as shown in Figure 29.

Three bowtie-filter thicknesses with a variation of 0.5 cm (that is, 4.0, 4.5, and 5.0 cm) and their corresponding percentage deviations from Figure 29 were plotted alone as shown in Figure 30. The exponential curves fitted to Figures 29 and 30 were compared as shown in Table 9.

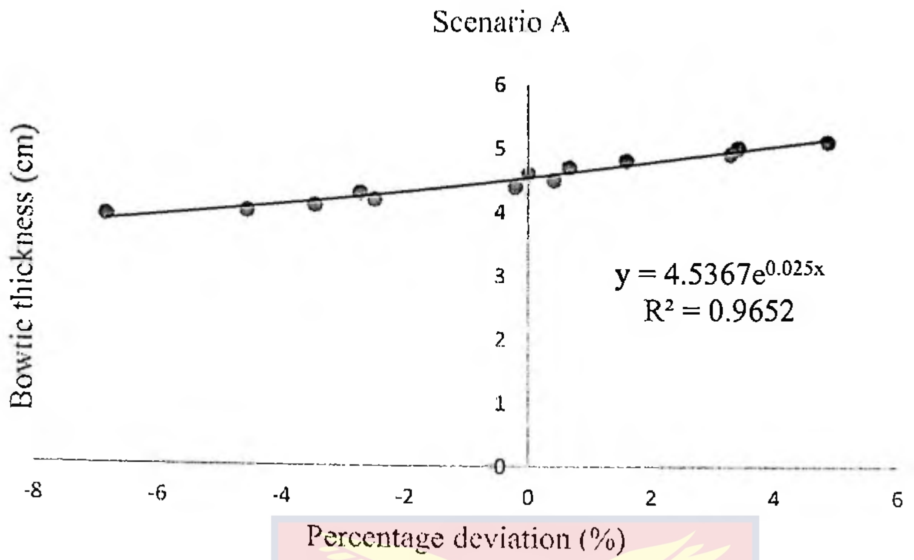

Figure 29: Exponential curve fitted to scatter graph of bowtie-filter thickness against percentage deviation

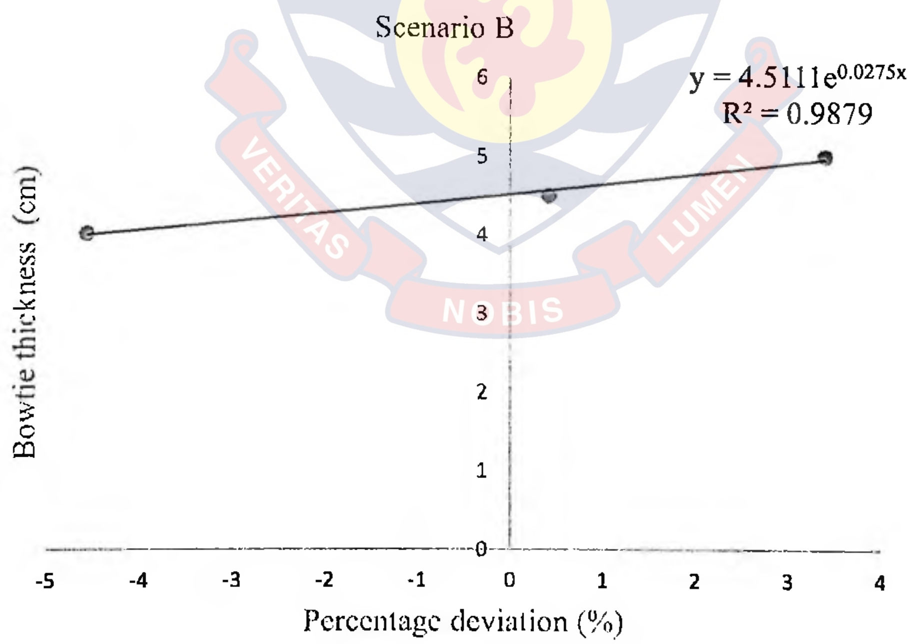

Figure 30: Exponential curve fitted to three-point curve of bowtie-filter thickness against percentage deviation

Table 9: Comparison of Exponential Curve trend for Scenario A and B

Percentage deviation (%)	Bowtie-filter thickness (cm)		
	Scenario A	Scenario B	(Scenario A - B)
5	5.14	5.18	-0.04
4	5.01	5.04	-0.03
3	4.89	4.90	-0.01
2	4.77	4.77	0.00
1	4.65	4.64	0.01
0	4.54	4.51	0.03
-1	4.42	4.39	0.03
-2	4.31	4.27	0.04
-3	4.21	4.15	0.06
-4	4.10	4.04	0.06
-5	4.00	3.93	0.07

It is clear from Table 9 that there was no significant difference in the observed exponential trends for both scenarios. Therefore, with a three point exponential curve, a bowtie-filter thickness with estimated percentage deviation (that is, deviation of measured $CTDI_c$ from simulated $CTDI_c$) of 0 % can be chosen and simulated for the CT scanner validation.

The three-point-exponential curve procedure was used to propose bowtie-filter thicknesses for all the four identified modelled CT scanners during validation. The CF used to convert MeV/g/particle to mGy/100 mA was estimated using equation 20. The details of the conversion and the conversion factors are given in Table 10 for all the CT scanners.

The measured CTDI and simulated CTDI has been compared at the category of center and weighted as illustrated in Table 11. The CT scanners

Table 10: Conversion Factor Generation for all Computed Tomography Scanners

CT Scanner	Peak Voltage (kVp)	Measured $CTDI_{100}$ in air (mGy/ 100 mA)	Simulated Energy in Ionisation Chamber in air (MeV/g/particle)	Conversion Factor (mGy.g.particle/ 100 mA/MeV)
Toshiba Aquilion One	120	44.75	2.23×10^{-08}	2.01×10^{09}
Siemens Somaton Emotion	130	69.96	5.63×10^{-08}	1.24×10^{09}
GE Discovery PET/CT 710	120	89.73	5.71×10^{-08}	1.57×10^{09}
Philip Brilliance	120	57.7	3.47×10^{-08}	1.66×10^{09}

were verified using the three point exponential curve procedure explained above. The bowtie-filter thickness estimated for the Toshiba Aquilion One, Siemens Somaton Emotion, GE LightSpeed Ultra and Philip Brilliance CT scanners were 13.4, 1.7, 2.9 and 8.5 cm respectively. The percentage relative error achieved for all the Monte Carlo simulations was 5 %. The simulated CTDI agrees well with the measured CTDI. They agreed within an absolute percentage deviation of 1.80 - 7.44 %. This was comparable with absolute percentage deviations of 1.80 – 3.40 %, 0.60 – 5.72 %, 2.90 – 7.00 % and 2.92 – 4.89 % by DeMarco et al (DeMarco, et al., 2005), Gu et al (Gu, Bednarz, C-

Table 11: Comparison of Measured and Simulated Computed Tomography Dose Index

CT Scanner	Tube Voltage (kVp)	Position	Measured CTDI (mGy)	Simulated CTDI (mGy/100 mA)	Percentage Deviation (%)
Toshiba Aquilion One	120	Centre	3.34	3.28	1.80
		Weighted	5.94	5.84	1.68
Siemens Somaton Emotion	130	Centre	16.27	15.06	7.44
		Weighted	26.13	26.81	-2.60
GE Discovery PET/CT 710	120	Centre	12.97	13.44	-3.62
		Weighted	22.98	23.92	-4.09
Philip Brilliance	120	Centre	5.25	5.39	-2.67
		Weighted	9.33	9.59	-2.79

(-) means simulated CTDI is greater than measured CTDI

-aracappa, & Xu, 2009), Figueira et al (Figueira, et al., 2013) and Oono et al (Oono, Araki, Tsuduki, & Kawasaki, 2014)respectively. The observed differences in measured and simulated CTDI could be explained by the already stated simulation relative error of 5 %, and the assumption of bowtie filter thickness and material of all the CT scanners since not readily available.

It was seen that the three-point-exponential curve was used to successfully validate all the modelled CT scanners without going through the stress of trial-and-error as indicated by some authors (DeMarco, et al., 2005; Figueira, et al., 2013). The methodological procedures for three-point-exponential curve approach have been validated and exhibited its ability to be applied to all the make of CT scanners. The three-point-exponential curve approach may always be engaged for validation of modelled CT scanners when information on bowtie-filter is not known. This is to enhance computational research studies (e.g. in radiation protection) with CT scanners.

Conventional use of Protective Equipment

Organ (thyroid and eye lens) and effective dose to staff positioned at 5 cm from the front of the staff to the patient table and 10 cm from the side of the staff to the gantry is given in Table 12. The staff dose focused on thyroid

Table 12: Organ and Effective Dose per 100 mA per rotation to MASH Staff with and without Protective Equipment

Dose Indicator	Protective Equipment	Without Protective Equipment
Thyroid Dose (μGy)	0.8 ± 0.2	2.6 ± 0.6
Eye lens Dose (μGy)	4.5 ± 1.3	4.8 ± 1.3
Effective Dose (μSv)	1.7 ± 0.4	7.6 ± 1.6

Values presented as mean ± standard error

and eye lens because of their radio-sensitivity and also the only radio-sensitive organs outside the thorax/abdomen region. Dosimetry of staff eye lens is also very necessary due to the reduction of equivalent dose limit of eye lens from 150 to 20 mGy per year (ICRP, 2007). The relative error associated with the simulation of organ doses of the staff varied from organ to organ depending on the size and the proximity of the organ to the source of radiation. The relative error in organ dose estimation ranged from 0.009 to 0.525.

The magnitude of radiation dose reduction per X-ray tube rotation to staff when lead apron, thyroid shield and goggles are worn was clearly demonstrated in Table 12. For the simulation, it must be mentioned that the staff was modelled to wear wrap-around lead apron (front: 0.35 mm lead equivalence and back: 0.25 mm lead equivalence), lead goggles (0.75 mm lead equivalence) and thyroid shield (0.35 mm lead equivalence) at the same time. The MASH staff was standing on the left side of the patient with the CT fluoroscopy gantry axis diagonal (30 degrees) to the axis of the room as shown in Figure 22. Generally, there is an overall reduction in effective and organ dose when protective equipment is worn by staff. The thyroid dose and effective dose to staff was reduced by about a factor of 3.3, and 4.5, respectively. Considering the uncertainties (standard error) in the dose estimation, the eye lens dose remains unchanged. The staff was modelled standing upright with head facing forward, hence considering only a fixed head position for this study. In a realistic scenario, the staff at a point in time may be looking at the patient or the monitoring screen for the procedure. Employing a movable phantom to take into account realistic staff head positions is planned for the future. The unchanged eye lens dose with or without lead goggle could be attributed to the unrealistic head positioning of the staff.

The eye lens dose was observed to be higher than the effective dose for the scenario with protective equipment. This indicates that there is a need to intensify research on eye lens dosimetry (Teles, et al., 2017; Ferrari, et al., 2016) due to the new dose limit of 20 mSv per year (ICRP, 2007). By the significant reduction in effective dose, emphasis is placed on the need to use protective equipment for staff during CT fluoroscopy-guided procedures.

Computed Tomography Gantry and Staff Positioning

Alternative dose reduction techniques, that is, CT gantry and staff positioning, apart from the conventional use of protective equipment have been investigated. The influence of CT fluoroscopy gantry positioning in the room and different positions of the staff on staff doses is shown in Table 13.

Table 13: Organ and Effective Dose per 100 mA per rotation to Staff for different Gantry and Staff Positions

Dose Indicators	Gantry Aligned (0^{o})		Gantry Diagonal (30^{o})	
	Staff on Right	Staff on Left	Staff on Right	Staff on Left
Thyroid Dose (μGy)	2.8 ± 0.6	3.3 ± 0.6	2.7 ± 0.6	2.6 ± 0.6
Eye Lens Dose (μGy)	5.0 ± 1.4	5.6 ± 1.4	5.3 ± 1.3	4.8 ± 1.3
Effective Dose (μSv)	9.4 ± 1.6	8.3 ± 1.6	8.6 ± 1.6	7.6 ± 1.6

Values presented as mean ± standard error

The positioning of the staff from the patient table and the gantry was 5 cm and 10 cm, respectively, for both aligned and diagonal positioning of the gantry. It must be mentioned that the positioning of the staff on the left or right of the gantry is related to the location of the point of interest as well as to the patient positioning (prone or supine) which allows the safest access from a clinical perspective.

The radiation dose to the thyroid, eye lens and effective dose of the staff positioned on the left side of the patient in the diagonal positioning of the gantry were lower than the others (right and left staff position with gantry aligned; and right staff positon with gantry diagonal) by a maximum factor of 1.3, 1.2, and 1.2, respectively. Generally, diagonal positioning of the gantry results in less dose to the staff than being aligned in the CT fluoroscopy room. It could also be seen generally that radiation dose to the staff on the left side of the patient is less as compared to the right side of the patient. This observation could be attributed to the scatter radiation from the walls of the CT fluoroscopy room, the concrete floor and the concrete ceiling. Another consideration is the shielding of the CT fluoroscopy gantry from scatter radiation to the staff. Moreover, the staff position with respect to the room and the opening of the doors varied from scenario to scenario.

The discussions and the results above indicate that diagonal positioning of CT fluoroscopy gantry should be considered in the design of a CT room and staff positioning away from walls of the room if possible is advised for staff dose reduction. It must be mentioned that the relative error associated with the simulation of organ doses of the staff for this scenario also varied from organ to organ depending on the size and the proximity of the organ to the source of radiation. The relative error in organ dose estimation ranged from 0.009 to 0.525.

Computed Tomography fluoroscopy room size variation

The alternate dose reduction technique included variation of room size (floor area). Organ and effective doses to the staff standing in room during CT fluoroscopy guided procedures by variation of the floor area is shown in Table 14. The scenario with less dose to the staff, that is, the CT fluoroscopy gantry positioned diagonal in the room and the staff standing on the left side of patient was considered. The floor dimension variation started from the allowable floor dimension (4.26 m x 5.87 m) by the Nuclear Regulatory Authority, Ghana (NRA, 2018) for diagnostic X-ray machines, that is, 25 square meters.

Table 14: Staff Organ and Effective Doses per 100 mA per rotation by variation of Room Floor Area

Room Floor Area (m^2)	Thyroid Dose (μGy)	Eye Lens Dose (μGy)	Effective Dose (μSv)
25.01 (4.26 x 5.87)	2.6 ± 0.6	4.5 ± 1.3	7.6 ± 1.6
33.75 (5.06 x 6.67)	2.6 ± 0.6	4.5 ± 1.3	7.6 ± 1.6

Values presented as mean ± standard error

It was seen that when the floor dimension was increased by approximately 0.8 m on both sides of the room , that is, from (4.6 m x 5.87 m) to (5.06 m x 6.67 m), within the uncertainties (standard error), there was no reduction in the thyroid and eye lens dose as well as the effective dose. This goes to suggest that increasing the room dimension above 4.6 m x 5.87 m to reduce staff doses is not justifiable. But further investigation is required to determine the extent to which a floor dimension could be increased or decreased to have a significant dose reduction to staff taking into consideration economic factors.

Lead drape and patient cover use

In this scenario, the dosimetry was performed with the staff wearing protective apron, thyroid shield and protective goggles. In addition to the use of the protective equipment, the use of lead drape (0.5 mm lead equivalence) and patient cover wrapped 180° around the patient (0.5 mm lead equivalence) were alternatively considered. The thyroid, eye lens and effective dose to staff for scenarios when both lead drape and patient cover are used or when lead drape and patient cover are used alternatively and, or when lead drape and patient cover are not used are shown in Table 15. The relative error associated

Table 15: Organ and Effective Dose to Staff per 100 mA per rotation for Lead Drape and Patient Cover Scenarios

Dose Indicator	Scenarios			
	Both Lead Drape and Patient Cover use	Only Lead Drape use	Only Patient Cover use	No Lead Drape or Patient Cover use
Thyroid Dose (μGy)	0.18 ± 0.03	0.30 ± 0.05	0.60 ± 0.03	1.04 ± 0.08
Eye Lens Dose (μGy)	0.68 ± 0.11	0.95 ± 0.16	3.18 ± 0.07	4.89 ± 0.14

Table 15 Continued				
Effective Dose (μSv)	0.98 ± 0.13	1.36 ± 0.18	2.58 ± 0.09	4.27 ± 0.12

Values presented as mean ± standard error

with the simulation of dose to organs of the staff varied from 0.006 to 0.502, this was dependant on the size of the organ and proximity to the point source.

It can clearly be seen that the use of both lead drape and patient cover significantly reduced the thyroid, eye lens and effective doses by a factor of 5.7, 7.1 and 4.3 respectively. When only patient cover was used, there was a reduction in dose to the thyroid, eye lens and effective dose of staff by a factor of 1.7, 1.5 and 1.7 respectively. The contribution of the lead drape to staffs' thyroid, eye lens and effective doses reduction during CT fluoroscopy procedures is more when compared with that of the patient cover for this study by a factor of 2.1, 3.4 and 1.8 respectively.

The radiation dose to the eye lens was lower than the effective dose by a factor of 1.4 for the scenario with the use of only lead drape. Contrarily, the scenario without lead drape resulted in the eye lens dose being higher than the effective dose by a factor of 1.2. Attention to the eye lens protection and dosimetry is very important (Pereira, et al., 2011; Teles, et al., 2017) due to the reduced annual dose limit proposed by ICRP (ICRP, 2007) from 150 mSv to 20 mSv average over 5 years. In this case, the eye lens dose would be the limiting quantity for occupational exposure.

The use of lead drape and patient cover should be encouraged where possible to augment the conventional protection provided by lead aprons, thyroid shield and protective goggles. Although the staff model was standing upright with a fixed head position facing forward with arms sideways, the doses are indicative enough to provide information on protection measures. Study with a movable phantom is planned for the future to account for realistic staff head and hand positions.

Protective face mask and apron use

The use of face mask (being used at the moment in interventional facilities) in place of thyroid shield and protective google have been investigated. The radiation dose to the thyroid, eye lens and effective dose of the FASH staff for the use of face mask and apron and without them have been shown in Table 16. The FASH staff was modelled standing approximately 1 cm and 2 cm distance from the patient and CT gantry respectively.

Table 16: Organ and Effective Dose of FASH Staff per 100 mA per rotation for Face Mask and Lead Apron Scenarios

Dose Indicator	Scenarios	
	Face Mask and Lead Apron	Without Face Mask and Lead Apron
Thyroid Dose (μGy)	1.34 ± 0.05	2.08 ± 0.08
Eye Lens Dose (μGy)	4.83 ± 1.05	5.16 ± 0.09
Effective Dose (μSv)	4.52 ± 0.80	12.75 ± 0.79

Values presented as mean ± standard error

It was seen from Table 16 that the use of protective face-mask and lead apron reduced the thyroid, eye lens and effective doses of the staff by a factor of 1.6, 1.1 and 2.8 respectively. There was no significant difference between the eye lens and thyroid dose within the uncertainties for protective face mask and lead apron use by the staff. However, the effective dose was more than the eye lens dose by a factor of 2.8 for staff without face mask and lead apron. Generally, there is a clear indication of the need to use face mask and lead apron because of the significant dose differences when used.

Comparing the staff dose results for the use of protective equipment (that is, lead apron, thyroid shield and protective goggle) shown in Table 12, and the use of protective facemask and lead apron shown in Table 16, it was seen that the use of protective equipment resulted in less thyroid and effective dose than the use of protective facemask and lead apron by a factor of 1.7 and 2.7 respectively. This could be attributed to the closeness of the FASH staff (1 cm and 2 cm from patient and CT gantry respectively) to the patient table and CT gantry than the MASH staff (5 cm and 10 cm from patient and CT gantry respectively). Additionally, the body mass index of FASH (22.75 kg/m^3) was smaller than that of MASH (23.60 kg/m^3) and could be a contributing factor. The same could be said for the scenarios without protective equipment (shown in Table 11), and protective facemask and lead aprons (shown in Table 16). However, there was no difference in the eye lens doses within the uncertainties in both the MASH and FASH scenarios.

Scatter radiation distribution in a room

The photon energy deposition in air was considered in a unit volume of

106074.03 cm^3 (50.60 x 60.64 x 34.57) or unit area of 3068.38 cm^2. The energy deposition in each unit area or volume in the CT fluoroscopy room has been considered for the dose distribution contour. The dose distribution at a height of 138.2 cm of the staff was considered because this is believed to be the trunk region of the human body (torso). Protection of the trunk region from radiation exposure is very important because of the presence of huge concentration of water that may interact with radiation to harm the body.

The radiation dose distribution in air in the CT fluoroscopy room with nothing, perspex phantom, MASH voxel phantom and boundless room with MASH voxel phantom on patient couch are illustrated in Figures 31 – 34 respectively. All the figures show room length and breadth on a linear scale representing x and y axis while the dose distribution in the room (mGy/100 mAs) was plotted on a log scale representing the z-axis.

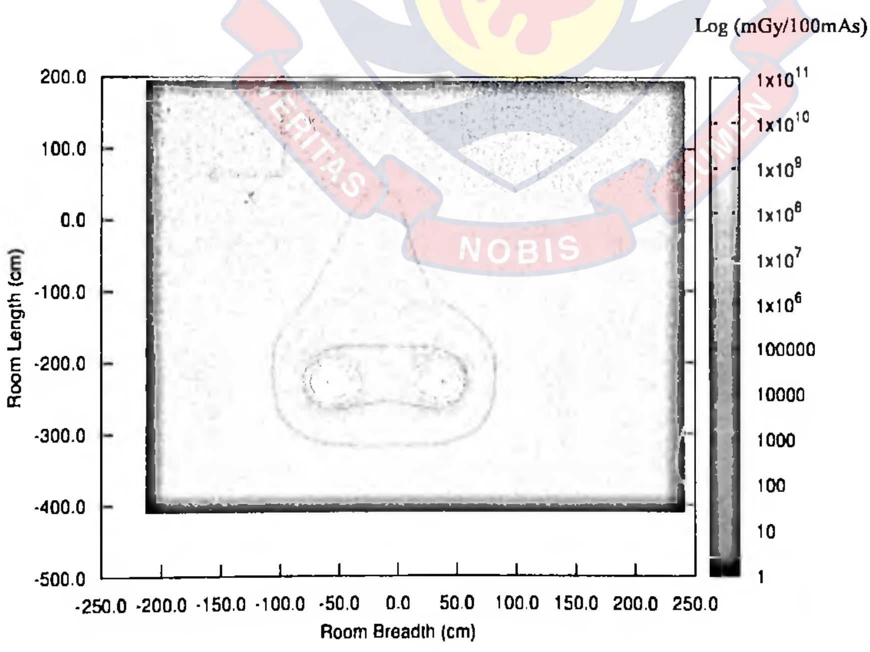

Figure 31: Dose distribution in the room with nothing on patient couch

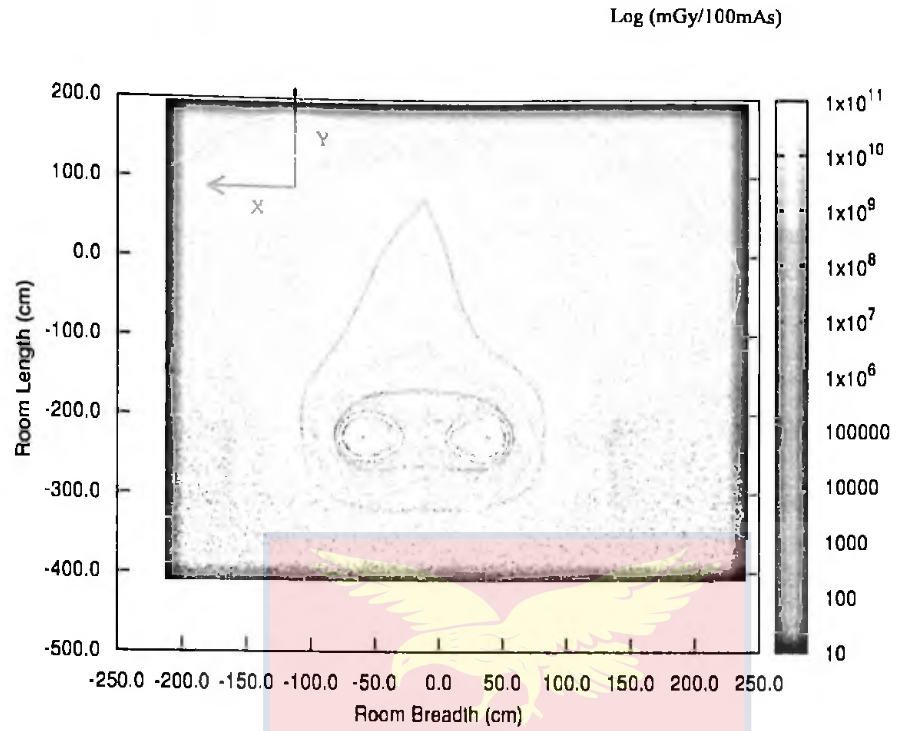

Figure 32: Dose distribution in the room with perspex phantom on patient couch

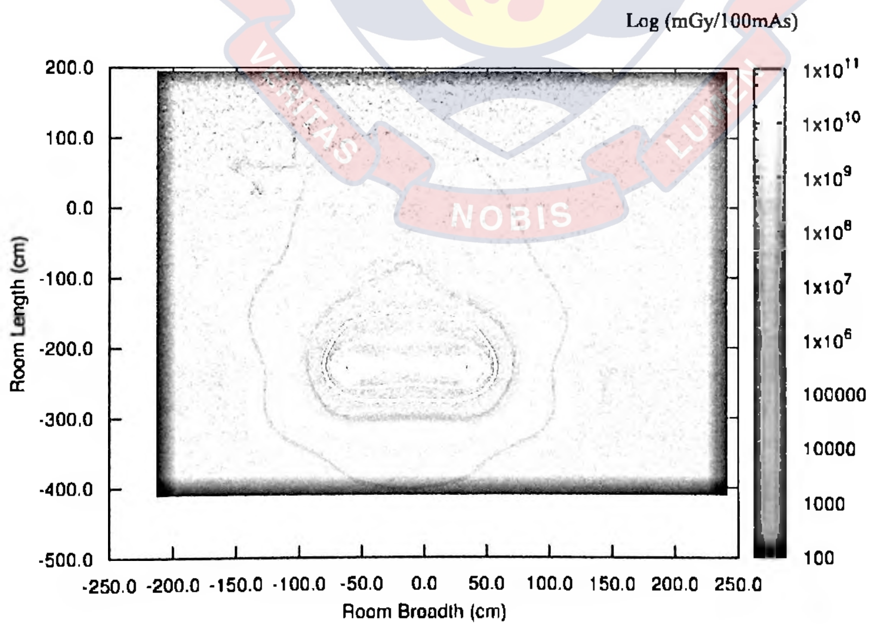

Figure 33: Dose distribution in the room with voxel phantom on patient couch

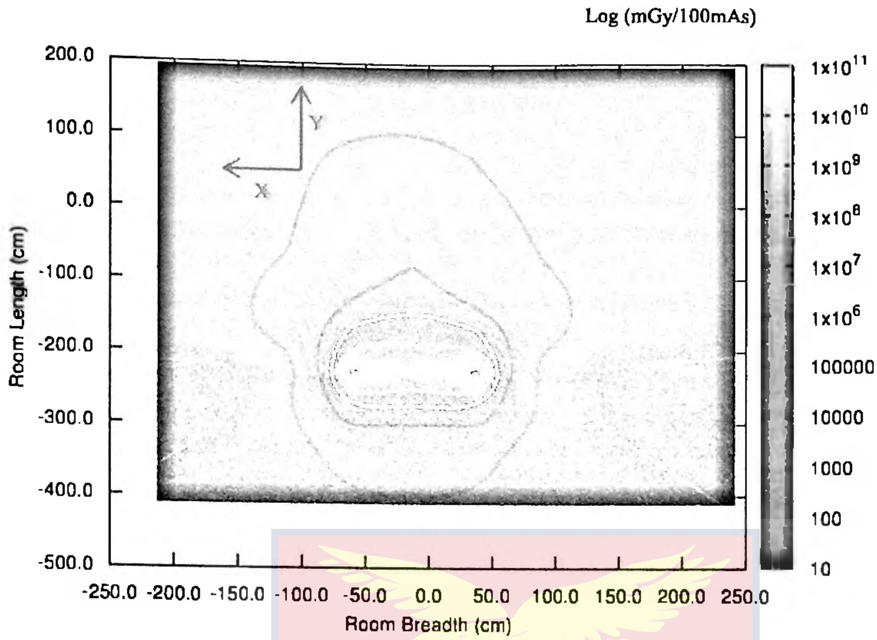

Figure 34: Dose distribution in a boundless room with voxel phantom on patient couch

The dose distribution was plotted on a logarithmic scale to clearly show the radiation distribution pattern at lower doses. The radiation dose in all the figures indicate a high dose in the magnitude of about 1.00 x 10^{11} mGy/100 mAs on the log scale (representing actual value of 1.58 x 10^{9} mGy/100 mAs). This high dose represents the modelled point source of radiation. Lowest doses in Figures 32, 33, 34 and 35 are in the magnitude of about 1, 10, 100, and 10 mGy/100 mAs on the log scale respectively (representing actual value of 0.78, 1.88, 18.40, and 2.89 mGy/100 mAs respectively). The dose distribution values in air (mGy/100 mAs) in the CT fluoroscopy room for when the couch had nothing, perspex phantom, voxel phantom, and boundless room with voxel on couch are shown in Appendices H – K respectively.

Comparing lowest doses of Figures 31, 32 and 33, it was seen that an object on the patient couch contributes more scatter radiation in the room. The lowest dose in air in the room with perspex and MASH voxel phantom on the couch was greater than the scenario with no phantom by a factor of about 2.4 and 23.5 respectively. It must be said that since the MASH voxel phantom has a greater volume and height than perspex phantom, the lowest distributed dose for the first is greater than the latter by a factor of 9.8. The surroundings (walls, roof and floor) of the CT fluoroscopy room contributed scatter radiation in the room as illustrated by a factor of 6.4 by comparing the lowest distribution dose in air for Figures 33 and 34. This was evidence that scatter radiation distribution in the room is influenced by its surroundings.

It was clear that the scatter radiation patterns in the room for all the scenarios are not the same. From all the Figures, the highest dose distribution in air are at the source of the radiation (yellow colour) whilst the lowest dose in air (indicated by the darkest colour) is at the sides of the CT fluoroscopy gantry (identified from the Cartesian coordinate of the model) parallel to the patient couch. The lowest dose at the sides of the CT fluoroscopy gantry could be explained by the shielding provided by the CT fluoroscopy gantry.

It is clear from the discussions above that a body on the couch increase the scatter radiation dose in the room. Objects that have more volume and height increase scatter radiation dose. The surroundings (walls, floor and ceiling) contribute to the scatter radiation dose in the room and hence larger rooms (recommended by regulatory body) (NRA, 2018) are advised to be used for radiation protection purposes. Occupancy in the room is recommended to be on the sides of the CT fluoroscopy gantry if possible for reduced radiation exposure. Alternatively, engineering techniques at the manufacturers' level should be explored to enable the staff stand on the sides of the CT fluoroscopy gantry during the procedure.

Effective dose estimation of staff

Radiation dose absorbed by the organs of MASH and FASH staff for effective dose estimation using Equation 14 is shown in Table 17. It could be seen that there was no distinction between the doses to the organs of the female

Table 17: Organ and Effective Dose per 100 mA per rotation for Female and Male Staff Voxel Phantom

Organ / Effective dose	120 kVp (µGy)	
	Male	Female
Bladder	0.10 ±0.01	0.16 ±0.03
Bone Surface	4.20 ±0.04	12.61 ± 1.01
Brain	1.27 ±0.02	1.64 ±0.03
Breast	1.76 ±0.09	1.82 ±0.07
Colon	0.30 ±0.06	0.36 ±0.04
Liver	0.98 ±0.00	1.18 ±0.05
Lungs	1.31 ±0.02	1.64 ±0.05
Bone Marrow	0.72 ±0.12	6.58 ±0.48
Oesophagus	0.97 ±0.07	1.27 ±0.23
Remainder Tissues	9.95 ±0.11	12.80 ±0.14
Salivary Glands	1.54 ±0.41	5.14 ±0.03
Skin	1.05 ±0.17	1.14 ±0.12

Table 17 Continued		
Stomach	0.43 ±0.08	0.43 ±0.03
Testes/ Uterus	0.20 ±0.01	0.24 ±0.02
Thyroid	0.83 ±0.15	1.32 ±0.21
Eye Lens	4.37 ±0.04	3.80±0.14
Effective Dose	1.95* ±0.11	3.21* ±0.28

(*) is in mSv; Values presented as mean ± standard error

or male phantom within uncertainty except bone surface, bone marrow remainder tissue and salivary glands that recorded more organ dose for female than male phantom. This could be attributed to the small body mass index of the female phantom compared to that of the male , that is, the surface organs shields the internal organs from radiation exposure e.g. surface bone dose is more than bone marrow dose. Additionally, organs dose absorption is also dependant on the volume, density of the organ and the proximity of the organ to the source of radiation.

However, the eye lens dose to the male phantom was more than that of the female phantom by a factor of 1.2. Also, the effective dose to the female phantom was more than that of the male phantom by a factor of 1.7. The dose to the eye lens in both male and female phantoms was more than their respective effective doses and hence warranting the need for eye lens dose optimisation considering the fact that the recommended eye lens dose limit is the same as effective dose, that is 20 mSv/year (ICRP, 2007).

Radiation dose measured with a TLD positioned at the neck over thyroid shield, under apron at the thorax and under apron at the waist for a CT fluoroscopy scan per 100 mA per tube rotation is illustrated in Table 17. The

TLD was modelled to measure dose equivalent at a depth of 10 mm and surface dose at a depth of 0.07 mm. It was seen from Table 18 that the TLD readings for the male phantom was more than that of the female by a maximum factor of 1.8. This could be attributed to the position of the TLD's (difference in phantom height) with respect to the source of radiation. Although the female and male phantoms were modelled to be equidistant from

Table 18: Modeled TLD Readings per 100 mA per rotation for Female and Male Voxel Phantoms during Computed Tomography Fluoroscopy

Peak Voltage (kVp)	Position	TLD Readings (μGy/100 mA)	
		Male	Female
120	Neck Over Collar	57.86 ±0.24	51.63 ±0.32
120	Thorax Under Apron	38.64 ±0.39	23.02 ±0.74
120	Waist Under Apron	16.50 ±0.17	9.26 ±0.22

Values presented as mean ± standard error

the patient and gantry, the male phantom is 13 cm taller than the female phantom. It was seen that TLD dosimetry at the thorax was more than that at the waist by a maximum factor of 2.5. Also, the TLD reading at the neck over the thyroid shield was more than that at the thorax and waist under apron by maximum factors of 2.2 and 5.6 respectively.

The TLD readings at the various positions (that is, neck over thyroid shield, thorax and waist under apron) of the staff were used to estimate staff effective dose using algorithms proposed by other studies (NCRP, 1995; Huyskens, Franken, & Hummel, 1994; Padovani, Foti, & Malisan, 2001;

Niklason, Marx, & Chan, 1994; Clerinx, Buls, Bosmans, & deMey, 2008; vonBoetticher, Lachmund, Hoffman, & Luska, 2003) in Table 6. The estimated effective doses from organ doses of this study were compared with that of the algorithms from other studies as shown in Table 19.

Table 19: Comparison of Estimated Effective Dose from Organ Absorbed Dose and TLD Readings

Source	Dosimetry Type	Estimated Effective Dose (μGy)	
		Male	Female
This Study (effective dose from organ doses)	-	1.95±0.32	3.21±0.43
NCRP Report 122, 1995	Single	2.75±0.23	2.46±0.31
Huyskens *et al.*, 1994	Single	11.57±0.29	10.32±0.14
Padovani *et al.*, 2001	Single	1.75±0.57	1.56±0.18
NCRP Report 122, 1995	Double	9.69±0.30	5.92±0.43
Niklason *et al.*, 1994	Double	17.33±0.44	10.11±0.25
Von Boetticher *et al.*, 2003	Double	26.06±0.61	15.84±0.07
Clerinx *et al.*, 2008	Double	67.61±0.15	41.62±0.28

(-) means not applicable; values presented as mean ± standard error

All the single dosimetry algorithms by other studies underestimated the effective dose to the staff for both sexes by a factor of 1.1 – 2.1 except that of Huyskens *et al* (Huyskens, Franken, & Hummel, 1994) and male staff dose by NCRP Report 122 (NCRP, 1995). Husykens *et al.* (Huyskens, Franken, & Hummel, 1994) overestimated the effective dose to the staff by a factor of 3.2 – 5.9. NCRP Report 122 (NCRP, 1995) overestimated effective dose for single and double dosimetry by a factor of 1.4 – 4.9 but underestimated for female staff dose single dosimetry by a factor of 1.3. All the double dosimetry algorithm by other studies overestimated the effective dose by a factor of 1.8 - 34.7.

Generally, it is clear that single or double dosimetry algorithm for a staff during CT fluoroscopy procedures overestimates or underestimates the actual absorbed dose. None of the algorithms from other studies (NCRP, 1995; Huyskens, Franken, & Hummel, 1994; Padovani, Foti, & Malisan, 2001; Niklason, Marx, & Chan, 1994; Clerinx, Buls, Bosmans, & deMey, 2008; vonBoetticher, Lachmund, Hoffman, & Luska, 2003) compared well with estimated effective dose from organ doses for both sexes. This lead to the need to propose effective dose algorithm for single and double TLD's for both male and female specifically for CT fluoroscopy as shown in Table 20.

The effective dose estimated from the proposed algorithm of this study compare well with that estimated from organ doses. The proposed algorithm overestimated the effective dose by a factor of 1.1 - 1.6 (10 – 60 %).

Table 20: Comparison of Algorithm and Organ Dose Estimated Effective Doses

Proposed Algorithm	Gender	Estimated Effective Dose from (mSv)	
		Algorithm	Organ Doses
Single Dosimetry			
$0.0625 \times H_p(0.07)_{\text{Neck,over collar}}$	Female	3.23±0.05	3.21±0.43
$(0.0625 \times H_p(0.07)_{\text{Neck,over collar}})/1.7$	Male	2.13±0.31	1.95±0.32
Double Dosimetry			
$(0.12 \times H_p(10)_{\text{under apron}}) + (0.01 \times H_p(0.07)_{\text{Neck,over collar}})$	Female	3.28±0.19	3.21±0.43
$[(0.12 \times H_p(10)_{\text{under apron}}) + (0.01 \times H_p(0.07)_{\text{Neck,over collar}})]/1.7$	Male	3.06±0.32	1.95±0.32

Values presented as mean ± standard error

Comparison of dose reduction factor

Radiation dose reduction factors observed for this study have been compared with published data by other studies in Table 21. It can be seen that studies by Karimian *et al.* (Karimian, Nikparvar, & Jabbari, 2014), Kicken *et al.* (Kicken, Kemerink, & van Engelshoven, 1999)and Marshall *et al.* (Marshall, Faulkner, & Clarke, 1992) observed significant dose reduction to the thyroid when protective equipment (lead apron, goggles and thyroid shield) are used by the staff. This observation was confirmed by this study as well but the reduction factors varied by 1.7 – 3.0 less.

Studies by Neeman *et al.* (Neeman, Sergio, Shawn, & Bradford, 2006) observed dose reduction to the hand of staff when fenestrated lead drape was

Table 21: Comparison of Dose Reduction Factors for Staff of this Study with other Studies

Protection	Organ	Dose Reduction Factor				
		This Study	Karimian et al. 2014	Kicken et al. 1999 & Marshal et al. 1992	Neeman et al. 2006	Cohen et al. 1997, McParland et al. 1990 & Kicken et al. 1999
Protective Equipment	Thyroid	3.0	8.9	5.0 – 7.0		
Lead Drape	Thyroid	3.5				
	Eye lens	5.1				
	Hand				1.3 – 2.7	
Patient Cover	Thyroid	1.7				
	Eye lens	1.7				
	Hand				1.4 – 5.5#	
Face mask/ shield	Thyroid	1.6				3.0 – 11.0

Protective equipment means lead apron, goggles and thyroid shield; # patient cover wrapped 360° around patient.

hanged on the gantry aperture and lead patient cover was wrapped 360° around the patient. The same could be said for this study when dose reduction to the thyroid and eye lens was observed when lead drape was also hanged on the gantry aperture and lead patient cover was wrapped 180° around the patient.

Ultimately, it can be said that the two studies observed dose reduction to staff when lead drape and lead patient cover was used.

The use of facial shield for protection of staff investigated by Cohen *et al.* (Cohen, et al., 1997), McParland *et al.* (McParland, Nosil, & Burry, 1990) and Kicken *et al.* (Kicken, Kemerink, & van Engelshoven, 1999) concluded on dose reduction factor of 3.0 – 11.0 to the thyroid of staff. It must be also said that there was an observed dose reduction factor of 1.6 to the thyroid of the staff when face mask was used for this study.

The staff dose reduction factors observed for applying protection measures for this study varied by a factor of 1.6 – 6.9 compared with other studies (Karimian, Nikparvar, & Jabbari, 2014; Kicken, Kemerink, & van Engelshoven, 1999; Marshall, Faulkner, & Clarke, 1992; Neeman, Sergio, Shawn, & Bradford, 2006; Cohen, et al., 1997; McParland, Nosil, & Burry, 1990). The variation could be attributed to the varying scenario settings and procedures considered.

Chapter Summary

A proposed three-point-exponential curve procedure was used verify all the four identified modelled CT scanners. The dose to the thyroid and effective dose to the staff was reduced by a factor of about 3.3, and 4.5 respectively when protective equipment were worn by the staff. Unfortunately, the eye lens remained unchanged within the uncertainties when protective equipment was worn by the staff.

The radiation dose to the thyroid, eye lens and effective dose of the sta-

-ff positioned on the left side of the patient in the diagonal positioning of the gantry were lower than the others (right and left staff position with gantry aligned; and right staff positon with gantry diagonal) by a maximum factor of 1.3, 1.2, and 1.2, respectively. When the floor dimension was increased by approximately 0.8 m on both sides of the room, that is, from (4.6 m x 5.87 m) to (5.06 m x 6.67 m), within the uncertainties (standard error), there was no reduction in the thyroid, eye lens and effective dose.

The application of both lead drape and patient cover significantly reduced the thyroid, eye lens and effective doses by a factor of 5.7, 7.1 and 4.3 respectively. The use of protective face mask and lead apron by the staff reduced the thyroid, eye lens and effective doses of the staff by a factor of 1.6, 1.1 and 2.8 respectively. Perspex and voxel phantom on the couch increased the scatter radiation dose in the room by a factor of about 2.4 and 23.5 respectively. The surroundings (walls, roof and floor) of the CT fluoroscopy room contributed to the scatter radiation in the room by a factor of 6.4. The CT gantry shielded the radiation and hence scatter radiation dose in the room were low on the sides of the gantry parallel to the patient couch.

Single or double dosimetry algorithm for staff effective dose estimation during CT fluoroscopy procedures overestimates or underestimates the actual absorbed dose. All the available dosimetry algorithms from literature did not compare well with estimated effective dose from organ doses for both sexes. Therefore, sex biased staff effective dose estimation algorithm for single and double dosimetry were proposed for CT fluoroscopy procedures. The staff dose reduction factors observed for applying protection measures for this study varied by a factor of 1.6 – 6.9 compared with other studies.

CHAPTER FIVE

CONCLUSIONS AND RECOMMENDATIONS

Overview and Summary

Staff dose reduction techniques during CT fluoroscopy procedures have been investigated using MCNP6 Monte Carlo code with the assistance of computational phantoms (FASH and MASH). Possible scenarios for dose reduction were investigated and conclusions and recommendations have been discussed below.

Conclusions

A systematic procedure or protocol called three-point-exponential curve have been proposed to effectively validate computational CT fluoroscopy machines. Since CT bowtie-filter is sophisticated and proprietary, this method would eliminate the trial-and-error methodology employed in other studies that can be very tedious and time-consuming. The three-point-exponential curve approach has successfully been used to validate four different brands of CT machines and the measured CTDI agreed with simulated CTDI within absolute value of 1.28 – 8.83 %. This was comparable with percentage deviations in studies other studies. Hence, the three-point-exponential curve is recommended for validation of CT scanners for computational studies when bowtie-filter thickness and shape is unknown.

Suggested dosimetry of male and female staff using single and double TLD dosimetry especially for CT fluoroscopy procedures has been proposed. It was observed that single dosimetry underestimated effective dose by a factor of 1.1 – 2.1 and in other instances overestimated by a factor of 3.2 – 5.9 using published algorithms. Double dosimetry also overestimated effective dose by a factor of 1.8 – 34.7. The proposed algorithm was additionally sex based since it was observed that estimated effective dose to staff from organ doses of a female was greater than that of the male by a factor of 1.7. The proposed algorithm from this study overestimated effective dose for male staff by 1.1 and 1.6 for single and double dosimetry respectively. The proposed algorithm for both single and double TLD dosimetry compared well with effective dose of females. Therefore, the proposed dosimetry algorithms of this study are recommended for use by radiation protection officers during staff dosimetry for CT fluoroscopy procedures.

The assessment and investigations into the effectiveness of already existing occupational dose reduction techniques published in literature in interventional radiology has successfully been conducted. The use of protective equipment (that is, lead apron, goggle and thyroid shield) by the staff reduced thyroid and effective dose by a factor of about 3.3 and 4.5 respectively. However, considering uncertainties (standard error) in the dose estimation, the staff eye lens dose was unchanged and it was attributed to unrealistic head position of the staff that is subject to future studies. The use of both lead drape and patient cover wrapped 180° around the patient reduced the thyroid, eye lens and effective doses by a factor of 5.8, 7.2 and 4.4 respectively. This concluded on lead drape contributing more dose reduction to the staff when compared with patient cover. The use of protective face mask and lead apron reduced the dose to the thyroid, eye lens and effective dose of staff by a factor of 1.6, 1.1 and 2.8 respectively. This led to additional conclusion that the closer a staff is to the patient and the lesser a body mass index, the more effective dose a staff would receive. The dose reduction factors observed by this study varied (1.6 – 6.9) when compared with published data by other studies due to varying scenarios. By the significant reduction in staff doses observed, emphasis is placed on the need to use these protections for the staff during CT fluoroscopy-guided procedures.

Alternative staff dose reduction techniques apart from the use of protection equipment were identified and investigated. The positioning of CT fluoroscopy gantry diagonally (30^{o}) as against aligned (0^{o}) in the CT room was generally observed to reduce thyroid, eye lens and effective dose by a factor of 1.1 – 1.3, 1.1 - 1.2 and 1.1 – 1.2 respectively. Staff standing on the left side of the patient as against the right side in a diagonal CT gantry positioning also resulted in reduction of thyroid, eye lens and effective dose by a maximum factor of 1.3, 1.2, and 1.2 respectively. The dose reduction was attributable to scatter radiation from the walls surrounding the room and hence, diagonal positioning of CT fluoroscopy gantry and staff positioning away from walls of the room if possible is advised for staff dose reduction. The CT fluoroscopy room size was found not to have any impact on the dose to the staff when increased from room size of 25 m^2 to 33.75 m^2. This suggests that increasing room size above the regulatory requirement (25 m^2) to reduce staff dose is not justifiable. The scatter radiation distribution investigation revealed that a body (that is, perspex or voxel phantom) on the couch increases the scatter radiation distribution in the room by a factor of 2.4 and 23.5 respectively. The voxel phantom scattered more radiation in the room than perspex phantom by a factor of 9.8 due to the greater volume and height of the first. The surroundings (that is, walls, floor, and ceiling) contributed a factor of 6.4 to the scatter radiation in the CT fluoroscopy room. The distribution of scatter radiation on the sides of the CT fluoroscopy gantry parallel to the patient table was found to be the lowest in the room. Therefore, staff is advised to stand by the sides of the CT fluoroscopy gantry if possible for reduced radiation exposure.

The study has successfully, addressed the objectives opined to enhance the protection of staff in CT fluoroscopy. The findings of this study have been promulgated in a publication at Oxford University Journal-Radiation Protection Dosimetry shown in Appendix L and a conference paper at International Conference on Radiation Protection in Medicine: Achieving Change in Practice, Vienna, Austria shown in Appendix M.

Recommendations

The study recommends further investigations in the application of the three-point-exponential curve in validating CT scanners by covering all tube voltages of a CT fluoroscopy scanner. Additionally, the employment of a movable phantom (that is, head and hand) to represent the staff phantom should be explored in the future for staff dose reduction. Lastly, further investigations on the impact of room floor area of the CT fluoroscopy scanner on staff dose reduction is recommended taking into consideration economic and social factors.

Engineering techniques are recommended to be explored by CT scanner manufacturers to enable the staff stand on the side of the gantry to perform clinical procedures since the scatter radiation in air was found to be less on the sides. Personnel service monitoring providers are recommended to apply the sex biased single or double TLD staff dosimetry algorithm proposed by this study specifically for CT fluoroscopy staff.

The radiation regulatory body is recommended to ensure that sex biased dosimetry of personnel is explored for implementation by the personnel service provider. The radiation regulatory body is encouraged to continue to ensure that radiation facilities, that is, CT fluoroscopy have protective equipment for staff.

Lastly, as an emphasis, the use of the three-point-exponential curve for validating CT scanners with unknown bowtie-filter, the need to use protection measures for staff dose reduction, the need to explore alternative dose reduction techniques , that is, gantry and staff positioning are recommended.

REFERENCES

AAPM. (2008). *The measurement, reporting and management of radiation dose in CT.* College Park: American Association of Physicist in Medicine (AAPM).

Bielajew, A. F. (2018). *National Research Council of Canada*. Retrieved from Photon Monte Carlo Simulation: http://rcwww.kek.jp/research/egs/docs/pdf/nrc-pirs0393.pdf

Bissoli, E., Bison, L., Gioulis, E., Chisena, C., & Fabbris, R. (2003). Multislice CT fluoroscopy: technical principles, clinical applications and dosimetry. *Radiol. Med., 106*, 201 - 212.

Buls, B., Vandenbroucke, F., & De Mey, J. (2012). Dose reduction in CT fluoroscopy. In D. Tack, M. K. Kalra, & P. A. Gevenois, *Radiation dose from multi-detector CT, Medical radiology imaging.* Berlin Heidelberg: Springer-Verlag.

Buls, N., Pages, J., de Mey, J., & Osteaux, M. (2003). Evaluation of patient and staff doses during various Ct fluoroscopy guided intervventions. *Helath Phys., 85*, 165 - 173.

Carlson, S. K., Bender, C. E., Classic, K. L., Zink, F. E., Quam, J. P., Ward, E. M., & Oberg, A. L. (2001). Benefits and Safety of CT Fluoroscopy in Interventional Radiologic Procedures. *Radiology, 219*, 515 - 520.

Cassola, V. F., de Melo Lima, V. J., Kramer, R., & Khoury, H. J. (2010). FASH and MASH: female and male adult human phantoms based on polygon mesh surfaces: I. Development of the anatomy. *Phys. Med. Biol., 55*, 133 - 162.

Cho, Y. B. (2014). CT Applications for radiation treatment of cancers. *Reference module in biomedical sciences*, 3973 - 3986.

Clerinx, P., Buls, N., Bosmans, H., & deMey, J. (2008). Double-dosimetry algorithm for workers in interventional radiology. *Radiat. Prot. Dosim., 129*(1 - 3), 321 - 327.

Cohen, R. V., Aldred, M. A., Paes, W. S., Fauto, A. M., Nucci, J. R., & Yoshimura, E. M. (1997). How safe is ERCP to the endoscopist? *Surg. Endosc., 11*, 615 - 617.

Cranley, K., Gilmore, B., Fogarty, G., & Deponds, L. (1997). *Catalogue of Diagnostic X-ray Spectra and other data* (Vol. Report No. 78). York: IPEM.

Daly, B., Krebs, T. L., Wong-You-Cheong, J. J., & Wang, S. S. (1999). Percutaneous abdominal and pelvic interventional procedures using Ct fluoroscopy guidance. *Am. J. Roentgenol., 173*, 637 - 644.

Deak, P., vanStraten, M., Shrimpton, P. C., Zankl, M., & Kalender, W. A. (2008). Validation of a Monte Carlo tool for patient specific-dose simulations in a multi-slice computed tomography. *Eur. Radiol., 18*, 759 - 772.

DeMarco, J. J., Cagnon, C. H., Cody, D. D., Stevens, D. M., McCollough, C. H., O'Daniel, J., & McNitty-Gray, M. F. (2005). A Monte Carlo based method to estimate radiation dose from mutidetector CT (MDCT): cylindrical and anthropomorphic phantoms. *Phys. Med. Biol., 50*, 3989 - 4004.

Ferrari, P., Becker, F., Carinou, E., Chumak, V., Farah, J., Jovanovic, Z., Krstic, D., Morgun, A., Principi, S., & Teles, P. (2016). Monte Carlo study of the scattered radiation field near the eyes of the operator in interventional procedures. *J. Radiol. Prot., 36*, 902 - 921.

Figueira, C., Becker, F., Blunck, C., DiMaria, S., Baptista, M., Esteves, B., Paulo, G., Santos, J., Teles, P., & Vaz, P. (2013). Medical staff extremity dosimetry in CT fluoroscopy: an anthropomorphic hand voxel phantom study. *Phys. Med. Biol., 58*, 5433 - 5448.

Froelich, J. J., Ishaque, N., Regan, J., Saar, B., Walthers, E. M., & Klose, K. J. (2002). Guidance of percutaneous pulmonary biopsies with real-time CT fluoroscopy. *Eur. J. Radiol., 42*(1), 74 - 79.

Froelich, J. J., Saar, B., Hoppe, M., Ishaque, N., Walthers, E. M., Regn, J., & Klose, J. K. (1998). Realtime CT-fluoroscopy for guidance of percutaneous drainage procedures. *J. Vasc. Interv. Radiol., 9*(5), 735 - 740.

Goldman, L. W. (2007). Princeiples of CT and CT Technology. *J. Nucl. Med. Technol.*, 115 - 128.

Gu, J., Bednarz, B., Caracappa, P. F., & Xu, X. G. (2009). The development, validation and application of a multi-detector CT (MDCT) scanner model for assessing organ dose to the pregnant patient and the fetus using Monte Carlo simulations. *Phys. Med. Biol., 54*, 2699 - 2717.

Gu, J., Bednarz, B., Xu, X. G., & Jiang, S. B. (2008). Assessment of patient organ doses and effective doses using the VIP-MAN adult male phantom for selecetd cone-beam CT imaging procdures during image guided radiation therapy. *Radiat. Prot. Dosim., 131*, 431 - 443.

Gyekye, P. K., Becker, F., Mensah, S. Y., & Emi-Reynolds, G. (2016). Optimisation of scatter radiation to staff during CT fluoroscopy: Monte Carlo studies. *Radiat. Prot. Dosim., 170*(1 - 4), 393 - 397.

Hohl, C., Suess, C., Wildberger, J. E., Honnef, D., Das, M., Muehlenbruch, G., . . . Mahnken, A. H. (2008). Dose reduction during CT fluoroscopy: Phantom study of angular beam modulation. *Radiology, 246*, 2.

Hounsfield, G. N. (1973). Computerised transverse axial scanning (tomography), part 1: description of system. *Br. J. Radiol., 46*, 1016 - 1022.

Huyskens, C. J., Franken, Y., & Hummel, W. A. (1994). Guidance on personal dosimetry for occupational exposure in interventional radiology. *J. Radiol. Prot., 14*, 229.

IAEA. (1999a). *Occupational radiation protection* (Vols. Safety Guide No. RS-G-1.1). Vienna: International Atomic Energy Commission (IAEA).

IAEA. (1999b). *Assessment of occupational exposure due to external sources of radiation* (Vols. Safety Guide No. RS-G-1.3). Vienna: International Atomic Energy Agency (IAEA).

IAEA. (2014a). *Diagnostic Radiology: A Handbook for teachers and students.* Vienna: International Atomic Energy Commission.

IAEA. (2014b). *Radiation Potection and Safety of Radiation Sources: International Basic Safety Standard* (Vol. General Safety Requirements Part 3). Vienna: International Atomic Energy Agency (IAEA).

ICRP. (1990). *1990 Recommendations of International Commission on Radiological Protection.* Oxford: Pergamon Press.

ICRP. (2000). *Avoidance of radiation injuries from medical interventional procedures* (Vol. ICRP Publication 85). Oxford: Pergamon Press.

ICRP. (2002). *Basic anatomical and physiological data for use in radiological protection: reference values* (Vol. Pulbication 89). Oxford: Pergamon.

ICRP. (2007). *The 2007 Recommendations of the International Commission on Radiological Protection* (Vol. 37). (J. Valtin, Ed.) Stockholm: Elsevier.

ICRU. (1985). *Determination of dose equivalent resulting from external radiation sources* (Vol. Report No. 39). Bethesda: International Commission on Radiation Units and Measurement (ICRU).

ICRU. (1993). *Quantities and units in radiation protection dosimetry* (Vol. Report No. 51). Bethesda: Internation Commission on Radiation Units and Measurments.

Iinuma, T. A., Tateno, Y., Umegaki, Y., & Wantanbe, E. (1977). Proposed system for ultrafast computed tomography. *J. Comput. Assist Tomogr., 1*, 494 - 499.

ILO. (2018, March 9). *Radiation Protection.* Retrieved from International Labour Organisation: http://www.ilo.org/safework/areasofwork/radiation-protection/lang--en/index.htm

Irie, T., Kajitani, M., Matsueda, K., Arai, Y., Inaba, Y., Kujiraoka, Y., & Itai, Y. (2001). Biopsy of Lung Nodules with Use of I-I Device Under

Intermittent CT Fluoroscopic Guidance: PreliminaryClinical Study. *J. Vasc. Interv. Radiol., 12*, 215 - 219.

ITN. (2012, November/December April, 2018). *WWW.ITNonline.com.* Retrieved from Imaging Technology News 2012 Comparison Chart: https://www.itnonline.com/chart/computed-tomography-systems

Joemai, R. M., Zweers, D., Obermann, W. R., & Geleijns, J. (2009). Assessment of patient and occupational dose in established and new applications of MDCT fluoroscopy. *Am. J. Roentgenol., 192*, 881 - 886.

Kalender, W. A., Seissler, W., Klotz, E., & Vock, P. (1990). Spiral volumetric CT with single-breath hold technique, continuos transparent and scanner rotation. *Radiology, 176*, 181 - 183.

Karimian, B., Nikparvar, B., & Jabbari, I. (2014). Assessment of physician and patient (child and adult) equivalent doses during renal angiography by Monte Carlo method. *Radiat. Prot. Dosim., 12*(1 - 2), 120 - 124.

Katada, K., Anno, H., Koga, S., Ida, Y., & Sata, S. (1993). Initial trial with CT fluoroscopy. *Radiology, 190*, 622 - 622.

Katada, K., Anno, H., Ogura, Y. K., Nonomura, K., & Kanno, T. (1995). Puncture and drainage of intracranial lesions with CT fluoroscopic guidance. *Radiology, 197(Suppl)*, 494.

Katada, K., Kato, R., Anno, H., Ogura, Y., Koga, S., Ida, Y., Sato, M., & Nonomura, K. (1996). Guidance with Real-Time CT Fluoroscopy: Early Clinical Experience. *Radiology, 200*, 851 - 856.

Kato, R., Katada, K., Anno, H., Suzuki, S., Ida, Y., & Koga, S. (1996). Radiation dosimetry at CT fluoroscopy: physician's hand dose and development of needle holders. *Radiology, 201*, 576 - 578.

Keat, N. (2001). Real-time CT and CT fluoroscopy. *Br. J. Radiol., 74*, 1088 - 1090.

Ketteringham, J., & Gempel, P. (1978). *History of computed tomography: 1967–1978 - excerpts from an ongoing study for the National Science Foundation.* Cambridge, MA: Arthur D. Little Inc.

Kicken, P. J., Kemerink, G. J., & van Engelshoven, J. M. (1999). Dosimetry of occupationally exposed person in diagnostic and interventional arteriography. Part I: Assessment of entrance doses. *Radiat. Prot. Dosim., 82*, 93 - 103.

Kramer, R., Khoury, H. J., Vieira, J. W., & Lima, V. J. (2006). MAX06 and FAX06: update of two adult phantoms for radiation protection dosimetry. *Phys. Med. Biol., 51*, 3331 - 46.

LANL. (2014). *MCNP6 users manual* (LA-CP-14-00745 ed.). (B. B. Pelowitz, J. A. Fallgreen, & E. G. McMathe, Eds.) Los Alamos: Los Alamos National Laboratory (LANL).

Marshall, N. W., Faulkner, K., & Clarke, P. (1992). An investigation into the effect of protective devices on the dose to radiosensitive organs in the head and neck. *Br. J. Radiol., 65*, 799 - 802.

Martin, C. J. (2009). A review of radiology staff doses and dose monitoring requirements. *Radiat. Prot. Dosim., 136*(3), 140 - 157.

McCollough, C. H. (1995). Principles and performance of electron beam CT. In L. W. Goldman, & J. B. Fowlkes, *Medical CT and ultrasound: Current technologies and applications* (pp. 487 - 518). Madison, WI: Advanced Medical Publishing.

McParland, B. J., Nosil, J., & Burry, B. (1990). A survey of the radiation exposures received by the staff at two cardiac catheterisation laboratories. *Br. J. Radiol., 63*, 885 - 888.

Meyer, C. A., White, C. S., Wu, J., Futterer, S. F., & Templeton, P. A. (1998). Real-time CT fluoroscopy: usefulness in thoracic drainage. *Am. J. Roentgenl., 171*, 1097 - 1101.

Nawfel, R. D., Judy, P. F., Silverman, S. G., Hooton, S., Tuncali, K., & Adams, D. F. (2000). Patient and personnel exposure during CT fluoroscopy-guided interventional procedures. *Radiology, 216*, 180 - 184.

NCRP. (1995). *Use of personal monitors to estimate effective dose equivalent and effective dose to workers for external exposure to low-LET* *radiation*. Bethesda: National Council on Radiation Protection and Measurements.

Neeman, Z., Sergio, A. D., Shawn, S., & Bradford, J. W. (2006). CT fluoroscopy shielding: Decreases in scattered radiation for the patient and operator. *J. Vasc. Interv. Radiol., 17*, 1999 - 2004.

Niklason, L. T., Marx, M. V., & Chan, H. P. (1994). The estimation of occupational effective dose in diagnostic radiology with two dosimeters. *Health Phys., 67*(6), 611 - 615.

NRA. (2018, May). *Structural shielding and room layout requirments for starting a diagnostic x-ray installation*. Retrieved from www.gnra.org.gh: https://www.gnra.org.gh/images/Download/client/Diagnostic_Radiology_Structural_shielding_Requirements_Room_Layout_Fin.pdf

Oono, T., Araki, F., Tsuduki, S., & Kawasaki, K. (2014). Monte Carlo calculation of patient organ doses from computed tomography. *Radiol. Phys. Technol., 7*, 176 - 182.

Padovani, R., Foti, C., & Malisan, M. R. (2001). Staff dosimetry protocols in interventional radiology. *Radiat. Prot. Dosim., 94*, 193 - 196.

Paulson, E. K., Sheafor, D. H., Enterline, D. S., McAdams, H. P., & Yoshizumi, T. T. (2001). CT Fluoroscopy-guided Interventional Procedures: Techniques and Radiation Dose to Radiologists. *Radiology, 220*, 161 - 167.

Pereira, M. F., Alves, J. G., Sarmento, S., Santos, J. A., Sousa, M. J., Gouvea, M., . . . Santos, L. M. (2011). Preliminary assessment of the dose to the interventional radiologist in fluoro-CT-guided procedures. *Radiat. Prot. Dosim., 144*(1 - 4), 448 - 452.

Poelz, S., Laubersheimer, S., Eberhardt, S. J., Henrrendorf, M. A., Keck, T., Benzler, A., & Breustedt, B. (2013). Voxel2MCNP: a framework for modeling, simulation nd evaluation of radation transport scenarios for Monte Carlo codes. *Phys. Med. Biol., 58*, 5381 - 5400.

Poludniowski, G. G. (2007b). Calculation of x-ray spectra emerging from an x-ray tube: Part II. X-ray production and filtration in x-ray targets. *Med. Phys.*, 2175 - 2176.

Poludniowski, G. G., & Evan, P. M. (2007a). Calculation of x-ray spectra emerging from an x-ray tube: Part I. Electron penetration characteristics in x-ray target. *Med. Phys.*, 2164 - 2174.

Poludniowski, G. G., Landry, G., DeBlois, F., Evans, P. M., & Verhaegen, F. (2009). SpekCalc: a programme to calculate photon spectra from tungsten anode x-ray tubes. *Phys. Med. Biol.*, N433 - N438.

RTIElectronic, A. (2018, March 23). *Ocean 2014*. Retrieved from RTIGroup.com: http://rtigroup.com/products/product-detail/ocean-2014

RTIElectronics, A. (2012). *CT Dose profiler*. Sweden: RTI Electronics Group AB.

Sato, K., Noguchi, H., Endo, A., Emoto, Y., Koga, S., & Saito, K. (2007). Development of a voxel phantom of Jappanesse adult male in upright posture. *Radiat. Prot. Dosim., 127*, 205 -8.

Seeram, E. (2010). Computed Tomography: Physical Principles and Recent Technical Advances. *Journal of Medical Imaging and Radiation Sources, 41*(2), 87 - 109.

Sheafor, D. H., Paulson, E. K., Kliewer, M. A., De-Long, D. M., & Nelson, R. C. (2000). Comparison of sonographic and CT guidance techniques: dose CT fluoroscopy decrease procedure time? *Am. J. Roentgenol., 174*, 939 - 942.

Siebel, R. M., Sehnert, C. P., & Schmit, A. M. (1997). Interventional procedures with real time CT. *Radiology, 205*, 383.

Silverman, S. G., Tuncali, K., Adams, D. F., Nawfel, R. D., Zou, K. H., & Judy, P. F. (1999). CT fluoroscopy guided abdominal interventions: techniques, results and radiation exposure. *Radiology, 212*, 673 - 681.

Sprawls, P. (2018, March 14). *Sprwals Educational Foundation*. Retrieved from Interaction of Radiation with Matter: http://www.sprawls.org/ppmi2/INTERACT/#CHAPTER CONTENTS

Stewart, F. A., Akleyev, A. V., Hauer-Jensen, M., Hendry, J. H., Kleiman, N. J., Macvittie, T. J., . . . Wallace, W. H. (2012). ICRP pulblication 118: Statement on tissue reactions/early and late effects of radiation in normal tissues and organs - threshold doses for tissue reactions in radiation protection context. *Ann ICRP, 41*(1 - 2), 1 - 322.

Stoeckelhuber, B. M., Leibecke, T., Schulz, E., Melchert, U. H., Bergmann-Koester, C. U., Helmberger, T., & Gellissen, J. (2005). Radiation Dose to Radiologist's hand during continuous CT fluoroscopy-guided interventions. *Cardiovasc. Intervent. Radiol., 28*, 589 - 594.

Teles, P., Nikodemova, D., Bakhanova, E., Becker, F., Knezevic, Z., Pereira, M. F., & Sarmento, S. (2017). A review of radiation protection requirements and dose estimation for staff and patients in CT fluoroscopy. *Radiat. Prot. Dosim., 174*, 518 - 534.

Theis, C., Buchegger, K. H., Forkel-Wirth, D., Roesler, S., & Vincke, H. (2006). Interactive three-dimensional visualisation and creation of geometries for Monte Carlo calculations. *Nuclear Instruments and Methods in Physics Research, A562*, 827 - 829.

Toki, Y. (1993). Principles of helical scanning. In K. S. Kimura, *Basic principles of clinical applications of helical scan: applications of continuos rotation CT* (pp. 110 - 120). Tokyo: Iryokagakusha.

Toth, T. L., Cesmeli, E., Ikhlef, A., & Horiuchi, T. (2005). Image quality and dose optimisation using novel x-ray source filters tailered to patient size. *Proc. SPIE, 5745*, 238 - 291.

Vano, E., & Faulkner, K. (2005). ICRP special radiation protection issues in interventional radiology, digital and cardiac imaging. *Radiat. Prot. Dosim., 117*(1 - 3), 13 - 17.

vonBoetticher, H., Lachmund, J., Hoffman, W., & Luska, G. (2003). Strahlenexposition des personals in der roentgendiagnostik:

Bestimmung de effektiven dosis mit dem 2-dosimeter-verfahren. *Proceedings of Jahrestagung, 12- 15 October, 2003* (pp. 109 - 113). Dortmund: ISBN 3-00-012084-X.

Williams, T., & Kelley, C. (2014). *GNUPlot 4.6.* GNUPlot.

X-5MonteCarloTeam. (2008). *MCNP-A General Monte Carlo N-Particle transport code version 5* (Vol. Volume I: Overview and Theory). Los Alamos, USA: Los Alamos National Laboratory.

Yoshimatsu, R., Yamagami, T., Kato, T., Hirota, T., Matsumoto, T., Shimada, J., & Nishimura, T. (2008). Percutaneous needle biopsy of lung nodules under CT fluoroscopic guidance with use of the I-I device. *Br. J. Radiol., 81*, 107 - 112.

Zankl, M., & Wittmann, A. (2001). The adult male voxel model "Golem" segmented from whole-body CTpatient data. *Radiat. Environ. Biophys., 40*, 153 - 62.

Zankl, M., Eckerman, K. F., & Bolch, W. E. (2007). Voxel-based models representing the male and female ICRP reference asult - the skeleton. *Radiat. Prot. Dosim.*(127), 174 - 86.

Zhang, J. Y., Na, Y. H., & Xu, X. G. (2008b). Development of whole-body phantoms representing an average adult male and female using surface-geometry methods. *Med. Phys., 35*, 2875.

Zhang, J., Na, Y. H., & Xu, X. G. (2008a). Size adjustable worker models for improved radiation protection dosimetry. *Helath Phys., 95*, S50.

Zhang, J., Na, Y. H., Caracappa, P. F., & Xu, X. G. (2009). RPI-AM and RPI-AF, a pari of mesh-based, size-adjustable adult male and female computational phantoms using ICRP-89 parameters and their calculations for organ doses from monoenergetic photn beams. *Phys. Med. Biol., 54*, 5885 - 908.

APPENDICES

APPENDIX A

TYPICAL MCNP6 SIMULATION INPUT FILE FOR COMPUTED TOMOGRAPHY VALIDATION

```
CT Validation/.......
c
c ---------------------------------------------------------------------
c --- Cells ------------------------------------------------------------
c ---------------------------------------------------------------------
c
read file=gantry-cells.i noecho
read file=perspex-cells.i noecho
read file=ionisationChanber-cells.i noecho

c
c ---------------------------------------------------------------------
c --- Surfaces ---------------------------------------------------------
c ---------------------------------------------------------------------
c
read file=gantry-surfaces.i noecho
read file=perspex-surfaces.i noecho
read file=ionisationChamber-surfaces.i noecho

c
c ---------------------------------------------------------------------
c --- Mode -------------------------------------------------------------
c ---------------------------------------------------------------------
c
mode p
c
imp:p 1 11r 0
c
c ---------------------------------------------------------------------
c --- Transformations --------------------------------------------------
c ---------------------------------------------------------------------
c
read file=transformations_20.i noecho
c
c ---------------------------------------------------------------------
c --- Materials --------------------------------------------------------
c ---------------------------------------------------------------------
c
read file=gantry-materials.i noecho
```

```
read file=perspex-materials.i noecho
read file=ionisationChamber-materials.i noecho
c
c ---------------------------------------------------------------------------
c --- Source ----------------------------------------------------------------
c ---------------------------------------------------------------------------
c
sdef par=p erg=d1 x=60 y=0 z=0 cell=6 rad=d2 wgt=1 tr=1
c
c ---------------------------------------------------------------------------
c --- Source Distributions --------------------------------------------------
c ---------------------------------------------------------------------------
c
read file=distributions.i noecho
read file=ct-distributions.i noechoc
c
c ---------------------------------------------------------------------------
c --- Tally -----------------------------------------------------------------
c ---------------------------------------------------------------------------
c
FC6: Energy in air of ionisation chamber
F6:p 32
FC26: Energy in wall of ion chamber
F26:p 30
FC36: Energy in build-up cap of ion chamber
F36:p 31
c
c
c ---------------------------------------------------------------------------
c --- Control ---------------------------------------------------------------
c ---------------------------------------------------------------------------
c
stop f6 0.05
c nps 1.5e9
prdmp j -60 1 1 100000
```

APPENDIX B

TYPICAL MCNP6 SCENARIO BASED SIMULATION INPUT FILE

```
Scenario/......
c
c --------------------------------------------------------------------------
c --- Cells ----------------------------------------------------------------
c --------------------------------------------------------------------------
c
read file=patient-lattice.i noecho
read file=patient-cells.i noecho
read file=staff-lattice.i noecho
read file=staff-cells.i noecho
read file=gantry-cells.i noecho
read file=mask-cells.i noecho
read file=room-cells.i noecho
read file=shield-cells.i noecho
read file=void-cells.i noecho

c
c --------------------------------------------------------------------------
c --- Surfaces -------------------------------------------------------------
c --------------------------------------------------------------------------
c
read file=patient-surfaces.i noecho
read file=staff-surfaces.i noecho
read file=gantry-surfaces.i noecho
read file=mask-surfaces.i noecho
read file=room-surfaces.i noecho
read file=shield-surfaces.i noecho

c
c --------------------------------------------------------------------------
c --- Mode -----------------------------------------------------------------
c --------------------------------------------------------------------------
c
mode p
c
imp:p 1 279r 0
c
c --------------------------------------------------------------------------
c --- Transformations ------------------------------------------------------
c --------------------------------------------------------------------------
c
read file=transformations_30.i noecho
```

```
c
c -----------------------------------------------------------------------
c --- Materials ---------------------------------------------------------
c -----------------------------------------------------------------------
c
read file=icrp-materials.i noecho
read file=gantry-materials.i noecho
read file=mask-materials.i noecho
read file=room-materials.i noecho
read file=shield-materials.i noecho
c
c -----------------------------------------------------------------------
c --- Source ------------------------------------------------------------
c -----------------------------------------------------------------------
c
sdef par=p wgt=0.9998052821 tr=6 erg=D2 cel=D1 x=60 y=0 z=0
rad=D3
c
c -----------------------------------------------------------------------
c --- Source Distributions ----------------------------------------------
c -----------------------------------------------------------------------
c
read file=distributions.i noecho
read file=ct-distributions.i noecho
c
c -----------------------------------------------------------------------
c --- Tallys ------------------------------------------------------------
c -----------------------------------------------------------------------
c
read file=tallys.i noecho
c
c -----------------------------------------------------------------------
c --- Control -----------------------------------------------------------
c -----------------------------------------------------------------------
c
stop nps=1900000000
prdmp j -60 1 1 100000
```

APPENDIX C

MODELLED ROOM AND GANTRY AT KORLE-BU TEACHING HOSPITAL, ACCRA

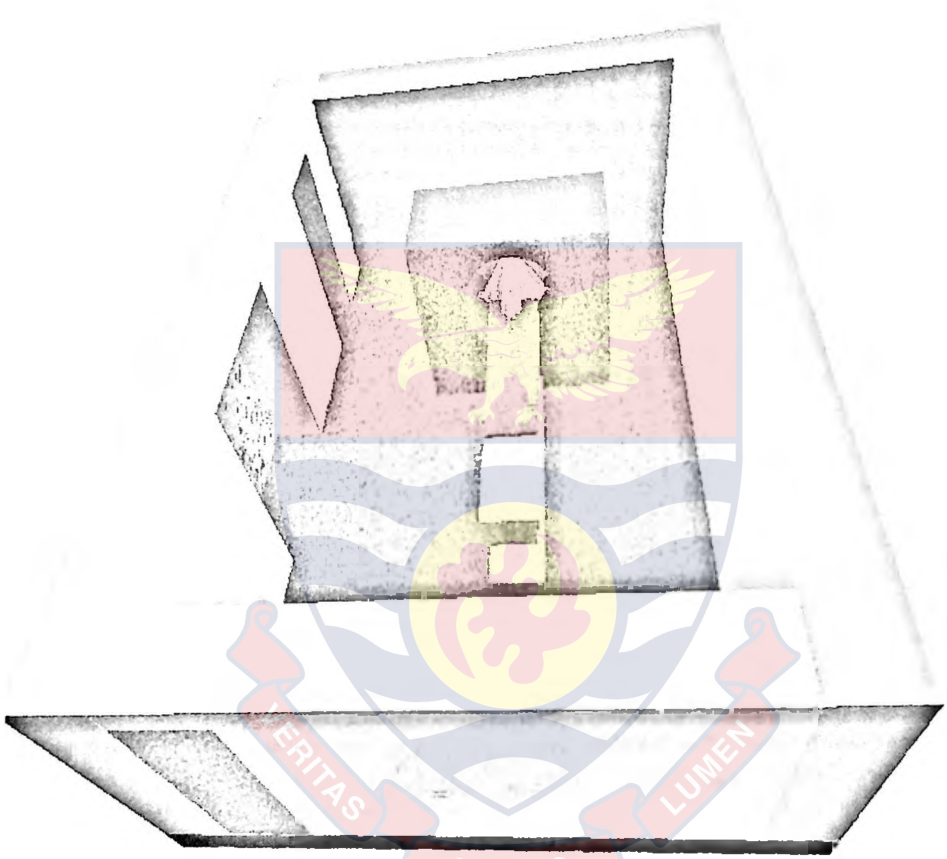

APPENDIX D

MODELLED ROOM AND GANTRY AT SWEDEN GHANA MEDICAL CENTRE, ACCRA

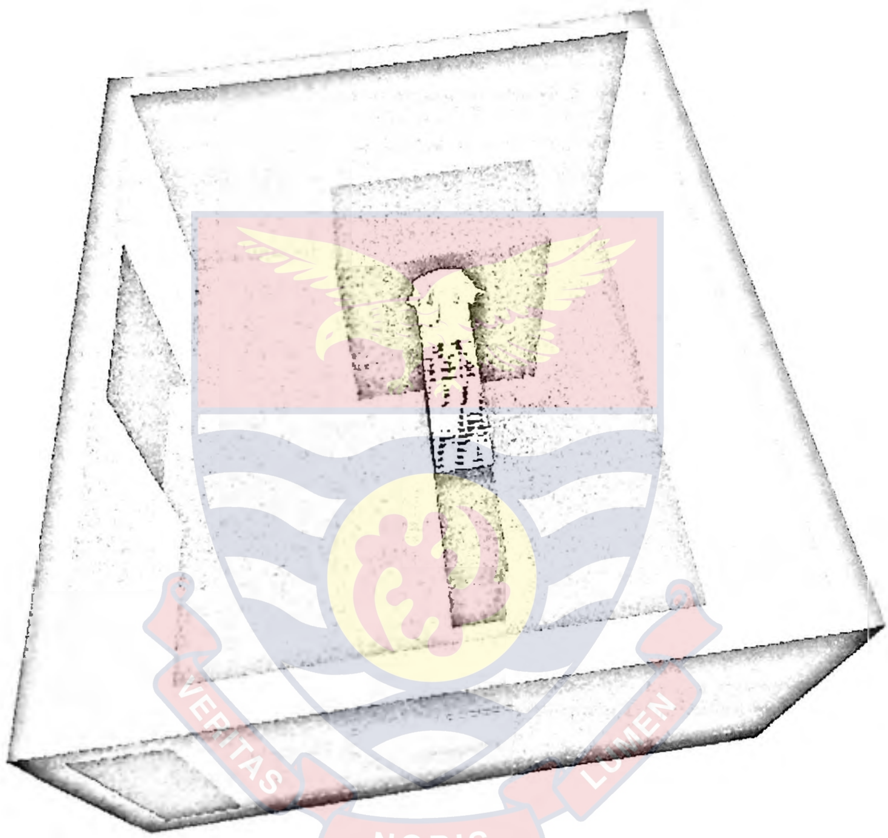

APPENDIX E

MODELLED ROOM AND GANTRY AT KARLSRUHE HOSPITAL, GERMANY

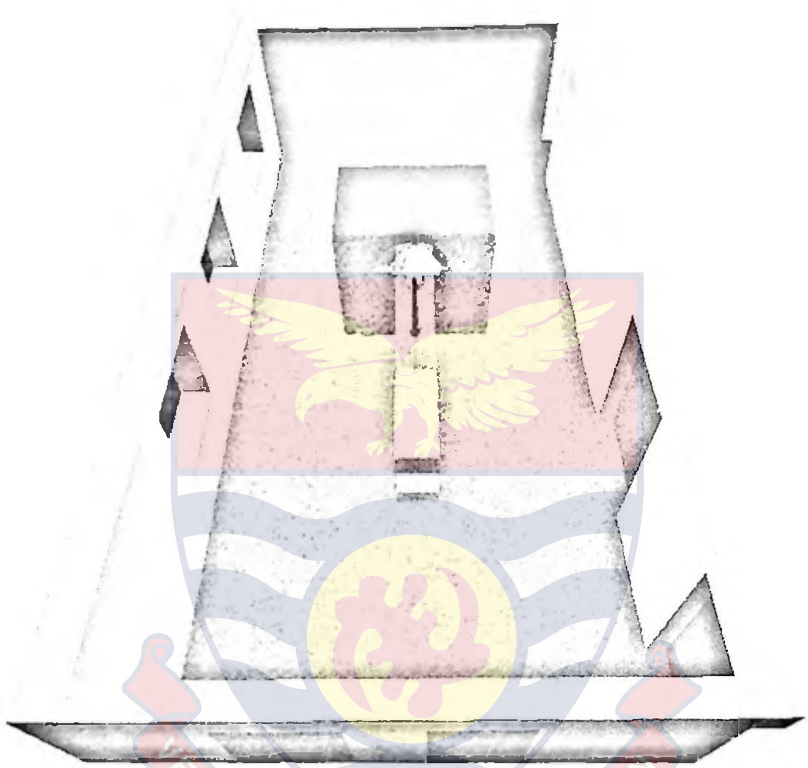

APPENDIX F

MODELLED ROOM AND GANTRY AT FOCOS ORTHOPAEDIC HOSPITAL, ACCRA

APPENDIX G

PHOTON ENERGY SPECTRUM FOR 130 KVP @ 2.5 MM AL FILTER AND 12 DEGREES TUNGSTEN ANODE ANGLE

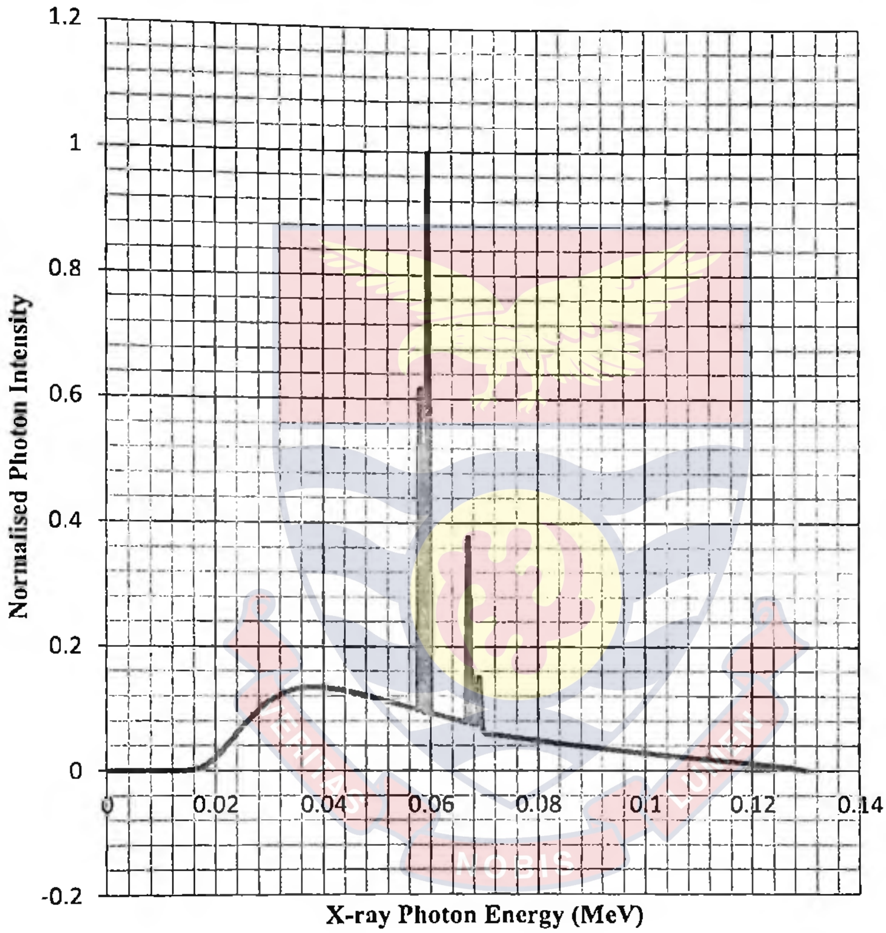

APPENDIX H

DOSE IN AIR IN A ROOM WITH NO PHANTOM

X-axis	Y-axis	Dose at 138.3 cm from the floor of room (mGy/100mAs)
-213.5	-410.75	3.603325551
-162.9	-410.75	8.048359352
-112.3	-410.75	16.28157195
-61.7	-410.75	28.01619608
-11.1	-410.75	30.34077981
39.5	-410.75	26.22825012
90.1	-410.75	13.85408596
140.7	-410.75	7.133348386
191.3	-410.75	2.837326993
241.9	-410.75	1.030710175
-213.5	-350.114	1.496241148
-162.9	-350.114	4.137054223
-112.3	-350.114	17.15577684
-61.7	-350.114	49.8276621
-11.1	-350.114	56.10528408
39.5	-350.114	44.65702501
90.1	-350.114	14.07690351
140.7	-350.114	3.015486329
191.3	-350.114	1.085365769
241.9	-350.114	0.78264415
-213.5	-289.477	1.259744294
-162.9	-289.477	1.379320433
-112.3	-289.477	386.2332005
-61.7	-289.477	18379.45769
-11.1	-289.477	5524.842122

39.5	-289.477	17503.18343
90.1	-289.477	337.1372988
140.7	-289.477	1.28346261
191.3	-289.477	1.119705162
241.9	-289.477	0.877185946
-213.5	-228.841	1.360080607
-162.9	-228.841	1.515784767
-112.3	-228.841	130.8610936
-61.7	-228.841	1578122253
-11.1	-228.841	201493.6915
39.5	-228.841	1578004952
90.1	-228.841	55.72748588
140.7	-228.841	1.002566441
191.3	-228.841	1.257226008
241.9	-228.841	1.134026797
-213.5	-168.205	5.72630375
-162.9	-168.205	11.44172814
-112.3	-168.205	594.1892683
-61.7	-168.205	71544.13124
-11.1	-168.205	59772.78748
39.5	-168.205	42021.75431
90.1	-168.205	437.8167012
140.7	-168.205	6.163014158
191.3	-168.205	2.833599069
241.9	-168.205	1.803750893
-213.5	-107.568	11.26219128
-162.9	-107.568	17.88995399
-112.3	-107.568	39.41463984
-61.7	-107.568	2248.154402
-11.1	-107.568	10025.71945

39.5	-107.568	447.1411845
90.1	-107.568	31.13398139
140.7	-107.568	14.09904229
191.3	-107.568	7.909810283
241.9	-107.568	5.169964008
-213.5	-46.9318	10.25051473
-162.9	-46.9318	14.80146873
-112.3	-46.9318	24.61779257
-61.7	-46.9318	651.4059497
-11.1	-46.9318	3280.906264
39.5	-46.9318	147.3289726
90.1	-46.9318	21.36460713
140.7	-46.9318	12.01600951
191.3	-46.9318	8.056462144
241.9	-46.9318	5.61690991
-213.5	13.7045	8.432177151
-162.9	13.7045	11.20020178
-112.3	13.7045	15.98954612
-61.7	13.7045	439.1328822
-11.1	13.7045	2110.260825
39.5	13.7045	94.36135875
90.1	13.7045	14.50439127
140.7	13.7045	9.800480468
191.3	13.7045	6.844692884
241.9	13.7045	5.524964501
-213.5	74.3409	6.833178876
-162.9	74.3409	8.837294912
-112.3	74.3409	11.13510271
-61.7	74.3409	157.3865261
-11.1	74.3409	726.3935184

APPENDIX I

DOSE IN AIR IN A ROOM WITH PERSPEX PHANTOM

X-axis	Y-axis	Dose at 138.3 cm from the floor of room (mGy/100mAs)
-213.5	-410.75	3.905450346
-162.9	-410.75	10.21573195
-112.3	-410.75	21.66725956
-61.7	-410.75	34.01869151
-11.1	-410.75	36.35776691
39.5	-410.75	32.43358901
90.1	-410.75	18.56270833
140.7	-410.75	8.407091766
191.3	-410.75	3.000641665
241.9	-410.75	1.156358057
-213.5	-350.114	1.668659162
-162.9	-350.114	4.46647459
-112.3	-350.114	22.52479273
-61.7	-350.114	60.91542503
-11.1	-350.114	68.04285007
39.5	-350.114	54.89677752
90.1	-350.114	17.37931698
140.7	-350.114	3.385809622
191.3	-350.114	1.312065907
241.9	-350.114	0.88172132
-213.5	-289.477	1.381823344
-162.9	-289.477	1.676643265
-112.3	-289.477	472.5243053
-61.7	-289.477	23228.19083
-11.1	-289.477	6666.809053
39.5	-289.477	21685.05976

90.1	-289.477	381.9703793
140.7	-289.477	1.413471646
191.3	-289.477	1.293452117
241.9	-289.477	1.041747154
-213.5	-228.841	1.563319178
-162.9	-228.841	1.741218999
-112.3	-228.841	149.3533207
-61.7	-228.841	1578042798
-11.1	-228.841	577698.7401
39.5	-228.841	1577976832
90.1	-228.841	60.97919086
140.7	-228.841	1.126521137
191.3	-228.841	1.417441867
241.9	-228.841	1.279710087
-213.5	-168.205	6.150434721
-162.9	-168.205	13.43591216
-112.3	-168.205	686.44788
-61.7	-168.205	69217.05075
-11.1	-168.205	79319.84727
39.5	-168.205	40634.34493
90.1	-168.205	508.1912871
140.7	-168.205	7.589095374
191.3	-168.205	3.155340971
241.9	-168.205	1.990944386
-213.5	-107.568	15.04775339
-162.9	-107.568	25.4291418
-112.3	-107.568	51.77472435
-61.7	-107.568	2528.441109
-11.1	-107.568	11591.14335
39.5	-107.568	514.8902653

90.1	-107.568	41.24215271
140.7	-107.568	20.13859864
191.3	-107.568	11.02262882
241.9	-107.568	6.439951483
-213.5	-46.9318	14.58962833
-162.9	-46.9318	20.16351399
-112.3	-46.9318	31.53277761
-61.7	-46.9318	736.6485067
-11.1	-46.9318	3652.311589
39.5	-46.9318	167.4301998
90.1	-46.9318	27.71773464
140.7	-46.9318	16.74422931
191.3	-46.9318	11.53334515
241.9	-46.9318	8.090573078
-213.5	13.7045	11.59784648
-162.9	13.7045	14.98548193
-112.3	13.7045	19.94813445
-61.7	13.7045	492.7597303
-11.1	13.7045	2325.037265
39.5	13.7045	116.758546
90.1	13.7045	18.53456133
140.7	13.7045	13.26603088
191.3	13.7045	9.524281102
241.9	13.7045	7.879751668
-213.5	74.3409	9.21474935
-162.9	74.3409	11.39369929
-112.3	74.3409	13.85931932
-61.7	74.3409	180.3399439
-11.1	74.3409	817.3289385
39.5	74.3409	51.74179907

90.1	74.3409	13.05766319
140.7	74.3409	10.45655416
191.3	74.3409	8.139778966
241.9	74.3409	6.693013369
-213.5	134.977	7.46495711
-162.9	134.977	8.898954169
-112.3	134.977	10.05240405
-61.7	134.977	9.57056498
-11.1	134.977	8.660376269
39.5	134.977	9.548521831
90.1	134.977	9.315125328
140.7	134.977	8.246259097
191.3	134.977	6.859291562
241.9	134.977	5.630499121
-213.5	195.614	6.275010533
-162.9	195.614	7.718837823
-112.3	195.614	7.861215363
-61.7	195.614	7.014837369
-11.1	195.614	6.412558438
39.5	195.614	7.004479189
90.1	195.614	7.528683883
140.7	195.614	7.061949605
191.3	195.614	5.74185009
241.9	195.614	4.676860604

APPENDIX J

DOSE IN AIR IN A ROOM WITH VOXEL PHANTOM

X-axis	Y-axis	Dose at 138.3 cm from the floor of room (mGy/100mAs)
-213.5	-410.75	62.23280824
-162.9	-410.75	173.3835102
-112.3	-410.75	420.3974514
-61.7	-410.75	697.0162857
-11.1	-410.75	780.2642313
39.5	-410.75	670.172098
90.1	-410.75	377.7785559
140.7	-410.75	146.9432014
191.3	-410.75	50.1756775
241.9	-410.75	18.43906327
-213.5	-350.114	29.4843751
-162.9	-350.114	76.68948093
-112.3	-350.114	411.1128795
-61.7	-350.114	1263.447619
-11.1	-350.114	1505.573257
39.5	-350.114	1167.162395
90.1	-350.114	310.9418694
140.7	-350.114	60.50125159
191.3	-350.114	26.79611279
241.9	-350.114	18.29282743
-213.5	-289.477	26.34233246
-162.9	-289.477	30.86849135
-112.3	-289.477	7731.908925
-61.7	-289.477	395978.9048
-11.1	-289.477	150491.4014
39.5	-289.477	390343.049

90.1	-289.477	6301.959265
140.7	-289.477	29.58502659
191.3	-289.477	25.12377429
241.9	-289.477	20.20142356
-213.5	-228.841	30.94672117
-162.9	-228.841	26.72643099
-112.3	-228.841	1978.796348
-61.7	-228.841	1574401822
-11.1	-228.841	39599861.44
39.5	-228.841	1571896113
90.1	-228.841	1390.921459
140.7	-228.841	26.29704022
191.3	-228.841	30.60085507
241.9	-228.841	26.83324136
-213.5	-168.205	80.62689905
-162.9	-168.205	206.7994705
-112.3	-168.205	13326.33137
-61.7	-168.205	1064865.109
-11.1	-168.205	3209556.988
39.5	-168.205	789743.6552
90.1	-168.205	9887.324735
140.7	-168.205	170.5227499
191.3	-168.205	69.2721763
241.9	-168.205	41.52446207
-213.5	-107.568	289.3241546
-162.9	-107.568	546.6455714
-112.3	-107.568	1107.506297
-61.7	-107.568	37161.96685
-11.1	-107.568	208923.7813
39.5	-107.568	10153.93186

90.1	-107.568	972.838862
140.7	-107.568	496.3312683
191.3	-107.568	250.9244484
241.9	-107.568	132.8847407
-213.5	-46.9318	310.67316
-162.9	-46.9318	418.4043774
-112.3	-46.9318	638.6092147
-61.7	-46.9318	12959.514
-11.1	-46.9318	55226.06414
39.5	-46.9318	3228.541019
90.1	-46.9318	601.3076533
140.7	-46.9318	388.2489668
191.3	-46.9318	276.8731842
241.9	-46.9318	190.6175937
-213.5	13.7045	236.657299
-162.9	13.7045	298.4053265
-112.3	13.7045	402.0926814
-61.7	13.7045	9406.277124
-11.1	13.7045	44711.8769
39.5	13.7045	2056.284768
90.1	13.7045	389.3857007
140.7	13.7045	280.700548
191.3	13.7045	214.8717907
241.9	13.7045	177.9684199
-213.5	74.3409	186.7272267
-162.9	74.3409	229.8551295
-112.3	74.3409	269.5154544
-61.7	74.3409	3312.173595
-11.1	74.3409	14340.75221
39.5	74.3409	820.302299

90.1	74.3409	267.3501899
140.7	74.3409	215.5473309
191.3	74.3409	171.323574
241.9	74.3409	146.0299646
-213.5	134.977	151.9563979
-162.9	134.977	179.7635978
-112.3	134.977	190.3654208
-61.7	134.977	177.8738381
-11.1	134.977	165.1609168
39.5	134.977	181.0379088
90.1	134.977	193.4878245
140.7	134.977	171.6767644
191.3	134.977	140.8366537
241.9	134.977	120.2557192
-213.5	195.614	125.9213547
-162.9	195.614	147.7555837
-112.3	195.614	147.3455921
-61.7	195.614	133.9119091
-11.1	195.614	122.8004024
39.5	195.614	137.1547785
90.1	195.614	149.3898405
140.7	195.614	143.2848702
191.3	195.614	116.8242736
241.9	195.614	99.25559322

APPENDIX K

DOSE IN AIR IN A BOUNDLESS ROOM WITH VOXEL PHANTOM

X-axis	Y-axis	Dose at 138.3 cm from the floor of room (mGy/100mAs)
-213.5	-410.75	41.28606435
-162.9	-410.75	149.7349348
-112.3	-410.75	408.4757208
-61.7	-410.75	696.4701959
-11.1	-410.75	773.9039456
39.5	-410.75	669.5646961
90.1	-410.75	365.0599831
140.7	-410.75	123.76331
191.3	-410.75	32.15971083
241.9	-410.75	5.727398697
-213.5	-350.114	6.057270449
-162.9	-350.114	46.85432615
-112.3	-350.114	421.0783418
-61.7	-350.114	1395.589358
-11.1	-350.114	1650.539497
39.5	-350.114	1285.936003
90.1	-350.114	308.7089279
140.7	-350.114	32.40141399
191.3	-350.114	5.484798612
241.9	-350.114	3.298760571
-213.5	-289.477	3.194658822
-162.9	-289.477	4.511074691
-112.3	-289.477	770.5366993
-61.7	-289.477	392432.6112
-11.1	-289.477	149089.6171
39.5	-289.477	385473.3178

90.1	-289.477	640.8065804
140.7	-289.477	4.592195469
191.3	-289.477	3.199316267
241.9	-289.477	2.888357793
-213.5	-228.841	4.909649829
-162.9	-228.841	3.394987374
-112.3	-228.841	70.34459396
-61.7	-228.841	1574397293
-11.1	-228.841	39573676.19
39.5	-228.841	1571896589
90.1	-228.841	92.33021834
140.7	-228.841	4.332240122
191.3	-228.841	5.533905184
241.9	-228.841	5.357861946
-213.5	-168.205	49.43841937
-162.9	-168.205	191.1990994
-112.3	-168.205	6209.862267
-61.7	-168.205	1060716.856
-11.1	-168.205	3194406.378
39.5	-168.205	786512.9314
90.1	-168.205	4794.415042
140.7	-168.205	157.2841312
191.3	-168.205	42.85031951
241.9	-168.205	16.63140457
-213.5	-107.568	272.3197977
-162.9	-107.568	584.5199736
-112.3	-107.568	1250.05735
-61.7	-107.568	34502.30876
-11.1	-107.568	193829.1214
39.5	-107.568	9830.889275

90.1	-107.568	1099.764982
140.7	-107.568	539.8190493
191.3	-107.568	254.6476862
241.9	-107.568	119.3517623
-213.5	-46.9318	290.6468572
-162.9	-46.9318	425.8621899
-112.3	-46.9318	684.3178838
-61.7	-46.9318	10098.6494
-11.1	-46.9318	42545.57035
39.5	-46.9318	2756.141613
90.1	-46.9318	653.1303143
140.7	-46.9318	407.1804303
191.3	-46.9318	282.0928341
241.9	-46.9318	185.5862557
-213.5	13.7045	213.1963866
-162.9	13.7045	290.0719993
-112.3	13.7045	411.5054707
-61.7	13.7045	6760.233394
-11.1	13.7045	32449.51478
39.5	13.7045	1592.335423
90.1	13.7045	402.3879142
140.7	13.7045	280.4894763
191.3	13.7045	208.2823287
241.9	13.7045	165.0646624
-213.5	74.3409	161.566742
-162.9	74.3409	214.8136888
-112.3	74.3409	262.1181147
-61.7	74.3409	2288.504258
-11.1	74.3409	9532.81394
39.5	74.3409	641.8978714

90.1	74.3409	265.9647638
140.7	74.3409	207.4334543
191.3	74.3409	158.3167943
241.9	74.3409	127.0685646
-213.5	134.977	127.9684535
-162.9	134.977	160.8846063
-112.3	134.977	174.9740951
-61.7	134.977	159.8692698
-11.1	134.977	145.0017722
39.5	134.977	165.5460854
90.1	134.977	182.1353925
140.7	134.977	159.4209565
191.3	134.977	125.8134928
241.9	134.977	100.9072689
-213.5	195.614	100.3574401
-162.9	195.614	122.3607755
-112.3	195.614	124.2839832
-61.7	195.614	110.5103502
-11.1	195.614	100.9052087
39.5	195.614	115.5569732
90.1	195.614	127.5401574
140.7	195.614	123.1547458
191.3	195.614	100.4884709
241.9	195.614	82.28211382

APPENDIX L

PUBLICATION - RADIATION PROTECTION DOSIMETRY

OPTIMISATION OF SCATTER RADIATION TO STAFF DURING CT-FLUOROSCOPY: MONTE CARLO STUDIES

P. K. Gyekye ✉, F. Becker, S. Y. Mensah, G. Emi-Reynolds

Radiation Protection Dosimetry, Volume 170, Issue 1-4, 1 September 2016, Pages 393–397, https://doi.org/10.1093/rpd/ncw135

Published: 07 September 2016 **Article history** ▾

Cite Permissions Share ▾

Abstract

Studies have shown that there is high radiation exposure to medical staff during computed tomography fluoroscopy (CTF)–guided procedures. This study aims to investigate staff dose reduction techniques considering the CTF gantry positioning in the room and room dimensions in addition to the conventional use of thyroid collars, aprons and eye goggles. A Toshiba Aquilion One 640 slice CT scanner and CTF room were modelled using SimpleGeo. Standing and supine adult mesh phantoms were used to represent the staff and patient. The

APPENDIX M

CONFERENCE PAPER

MONTE CARLO STUDIES INTO STAFF DOSE: LEAD DRAPE AND PATIENT COVER USE DURING COMPUTED TOMOGRAPHY FLUOROSCOPY PROCEDURES

P. K. GYEKYE
Nuclear Regulaotry Authority
Accra, Ghana
E-mail: p.gyekye@gnra.org.gh

F. BECKER
Institute for Nuclear Waste Disposal, Karlsruhe Instiute of Technology
Karlsruhe, Germany

S. Y. MENSAH
University of Cape Coast
Cape Coast, Ghana

G. EMI-REYNOLDS
Nuclear Regulaotry Authority
Accra, Ghana

Abstract

Reduction of staff radiation dose through the use of lead drape on the computed tomography fluoroscopy (C